1990

Development, characterization, and applications of optical pH sensors supported at cellulosic films

Thomas P. Jones
Iowa State University

INFORMATION TO USERS

The most advanced technology has been used to photograph and reproduce this manuscript from the microfilm master. UMI films the text directly from the original or copy submitted. Thus, some thesis and dissertation copies are in typewriter face, while others may be from any type of computer printer.

The quality of this reproduction is dependent upon the quality of the copy submitted. Broken or indistinct print, colored or poor quality illustrations and photographs, print bleedthrough, substandard margins, and improper alignment can adversely affect reproduction.

In the unlikely event that the author did not send UMI a complete manuscript and there are missing pages, these will be noted. Also, if unauthorized copyright material had to be removed, a note will indicate the deletion.

Oversize materials (e.g., maps, drawings, charts) are reproduced by sectioning the original, beginning at the upper left-hand corner and continuing from left to right in equal sections with small overlaps. Each original is also photographed in one exposure and is included in reduced form at the back of the book.

Photographs included in the original manuscript have been reproduced xerographically in this copy. Higher quality 6" x 9" black and white photographic prints are available for any photographs or illustrations appearing in this copy for an additional charge. Contact UMI directly to order.

UMI

University Microfilms International
A Bell & Howell Information Company
300 North Zeeb Road Ann Arbor MI 48106-1346 USA
313 761-4700 800 521-0600

Order Number 9101357

Development, characterization, and applications of optical pH sensors supported at cellulosic films

Jones, Thomas P., Ph.D.

Iowa State University, 1990

U·M·I
300 N. Zeeb Rd.
Ann Arbor, MI 48106

Development, characterization, and applications of optical pH sensors supported at cellulosic films

by

Thomas P. Jones

A Dissertation Submitted to the
Graduate Faculty in Partial Fulfillment of the
Requirements for the Degree of
DOCTOR OF PHILOSOPHY

Department: Chemistry
Major: Analytical Chemistry

Approved:

Signature was redacted for privacy.

Signature was redacted for privacy.

In Charge of Major Work

Signature was redacted for privacy.

For the Major Department

Signature was redacted for privacy.

For the Graduate College

Iowa State University
Ames, Iowa

1990

TABLE OF CONTENTS

GENERAL INTRODUCTION

Explanation of Dissertation Format

This dissertation is organized as the "Alternate Thesis Format" described in the Iowa State University Graduate College Thesis Manual. Each section of this dissertation represents work done by the author of this dissertation, under the direction of Marc D. Porter, his Thesis Advisor. Section I reviews the literature on optical chemical sensor development, and Sections II through VI are typescripts of manuscripts as submitted to or published in scholarly journals. In Section II, Scott M. Stole is listed as co-author due to his contributions in the collection and interpretation of data. The dissertation closes with a short summary and discussion.

Overview of Dissertation

The design, fabrication, and characterization of optical chemical sensors for the determination of pH have been studied. Section I is a review and discussion of the literature pertaining to the development of optical chemical sensors, including those for ions, gasses, and biocomponents. Section II is a study of the hydrolysis of cellulose acetate by internal reflection spectroscopy. Section III describes the fabrication and initial characterization of a sensor for the determination of pH, which was based on the immobilization of Congo Red at hydrolyzed cellulose acetate films. Section IV describes the development of a pH sensor based on infrared internal reflection spectroscopy, as well as structural characterization of immobilized Congo Red by infrared internal reflection spectroscopy. Section

V reports further characterizations of Congo Red immobilized at cellulose acetate, including the effects of ionic strength on the optical response characteristics, and includes a discussion on calibration of optical sensors based on the immobilization of colorimetric indicators. Section VI reports the development of a solid-state two-wavelength fiber-optic sensor device based on light-emitting-diode (LED) sources and photodiode detectors.

SECTION I. LITERATURE REVIEW OF CHEMICAL SENSORS

DEFINITION OF CHEMICAL SENSORS

Chemical sensors are self-contained devices that provide real-time information about the chemical composition of a system. The chemical selectivity of an immobilized reagent provides for the determination of analyte concentration in the presence of potential interferents. Thus, chemical sensors can be used with a minimum, or preferably, no sample preparation. Additionally, chemical sensors provide a means of continuous monitoring of analyte concentration, which is a desirable capability for applications in environmental, biomedical, or process-control analyses. Transduction of the sensor response most often involves electrochemical or optical measurements, or mass-sensitive methods based on piezoelectric oscillators.

This section consists of a review of the literature pertaining to the development, characterization, and applications of chemical sensors based on the immobilization of colorimetric indicators. The literature review is followed by a discussion of immobilization chemistry, including the schemes that have been used to immobilize colorimetric indicators, and the effect of immobilization on the response time, reactivity, and stability. A discussion on the calibration of optical sensors follows, including the use of multiple indicators to extend the dynamic range. The section closes with a comparison of optical methods with electrochemical methods with respect to dynamic range, ionic-strength effects, and calibration of the sensor response.

LITERATURE REVIEW

Development, characterization, and application of optical chemical sensors for pH, metal ions, gasses, and biological materials have in recent years become an area of rapidly increasing research activity.[1-11] Chemical sensors involving the immobilization of colorimetric reagents at optical fibers have been developed for applications in biomedical[11] and environmental analyses,[12] as well as in process analytical chemistry.[10,12]

Optical pH Sensors

The large number of optical pH sensors developed is, in part, a result of the availability of acid-base indicators on which to base the sensor design, and, in part, due to the importance of pH determination. Sensors for pH utilizing fluorescence,[13-21] UV-visible absorbance,[22-29] UV-visible diffuse reflectance,[30-34] and infrared internal reflection[35] spectroscopy have been developed. A novel approach developed by Jordan *et al.*[36] utilizes the energy transfer from a fluorescent reagent to a colorimetric acid-base indicator. The attenuation of the fluorescence by the absorbing indicator provides a means of determining pH. Sensors for pH have employed acid-base indicators that have been immobilized at a variety of polymeric materials,[18-20,25-29,31-36] electrostatically immobilized in ion-exchange resins;[17,30] covalently bound at porous[13-15,24] or "sintered"[16] glasses, or bound as a monolayer to glass plates.[21-23]

Optical Ion Sensors

Sensors for the detection of ionic species make up the second-largest class of optical chemical sensors. Sensors which provide selective detection of Al(III),[37] K(I),[38-40] Na(I),[41] Mg(II),[42] Ca(II),[43,44] carbonate,[45] iodide,[46] and fluoride[47] have been developed. Less-specific sensors, which respond to multiple metal ions,[48-50] ionic strength,[51] and anions,[52] have also been developed. Ion sensors have employed reagents immobilized in polymeric materials,[37,39,40,42,43,45-47,51,52] immobilized electrostatically in ion-exchange resins,[44,48-50] trapped in an internal solution by a semi-permeable membrane across which analyte diffused,[41] or deposited as a Langmuir-Blodgett film.[38] Optical methods used by ion sensors include absorbance,[39,43,45,52] fluorescence,[37,38,41,42,46,48-50] fluorescence with energy transfer,[51] and diffuse reflectance[40,44,47] detection schemes.

Optical Gas Sensors

Optical sensors for the detection of gasses such as oxygen,[53-58] carbon dioxide,[59-60] ethanol,[61-64] ammonia,[65-67] trichloroethane,[68] carbon tetrachloride,[68] sulfur compounds,[69] and other organic vapors[70] have been developed. These sensors have utilized reagents immobilized at a variety of polymeric materials.[53-57,59,62-64,65,67] Reagents have also been bound covalently to the distal end of an optical fiber[58] or at porous glass.[69] Semipermeable membranes have also been used to trap reagents in a reservoir solution.[60,61,66,68] Gas sensors have employed fluorescence,[53-55,57-62,65] ab-

sorbance,[63,64,66-69] internal reflection,[70] and fluorescence with energy transfer[56] as methods of optical measurement.

Optical Biosensors

Biosensors are sensors which utilize immobilized antigens, antibodies or enzymes to interact with analyte. Because of the specificity of biochemical interactions, such sensors have a very high selectivity. In addition to selectivity, biosensors based on immobilized antibodies or antigens have extremely low limits of detection, due to the extremely strong binding constant of antibody-antigen interactions, but usually have an irreversible response, which necessitates disposable devices. For example, a fiber-optic sensor based on immobilized antibody had sensitivity of ~1 fmol in the detection of the carcinogen benzo(a)pyrene,[71] and other antibody-based sensors have attained similar limits of detection.[72] Sensors that utilize a natural acetylcholine receptor incorporated into artificial lipid bilayer membranes have also been developed,[73] providing detection of carbamylcholine at micromolar concentrations and α-bugarotoxin at nanomolar concentrations. An assay based on competitive binding of fluorescent-labelled antibodies with non-labelled antibodies has also been developed for the detection of rabbit immunoglobin G with a 10 fmol limit of detection.[74] Biosensors based on immobilized enzymes, which operate by the detection of either the enzyme reaction products or by depletion of reactants, have been developed for the detection of glucose,[75,76] carboxylic esters,[77] p-nitrophenyl phosphate,[78] lactate, and pyruvate, NADH, and glutamate.[79] Optical biosensors for penicillin have also been developed,[80,81] which operate

by measuring the pH change caused by the reaction with the enzyme penicillinase.

DISCUSSION

Issues in Sensor Construction and Performance

Immobilization schemes

Optical sensors have been fabricated which feature the immobilization of colorimetric indicators at a variety of polymeric materials, ion-exchange materials, and glasses. The support material is the primary factor in determining the response time of the sensor, as a result of barriers to diffusion from solution to the analytical reagent. The immobilization chemistry is also a large determining factor in the long-term stability of the sensor. Weak immobilization chemistry results in sensors in which the reagent "bleeds" from the support material.

Polymeric materials and ion-exchange resins A common immobilization scheme is to bond or trap the indicator at a support material such as a polymeric material or ion-exchange resin. Many different bonding schemes have been utilized to immobilize the indicator. The simplest is to entrap physically the indicator in a polymer, by mixing the indicator with the plasticizer material. When the polymer forms, the indicator is trapped in the polymer matrix, in which the pore size is smaller than the size of the colorimetric reagent, but larger than that of the analyte, allowing analyte to diffuse through the pores to the trapped colorimetric reagent. The principal drawback to this immobilization scheme is the slow response times due to mass transport barriers in the relatively nonporous material. Another approach is to bond the analytical reagent chemically to

the polymer. This may improve the response time of the sensor, if the polymer is sufficiently porous. A fabrication scheme for porous polymer films has been reported.[27,29]

Ion-exchange resins have also been utilized as support materials.[17,30,44,49,50] In these materials, the reagent is electrostatically trapped in the resin. The immobilization chemistry works primarily for ionic indicators with poor solubilities in aqueous solutions, but some of these sensors suffer from poor long-term stability as a result of indicator bleeding.

Covalent immobilization at glass Indicators can also be covalently bonded to glass plates or at porous glass, utilizing silanization reactions developed for chromatographic applications. The "fastest" sensor made to date consisted of a monolayer of reagent covalently bonded to a glass plate,[21] but the sensor suffered from a weak analytical signal due to the small amount of indicator bound to the surface per unit area. To increase the amount of indicator bound to a surface, several sensors that have been reported have utilized porous glass substrates.[13-16,24,69]

Semipermeable membranes Another immobilization scheme that has been utilized is to trap the reagent in a solution reservoir behind a semipermeable membrane.[41,60,61,66] Such a membrane allows the selective transport of analyte from solution to an internal reservoir which contains the reagent in the solution. The principal advantage of this sensor geometry is that it allows use of the many reagents developed for conventional solution analyses without chemical modification to the reagent. Although this method offers versatility with respect to selection of the reagent, the

response time to changes in analyte concentration is generally very long, due to barriers to mass transport through the semipermeable membrane. The response time can be minimized by reducing the volume of the internal reservoir, but the ultimate limit depends mass transport through the membrane.

Effects of immobilization on reactivity

As in the case of electrochemical sensors,[82] the selectivity and sensitivity of optical chemical sensors are governed by a complex combination of chemical interactions, as well as instrumentation performance characteristics. In many cases, immobilized indicators display remarkably different behavior compared to their solution analogs. For example, Congo Red immobilized at hydrolyzed cellulose acetate has an acid strength of almost two orders of magnitude greater than the solution form of the indicator.[27] Several metallochromic indicators exhibit even greater differences; some lose their reactivity to the analyte completely when immobilized.[29] Many of the metallochromic indicators form complexes through multiple coordination sites; loss of reactivity may occur when the immobilization sites force the indicator into conformations which are not favorable for complex formation. Additional factors which may affect the reactivity of immobilized indicators include the dielectric constant and the ionic characteristics of the polymeric support.

Sensor Calibration

In an analysis, a probe consisting of a colorimetric reagent immobilized at a support material is inserted into a solution, and an optical property is measured. Such optical properties include absorbance, fluorescence, diffuse reflectance and Raman scattering. In some cases, an energy transfer is utilized, in which the excitation radiation is absorbed by one reagent, which transfers the energy to a second reagent; the second compound then emits a fluorescent photon upon relaxation.[36,51,56] The advantage of this approach is that it allows coupling a reagent which has a large absorptivity with a reagent which has a high quantum fluorescence efficiency; this results in a stronger analytical signal.

In most cases, the concentration of analyte is calculated through the use of a calibration curve relating the optical property to concentration of analyte. A sensor, however, can be internally calibrated if the immobilized reagent is a "two-color" indicator (i.e., an indicator in which both forms absorb light of different wavelengths), because the ratio of the two forms of the indicator can be used to determine pH. Some pH sensors have been fabricated by immobilizing multiple indicators with overlapping dynamic ranges. This approach extends the dynamic range of the sensor. It should be noted, however, that in sensors using multiple immobilized indicators, the optical response is also a function of the concentration relative concentrations of the indicators, which may change with time due to unequal degradation of the indicators. Therefore if the relative

concentrations of the multiple indicators change as a function of time, the sensor may require periodic recalibration.

Comparison of Optical and Electrochemical Sensors

Electrochemical devices, such as ion-sensitive field-effect transistors, offer many of the same advantages as optical sensors, including potential for miniaturization and use in low-cost instrumentation. It is instructive to compare the advantages and disadvantages of optical sensors and electrochemical sensors, which has been discussed previously.[83] The most common form of an electrochemical sensor for pH and metal-ion determination is based on potentiometric measurements across an ion-selective membrane. In the following discussion, the relative advantages and disadvantages of sensors based on potentiometric and optical methods will be discussed.

Dynamic range

Because the potential of potentiometric electrochemical sensors follows the Nernst equation, the dynamic range of potentiometric sensors (as many as 15 decades of concentration) is much greater than that of optical sensors, in which the response is governed by complex-formation equilibria. Optical sensors operate through measurement of the ratio of the complexed and uncomplexed forms of an indicator. If the ends of the dynamic range are defined as where the ratio of the two forms of an indicator varies from 1:10 to 10:1, the dynamic range of a single-step optical sensor is limited to only 2 decades of concentration. This limitation can be overcome

through the use of multiple optical reagents either multiple indicators or indicators containing multiple complexation sites.

Ionic strength effects

Optical absorption by an immobilized indicator is proportional to its concentration (i.e., number of moles). The response of optical chemical sensors is a result both of the complex formation between the analyte and immobilized reagent, and the optical absorptivity of each the various forms of the indicator. Consider the case of a monoprotic acid-base indicator. The pH is given by

$$pH = pK + \log([A^-]/[HA]) + \log (\gamma_A/\gamma_{HA}) \quad (1)$$

where $[A^-]$ and [HA] are the concentrations of the basic and acid forms of the indicator, respectively, and γ_A and γ_{HA} are their activity coefficients. The equilibrium constant K is defined in terms of activities. Spectroscopic methods can be used to determine the second term above in Equation 1, but it is clear that changes in the activity coefficient in the third term will affect the calibration of the sensor. Because the activity coefficients of large aromatic molecules are not easily predicted, optical sensors should be calibrated for the ionic strength of the medium in which they are used. In contrast, potentiometric methods respond to the *activity* of analyte, and therefore are not affected by ionic strength changes.

Calibration

Optical sensors can be internally calibrated if the indicator is a "two-color" indicator, because the the pH is a function of the ratio of the

concentrations in the second term of Equation 1. The accuracy of the sensor will be affected by ionic strength changes, but the response will remain calibrated even if some of the indicator is lost by bleeding. In contrast, due to the variability in the junction potential, potentiometric methods need an external reference (e.g., a standard solution) for calibration, and may require periodic recalibration.

Perhaps the most significant advantage that optical sensors offer, however, is the capability for remote sensing through fiber optics. Low-cost fiber-optics are available for the transmission of light across long distances with low losses, so that the possibility of locating the spectrometer literally kilometers from the sample is technically and economically feasible. Optical sensors based on fiber-optic transmission can also probe into hostile environments, and the transmission is unaffected by electronic noise that would require extensive electrical shielding.

REFERENCES

1. Janata, J. *Principles of Chemical Sensors*; Plenum: New York, 1989, chapter 1.
2. Wohltjen, H. *Anal. Chem.* **1984**, *56*, 87A-103A.
3. Janata, J.; Bezegh, A. *Anal. Chem.* **1988**, *60*, 62R-74R.
4. Seitz, W. R. *Anal. Chem.* **1984**, *56*, 16A-34A.
5. Narayanaswamy, R. *Anal. Proc. (London)* **1985**, *22*, 204-206.
6. Alder, J. F. *Fresenius' Z. Anal. Chem.* **1986**, *324*, 372-375.
7. Wolfbeis, O. S. *Fresenius' Z. Anal. Chem.* **1986**, *325*, 387-392.
8. Angel, S. M. *Spectroscopy (Springfield, Oreg.)* **1987**, *2*, 38-4.
9. Wolfbeis, O. S. *Anal. Proc. (London)* **1987**, *24*, 14-15.
10. Hirschfeld, T.; Callis, J. B.; Kowalski, B. R. *Science* **1984**, *226*, 312-318.
11. Peterson, J. I.; Vurek G. G. *Science* **1984**, *224*, 123-12.
12. Callis, J. B.; Illman, D. L.; Kowalski, B. R. *Anal. Chem.* **1987**, *59*, 624A-637A.
13. Saari, L. A.; Seitz, W. R. *Anal. Chem.* **1982**, *54*, 821-823.
14. Wolfbeis, O. S.; Offenbacher, H. *Sens. Actuators* **1986**, *9*, 85-91.
15. Fuh, M.-R. S.; Burgess, L. W.; Hirschfeld, T.; Christian, G. D.; Wang, F. *Analyst (London)* **1987**, *112*, 1159-1163.
16. Offenbacher, H.; Wolfbeis, O. S.; Fürlinger, E. *Sens. Actuators* **1986**, *9*, 73-84.
17. Zhujun, Z.; Seitz, W. R. *Anal. Chim. Acta* **1984**, *160*, 47-55.
18. Kirkbright, G. F.; Narayanaswamy, R.; Welti, N. A. *Analyst (London)* **1984**, 109, 1025-1028.

19. Munkholm, C.; Walt, D. R.; Milanovich, F. P.; Klainer, S. M. *Anal. Chem.* **1986**, *58*, 1427-1430.

20. Zhang, Z.; Zhang, Y.; Ma, W.; Russel, R.; Shakhsher, Z. M.; Grant, C. L.; Seitz, W. R.; Sundberg, D. C. *Anal. Chem.* **1989**, *61*, 202-205.

21. Kawabata, Y.; Tsuchida, K.; Imasaka, T.; Ishibashi, N. *Anal. Sci.* **1987**, *3*, 7-9.

22. Harper, G. B. *Anal. Chem.* **1975**, *47*, 348-351.

23. Mimms, L. T.; McKnight, M. A.; Murray, R. W. *Anal. Chim. Acta* **1977**, *89*, 355-361.

24. Macedo, P. B.; Barkatt, A.; Feng, X.; Finger, S. M.; Hojaji, H.; Laberge, N.; Mohr, R.; Penafiel, M.; Saad, E. *Proc. SPIE-Int. Soc. Opt. Eng.* **1988**, *986*, 200-205.

25. Kirkbright, G. F.; Narayanaswamy, R.; Welti, N. A. *Analyst (London)* **1984**, *109*, 15-17.

26. Boisdé, G.; Pérez, J. J. *Proc. SPIE-Int. Soc. Opt. Eng.* **1987**, *798*, 238-245.

27. Jones, T. P.; Porter, M. D. *Anal. Chem.* **1988**, *60*, 404-406.

28. Guthrie, A. J.; Narayanaswamy, R.; Welti, N. A. *Talanta* **1988**, *35*, 157-159.

29. Stole, S. M; Jones, T. P.; Chau, L.-K.; Porter, M. D. In *Chemical Sensors and Microinstrumentation*; Murray, R.; Dessy, R. E.; Heineman, W. R.; Janata, J.; Seitz, W. R.; Eds.; ACS Symposium Series 403; American Chemical Society: Washington, DC, 1989; pp 283-302.

30. Moreno, M. C.; Martinez, A.; Millan, P.; Camara, C. *J. Mol. Struct.* **1986**, *143*, 553-556.

31. Ruzicka, J.; Hansen, E. H. *Anal. Chim. Acta* **1985**, *173*, 3-21.

32. Woods, B. A.; Ruzicka, J.; Christian, G. D.; Charlson, R. J. *Anal. Chem.* **1986**, *58*, 2496-2502.

33. Peterson, J. I.; Goldstein, S. R.; Fitzgerald, R. V.; Buckhold, D. K. *Anal. Chem.* **1980**, *52*, 864-869.

34. Narayanaswamy, R.; Sevilla, F., III *Anal. Chim. Acta* **1986**, *189*, 365-369.

35. Jones, T. P.; Porter, M. D. *Appl. Spectrosc.* **1989**, *43*, 908-911.

36. Jordan, D. M.; Walt, D. R.; Milanovich, F. P. *Anal. Chem.* **1987**, *59*, 437.

37. Saari, L. A.; Seitz, W. R. *Anal. Chem.* **1983**, *55*, 667-670.

38. Wolfbeis, O. S.; Schaffar, B. P. H. *Anal. Chim. Acta* **1987**, *198*, 1-12.

39. Alder, J. F.; Ashworth, D. C.; Narayanaswamy, R.; Moss, R. E.; Sutherland, I. O. *Analyst (London)* **1987**, *112*, 1191-1192.

40. Al-Amir, S. M. S.; Ashworth, D. C.; Narayanaswamy, R.; Moss, R. E. *Talanta* **1989**, *36*, 645-650.

41. Zhujun, Z.; Mullin, J. L.; Seitz, W. R. *Anal. Chim. Acta* **1986**, 184, 251-258.

42. Wangbai, M.; Zhujun, Z.; Seitz, W. R. In *Chemical Sensors and Microinstrumentation*; Murray, R.; Dessy, R. E.; Heineman, W. R.; Janata, J.; Seitz, W. R.; Eds.; ACS Symposium Series 403; American Chemical Society: Washington, DC, 1989; pp 271-282.

43. Ashworth, D. C.; Huang, H. P.; Narayanaswamy, R. *Anal. Chim. Acta* **1988**, 213, 251-257.

44. Chau, L.-K.; Porter, M. D. *Anal. Chem.*, in press.

45. Morf, W. E.; Seiler, K.; Lehmann, B.; Behringer, C.; Hartman, K.; Simon, W. *Pure Appl. Chem.* **1989**, *61*, 1613-1618.

46. Wyatt, W. A.; Bright, F. V.; Hieftje, G. M. *Anal. Chem.* **1987**, *59*, 2272-2276.

47. Narayanaswamy, R.; Russell, D. A.; Sevilla, F., III *Talanta* **1988**, *35*, 83-88.

48. Carroll, M. K.; Bright, F. V.; Hieftje, G. M. *Anal. Chem.* **1989**, *61*, 1768-1772.

49. Zhujun, Z.; Seitz, W. R. *Anal. Chim. Acta* **1985**, *171*, 251-258.

50. Bright, F. V.; Poirier, G. E.; Hieftje, G. M. *Talanta* **1988**, *35*, 113-118.

51. Christian, L. M.; Seitz, W. R. *Talanta* **1988**, *35*, 119-122.

52. Tan, S. S. S.; Hauser, P. C.; Chaniotakis, G. S.; Simon, W. *Chimia* **1989**, *43*, 257-261.

53. Zhujun, Z.; Seitz, W. R. *Anal. Chem.* **1986**, *58*, 220-222.

54. Cox, M. E.; Dunn, B. *Proc. SPIE-Int. Soc. Opt. Eng.* **1985**, *576*, 60-65.

55. Lee, E. D.; Werner, T. C.; Seitz, W. R. *Anal. Chem.* **1987**, *59*, 279-283.

56. Sharma, A.; Wolfbeis, O. S. *Appl. Spectrosc.* **1988**, *42*, 1009-1011.

57. Wolfbeis, O. S.; Weis, L. J.; Leiner, M. J.P.; Ziegler, W. E. *Anal. Chem.* **1988**, *60*, 2028-2030.

58. McFarlane, R.; Hamilton, M. C. *Proc. SPIE–Int. Soc. Opt. Eng.* **1987**, *798*, 324-330.

59. Munkholm, C.; Walt, D. R.; Milanovich, F. P. *Talanta* **1988**, *35*, 109-112.

60. Kawabata, Y.; Kamichika, T.; Imasaka, T.; Ishibashi, N. *Anal. Chim. Acta* **1989**, *219*, 223-229.

61. Walters, B. S.; Nielsen, T. J.; Arnold, M. A. *Talanta* **1988**, *35*, 151-155.

62. Wolfbeis, O. S.; Posch, H. E. *Fresenius' Z. Anal. Chem.* **1988**, *332*, 255-257.

63. Posch, H. E.; Wolfbeis, O. S.; Pusterhofer, J. *Talanta* **1988**, *35*, 89-94.

64. Gumbrecht, W.; Schelter, W. *Siemens Forsch–Entwicklangsber.* **1986**, *15*, 101-104.

65. Wolfbeis, O. S.; Posch, H. E. *Anal. Chim. Acta* **1986**, *185*, 321-327.

66. Rhines, T. D.; Arnold, M. A. *Anal. Chem.* **1988**, *60*, 76-81.

67. Çağlar, P.; Narayanaswamy, R. *Analyst (London)* **1987**, *112*, 1285-1288.

68. Angel, S. M.; Ridley, M. N.; Langry, K.; Kulp, R. J.; Myrick, M. L. In *Chemical Sensors and Microinstrumentation*; Murray, R.; Dessy, R. E.; Heineman, W. R.; Janata, J.; Seitz, W. R.; Eds.; ACS Symposium Series 403; American Chemical Society: Washington, DC, 1989; pp 345-363.

69. Novak, T. J.; Mackay, R. A. *Spectrosc. Lett.* **1988**, *21*, 127-145.

70. Giuliani, J. F. In *Chemical Sensors and Microinstrumentation*; Murray, R.; Dessy, R. E.; Heineman, W. R.; Janata, J.; Seitz, W. R.; Eds.; ACS Symposium Series 403; American Chemical Society: Washington, DC, 1989; pp 364-379.

71. Vo-Dinh, T.; Tromberg, B. J.; Griffin, G. D.; Ambrose, K. R.; Sepaniak, M. J.; Gardenhire, E. M. *Appl. Spectrosc.* **1987**, *41*, 735-738.

72. Sepaniak, M. J., Tromberg, B. J.; Alarie, J.-P.; Bowyer, J. R.; Hoyt, A. M.; Vo-Dinh, T. In *Chemical Sensors and Microinstrumentation*; Murray, R.; Dessy, R. E.; Heineman, W. R.; Janata, J.; Seitz, W. R.; Eds.; ACS Symposium Series 403; American Chemical Society: Washington, DC, 1989; pp 318-330.

73. Krull, U. J.; Brown, R. S.; Dyne, K.; Hougham, B. D.; Vandenberg, E. T. In *Chemical Sensors and Microinstrumentation*; Murray, R.; Dessy, R. E.; Heineman, W. R.; Janata, J.; Seitz, W. R.; Eds.; ACS Symposium Series 403; American Chemical Society: Washington, DC, 1989; pp 331-344.

74. Tromberg, B. J.; Sepaniak, M. J.; Vo-Dinh, T.; Griffin, G. D. *Anal. Chem.* **1988**, *59*, 1226-1230.

75. Parker, J. W.; Cox, M. E. *Proc. SPIE-Int. Soc. Opt. Eng.* **1987**, *713*, 113.

76. Zhujun, Z.; Seitz, W. R. *Anal. Chem.* **1986**, *58*, 220.

77. Wolfbeis, O. S. *Anal. Chem.* **1986**, *58*, 2874.

78. Arnold, M. A. *Anal. Chem.* **1985**, *57*, 565.

79. Arnold, M. A. In *Chemical Sensors and Microinstrumentation*; Murray, R.; Dessy, R. E.; Heineman, W. R.; Janata, J.; Seitz, W. R.; Eds.; ACS Symposium Series 403; American Chemical Society: Washington, DC, 1989; pp 303-317.

80. Walt, D. R.; Munkholm, C. M.; Yuan, P.; Luo, S; Barnard, S. In *Chemical Sensors and Microinstrumentation*; Murray, R.; Dessy, R. E.; Heineman, W. R.; Janata, J.; Seitz, W. R.; Eds.; ACS Symposium

Series 403; American Chemical Society: Washington, DC, 1989; pp 252-272.

81. Fuh, M.-R. S.; Burgess, L. W.; Christian, G. D. *Anal. Chem.* **1988**, *60*, 433-435.

82. Murray, R. in *Electroanalytical Chemistry*; Bard, A. J., Ed.; Dekker: New York, 1984; vol. 13.

83. Janata, J. *Anal. Chem.* **1987**, *59*, 1351-1356.

SECTION II. MONITORING THE PROGRESS OF THE BASE HYDROLYSIS OF CELLULOSE ACETATE USING INTERNAL REFLECTION INFRARED SPECTROSCOPY

MONITORING THE PROGRESS OF THE BASE HYDROLYSIS OF CELLULOSE ACETATE USING INTERNAL REFLECTION INFRARED SPECTROSCOPY

Thomas P. Jones, Scott M. Stole and Marc D. Porter
Department of Chemistry and Ames Laboratory–USDOE
Iowa State University
Ames, IA 50011

INTRODUCTION

Thin films of polymeric materials have been used in the modification of surface properties in a wide range of applications, including electroanalysis[1-6] and lubrication,[7] as well as in the construction of biocompatible materials for artificial hearts and joint replacements.[8,9] These materials have also gained importance in the design and construction of optical and electrochemical sensors. Electrochemical applications utilize the chemical and physical properties of thin films to control the selectivity of analyses. In optical sensor applications, thin polymeric films have found widespread applicability as support materials for the immobilization of colorimetric indicators.

As part of our interest in this area, we have utilized cellulose acetate films for the fabrication of optical sensors for pH determination.[10,11] Due to the *porous* nature of the hydrolyzed cellulose acetate film, these sensors exhibit dramatically faster response times in comparison with other sensors based on immobilization of optical reagents at comparatively impermeable polymeric materials. In this paper, we present the results of a characterization of the base-hydrolysis mechanism of cellulose acetate by infrared internal reflection spectroscopy (IR-IRS). The utilization of infrared internal reflection spectroscopy offers the advantages of *in-situ* spectroscopy of the polymer, such that data can be taken continually as the hydrolysis proceeds without removing the sample from the hydrolysis solution. The results of this study are compared to results obtained in

emersion studies using infrared external reflectance spectroscopy (IR-ERS) at glassy carbon substrates.[11,12]

Infrared Internal Reflection Spectroscopy (IR-IRS)

Infrared internal reflection spectroscopy provides a facile means to detect subtle changes in the composition and structure of thin films in the presence of strongly absorbing solvents,[13,14] as well as to monitor the diffusion of small organic molecules into such materials.[15] The evanescent wave from IR-transmitting fibers has been used to detect adsorbed films containing organic moieties after solvent evaporation,[16] and to monitor the progress of a composite curing reaction.[17]

When light is reflected from one medium to a medium of lower refractive index, interference between the incident and reflected waves creates an evanescent wave which extends into the rarer medium. The electric field is non-zero at the interface, and decreases exponentially as a function of distance into the rarer medium, as depicted in Figure 1. The decay of the electric field as a function of distance from the interface within the rarer medium is given[18] by

$$E(z) = E_0 \exp(-z/d_p) \qquad (1)$$

where E_0 is the value of the electric field at the surface, z is the distance from the interface between the two media, and d_p is the "depth of penetration," which is defined as value of z for which the electric field has dropped to e^{-1} of its value at the interface. The depth of penetration is given[18] by

$$d_p = \lambda_1 / \{2\pi(\sin^2 \Theta - n_{21}^2)^{1/2}\} \qquad (2)$$

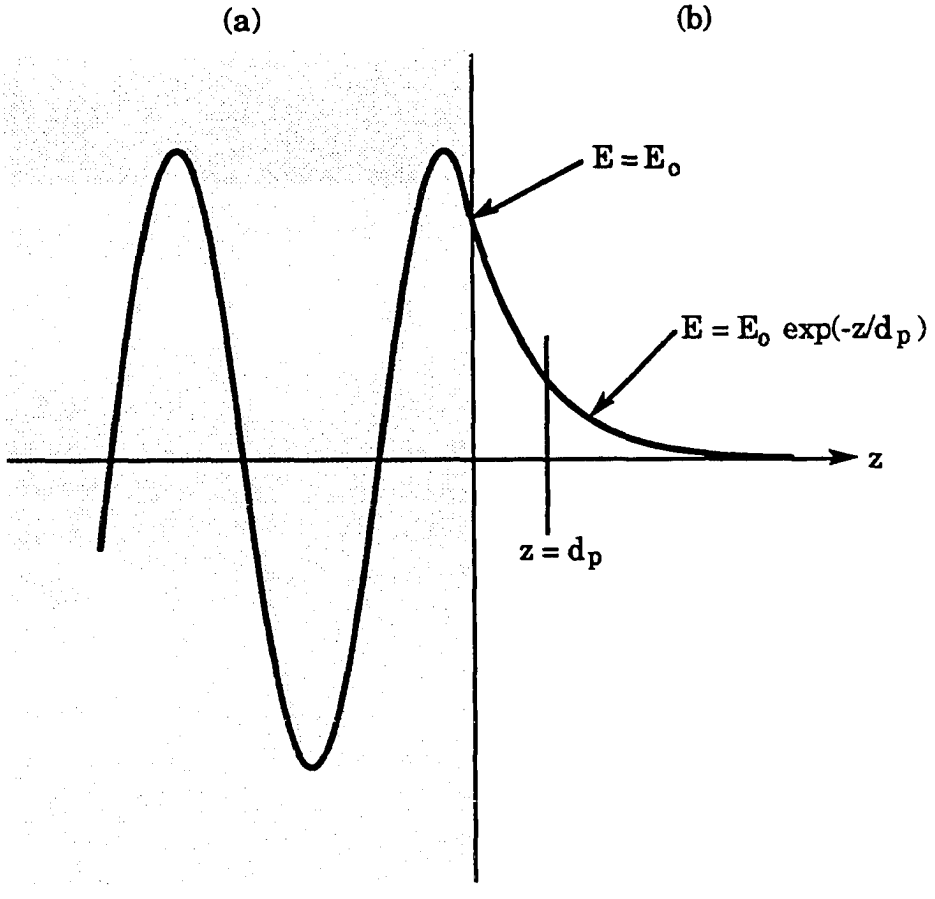

Figure 1. Electric field amplitude of evanescent wave as a function of distance from the interface between two media: (a) denser medium, (b) rarer medium. Electric field varies sinusoidally in denser medium; $E = E_0$ at surface, and E decays exponentially in rarer medium

where ($\lambda_1 = \lambda/n_1$) is the wavelength of light, and ($n_{21} = n_2/n_1$) is the ratio of the refractive index of the rarer medium to that of the denser medium, and Θ is the angle of incidence. The amount of light absorbed as a function of distance from the interface is proportional to the square of the electric field.

EXPERIMENTAL

CIRCLE® Cell

Spectra of cellulose acetate as a function of hydrolysis time were collected by internal reflection spectroscopy (IRS) of a cellulose acetate film coated at the cylindrical internal reflection element of a CIRCLE® cell (Spectra Tech, Inc., Stamford CT). A schematic diagram of the sensor and flow cell is shown in Figure 2. A pair of mirrors in a "Cassegrain-like" arrangement directs the IR beam onto the IRE at an average angle of incidence of 45°. A similar pair of mirrors collects and redirects the beam to an IR detector after propagation through the IRE. Teflon® O-rings were used to mount the IRE in the flow cell. The O-rings restrict solution contact to a 6.0-cm segment of the thin film sensor. With this arrangement, the light undergoes ~10-11 reflections as it passes through the IRE.

Fabrication of Cellulose Acetate Film

A film of cellulose acetate (Aldrich, Inc., Milwaukee, WI) was coated onto the IRE by the slow evaporation of a polymer solution (2.5% w/v cellulose acetate in cyclohexanone). The optical element was positioned horizontally in a chuck attached to an electric motor, and was rotated at 300 rpm to ensure a uniform film thickness. After drying for 24 h, the thickness of the resulting film was 5.1 μm, as estimated by the mass difference of the IRE before and after film deposition. The polymer-modified IRE was then mounted in the CIRCLE® cell.

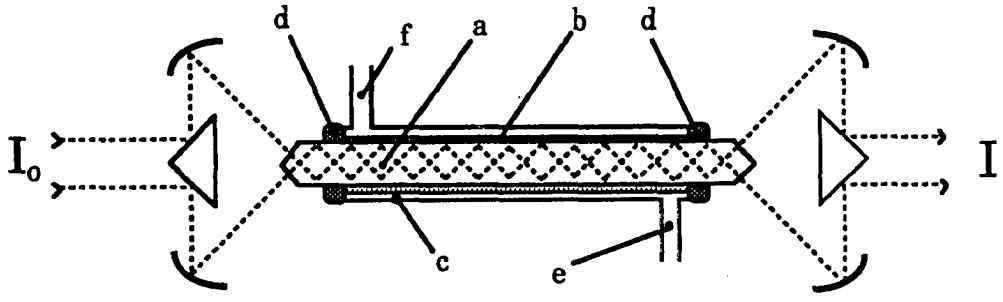

Figure 2. CIRCLE® cell: (a) ZnSe internal reflection element; (b) cellulose acetate film; (c) flow cell; (d) Teflon® O-rings; (e) solution inlet; and (f) solution outlet. The dashed lines represent the light path through the cell

Hydrolysis and Spectra Collection

Spectra were collected with a Nicolet 740 Fourier transform infrared spectrometer (Madison, WI). Each spectrum represents the ratio of 25 sample and 25 reference scans, and required 5 s for collection of each sample spectrum. Interferograms were coadded at 4 cm^{-1} resolution with Happ-Genzel apodization. The optical signal was monitored with a liquid-N_2 cooled narrow-band MCT detector. The spectrometer was purged with liquid-N_2 boil-off to minimize absorption by water vapor and CO_2.

The flow cell was filled with 0.07-M KOH, and spectra were collected at 2-min intervals up to 120 min of hydrolysis. Between spectra collection, 30 mL of additional 0.07 M KOH was injected into the cell to refresh the solution in contact with the cellulose acetate film and to remove hydrolysis products. Spectra of the cellulose acetate film were given as $-\log(R/R_0)$ where R is the single-beam spectrum of the cellulose acetate film in contact with the IRE, and R_0 is the single-beam spectrum of the IRE in contact with 0.07-M KOH. Similarly, a spectrum of liquid water was obtained by referencing the single-beam spectrum of the IRE in contact with 0.07-M KOH to the single-beam spectrum of the dry IRE. The spectrum of liquid water was subtracted interactively from the spectra of the cellulose acetate film to eliminate residual liquid water bands.

RESULTS AND DISCUSSION

Hydrolysis of Cellulose Acetate

Figure 3 shows the effect of the hydrolysis reaction on the structure of cellulose acetate. Cellulose acetate is acetyl-substituted cellulose that contains an average of 2.4 acetyl groups per glucose unit. Cellulose acetate contains both amorphous and crystalline regions, the relative amounts of which depend on the fabrication parameters, such as solvent, rotation rate, and acetyl content.[19] The hydrolysis of cellulose acetate has been used to control the permselectivity of glassy-carbon electrodes coated with a thin film of cellulose acetate,[3] and in our previous study by cyclic voltammetry and infrared external reflection spectroscopy,[11,12] the increase in permselectivity of a cellulose acetate film was correlated to the replacement of acetyl by hydroxyl groups. Figure 4 illustrates the proposed model explaining the structural changes responsible for the increase in permselectivity. The "bulky" acetyl groups limit the interchain spacing of the cellulose acetate film,[20] but as the acetyl functionalities are replaced by hydroxyl groups, hydrogen-bonding interactions between chains opens up small channels and pinholes in the film, which increase porosity.

Transmission Spectrum and Band Assignments

A transmission spectrum of a 3.0-μm film of cellulose acetate is shown in Figure 5. The major peaks in the spectrum are assigned as given in Table 1. Bands at 1755, 1369, and 1233, and 1052 cm^{-1} are assigned to the acetyl functionality, arising from the C=O stretching, the methyl bending,

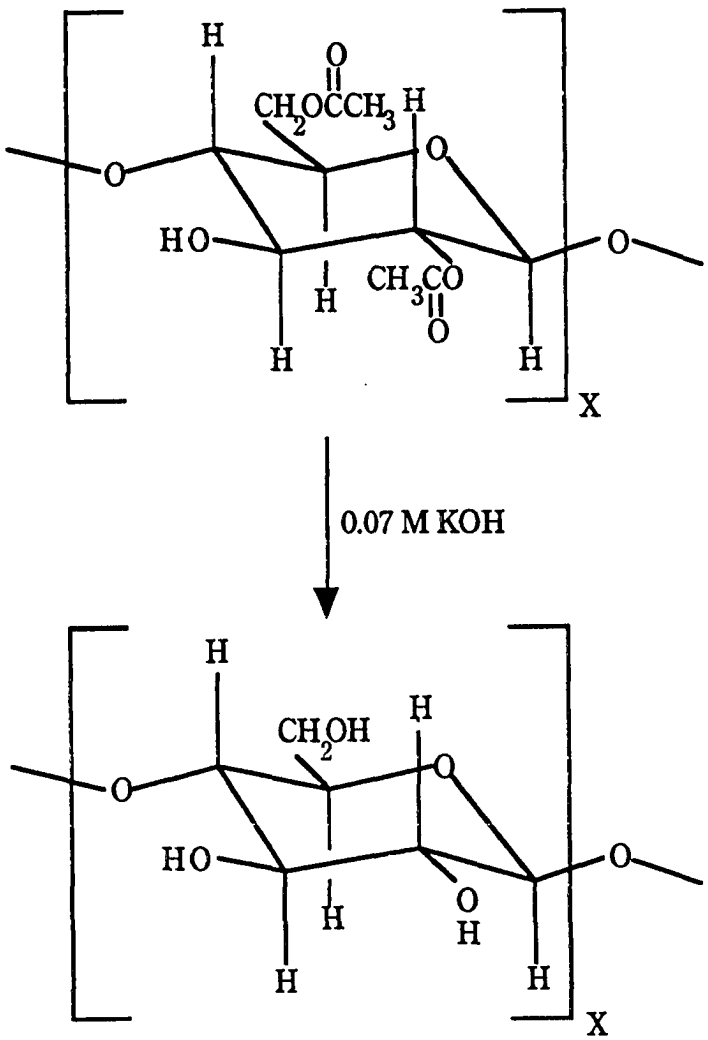

Figure 3. Effect of hydrolysis on the structure of cellulose acetate. Acetate groups are replaced by hydroxyl groups, resulting in a "cellulosic" material

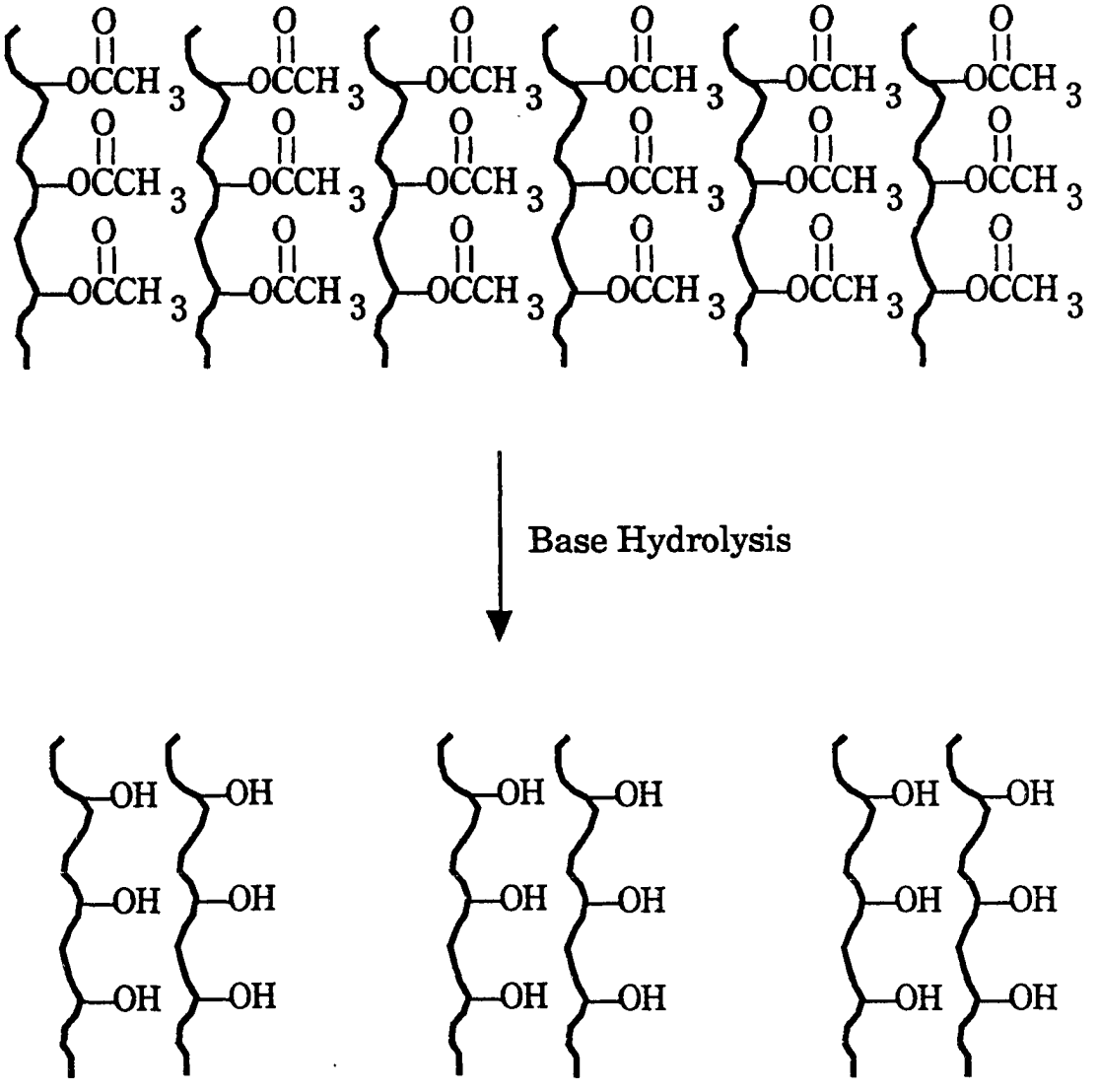

Figure 4. Depiction of permeability increase upon hydrolysis. Porosity increases as bulky acetyl groups are replaced by smaller hydroxyl groups. Pinholes and channels open up as chains are pulled together by hydrogen bonding between adjacent chains

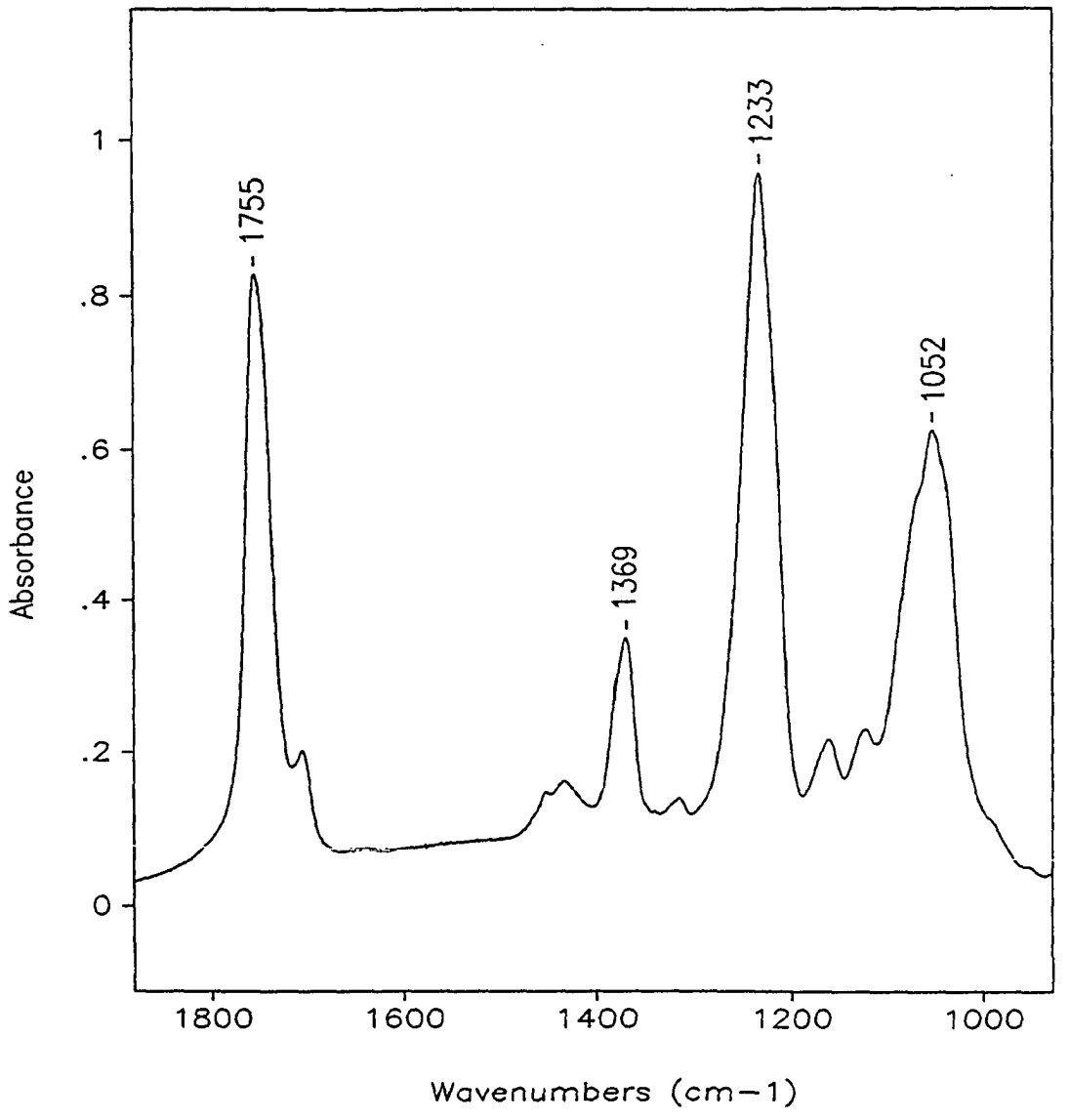

Figure 5. Infrared transmission spectrum of cellulose acetate film. Peak assignments are listed in Table 1

Table 1. Peak assignments infrared transmission and internal-reflection spectra of cellulose acetate. Peak positions are in wavenumbers (cm^{-1})

Assignment	Transmission	Internal Reflection
ν(C=O)	1755	1732
$\delta(CH_3)$	1369	1369
ν(C-O) acetyl	1233	1227
ν(C-O)[a]	1052	1034

[a]Overlapping C-O stretches of acetyl, alcohols and ethers.

and the two C-O stretching modes of the acetyl group, respectively. The latter of the C-O stretches is overlaid by C-O stretches of the alcohol and ether functionalities of the cellulose support.

IR-IRS Spectra vs. Hydrolysis Time

Figure 6 shows infrared internal reflection spectra as a function of hydrolysis time, at 10 min intervals. The peak positions of these bands are given in Table 1. The absorbance of a number of bands decreases as a function of hydrolysis time, which we attribute to the removal of the acetyl group. The band at 1732 cm^{-1} is assigned to the carbonyl C=O stretch of the acetyl group; it disappears completely by 80 min of hydrolysis. Also attributed to the acetyl group is the methyl bending mode at 1369 cm^{-1}, and two C-O stretches at 1227 and 1034 cm^{-1}. The latter of these C-O bands is superimposed on C-O stretches of the alcohol and ether groups of cellulose.

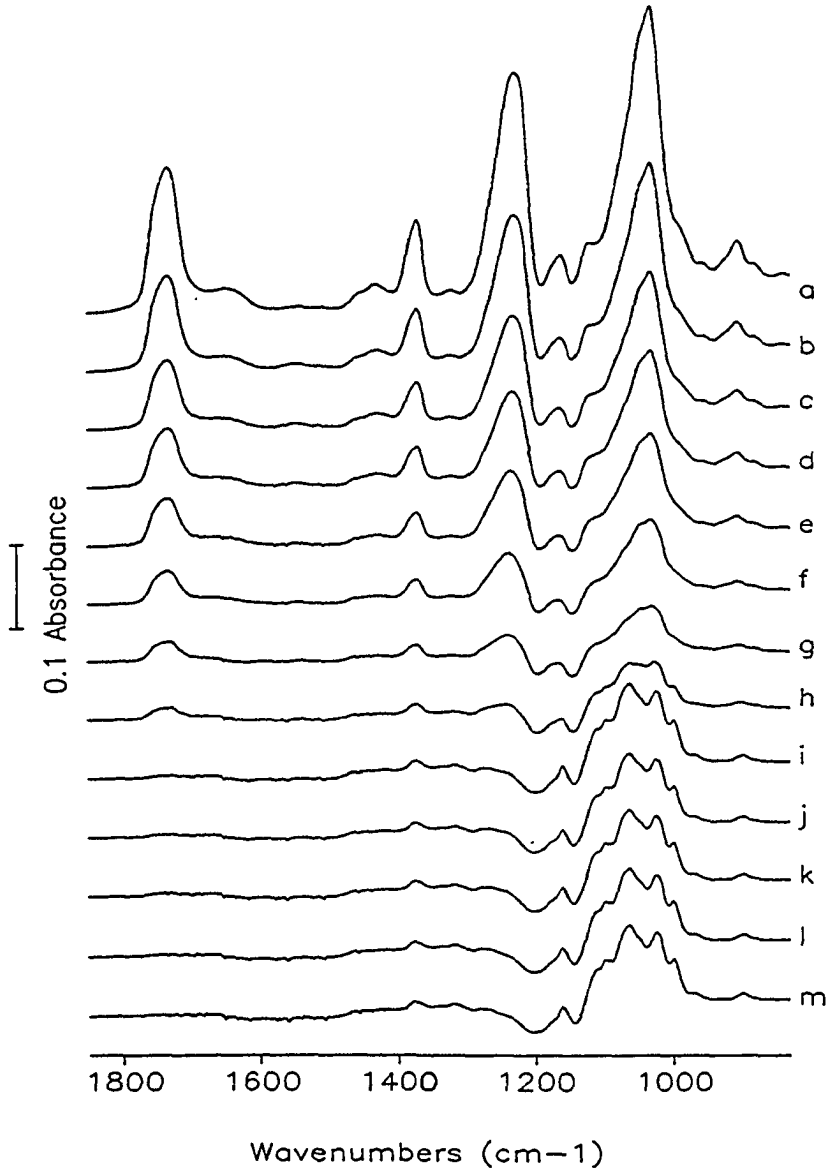

Figure 6. Infrared internal reflection spectra as a function of hydrolysis time: (a) 2 min; (b) 10 min; (c) 20 min; (d) 30 min; (e) 40 min; (f) 50 min; (g) 60 min; (h) 70 min; (i) 80 min; (j) 90 min; (k) 100 min; (l) 110 min; (m) 120 min

Kinetics of Hydrolysis

The base hydrolysis of an ester is a second-order reaction, the rate of which depends on both the concentration of ester and the concentration of base. Because the base was present in excess, and the flow cell was flushed with fresh solution between data collection, the kinetics of the reaction can be treated as pseudo first-order, i.e., the rate depends only on the concentration of acetyl groups in the cellulose acetate. In hydrolysis reactions at polymers, an initial "break-in" period is often observed before the hydrolysis reaction proceeds, during which solvent is incorporated into the material.[21] In our previous study by IR-ERS, a pseudo first-order plot showed two linear regions. The first linear region corresponded to the break-in period (the first 40 min of immersion), during which only small changes were observed in acetyl marker peak areas. The break-in period was followed by a second linear region corresponding to a tenfold increase in rate from 40 minutes of immersion to the completion of the hydrolysis reaction. This break-in period is attributed to the incorporation of solvent into the polymer.

IR-IRS Data

Similar features in the infrared spectra as a function of immersion time in basic solution are observed by IR-IRS as observed in our earlier studies of the hydrolysis of cellulose acetate using infrared external reflection spectroscopy (IR-ERS).[11,12] A number of significant differences are observed, however, which arise from the difference in the depth-

sensitivity of the two methods. IR-ERS does not have a significant depth-sensitivity because the magnitude of the electric field does not change significantly over the thickness of the film. In IR-IRS, however, the evanescent wave decays exponentially, as was shown in Figure 1. Because 99.8% of the intensity of the evanescent wave lies within the cellulose acetate film (i.e., the depth of penetration, 1.62 μm at 1000 cm^{-1}, is significantly less than the 5.1-μm film thickness), it can be treated as absorption at an infinitely thick layer where the resulting light absorption is proportional to the concentration. Therefore, many of the differences in the spectral data obtained by IR-ERS and IR-IRS can be attributed to either to changes in the film thickness, which result in an increase of the concentration of absorbing moieties in the evanescent wave, or to changes in the refractive index, which would result in changes in the depth of penetration of the evanescent wave. Changes in both thickness and refractive index are expected for cellulose acetate films as solvent is absorbed by the film. However, because the refractive index resulting from solvent incorporation would be between that of dry cellulose acetate (1.4) and water (1.33), such a change would cause less than an 8% reduction in absorbance. Changes in absorbance much greater than this suggest that changes in film thickness are occurring.

Figure 7 shows a pseudo first-order plot of the marker bands for the acetyl group as a function of hydrolysis time, as measured by IR-IRS. The abscissa is given as $\ln\{(A - A_\infty)/(A_0 - A_\infty)\}$, where A is the peak area at time t, A_0 is the initial peak area, and A_∞ is the peak area after reaction completion. Similar to the IR-ERS data from our previous study, the plot in

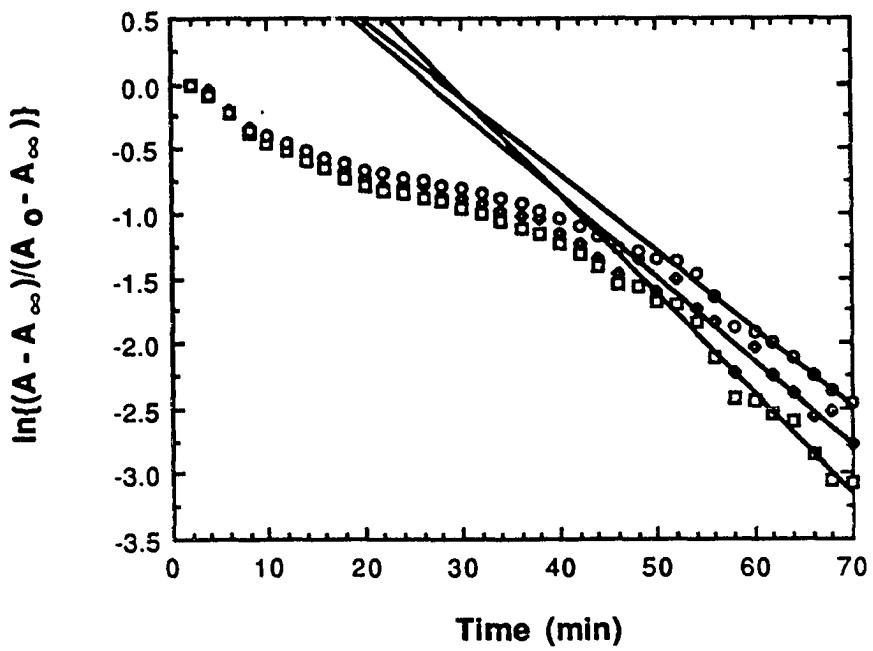

Figure 7. Pseudo-first-order kinetics plot of the acetyl marker bands between 0 and 70 min of hydrolysis: (•) ν(C=O), (▫) ν(C-O), and (o) $\delta(CH_3)$. The straight lines indicate a linear regression curve-fit of the points from 52 to 70 min

Figure 7 shows a linear region after 50 min of immersion, where the hydrolysis proceeds according to a pseudo first-order kinetics. The slope of the curves between 52 and 70 min, which are indicated by the straight lines in Figure 7, yielded a rate constant of 0.91 ± 0.11 M^{-2} min^{-2}. Unlike the IR-ERS data, considerable spectral change is observed during the "break-in" period by IR-IRS, as the absorbance of the acetyl marker bands decreases by 49% over the first 25 min of immersion. This change affects all bands in the spectrum equally, and is attributed to an expansion of the film by uptake of solvent by the film. Because the amount of light absorbed is proportional to the concentration of absorbers in the film, the observed decrease corresponds to an expansion by a factor of 195% to a thickness of 10.0 μm.

Near the completion of the hydrolysis reaction (after 70 min), additional changes are observed in the spectrum that suggest a collapse of the film. Figure 8 shows spectra of cellulose acetate at hydrolysis times between 60 and 84 min. During this time, the shape of the overlapping C-O bands in the 1200 to 1000 cm^{-1} region changes as the individual bands become better resolved, and the absorbance of the C-O stretching region increases by 57%. Concurrent with the intensity increase, the overlapping C-O bands sharpen, revealing at least 6 overlapping individual bands. The increase in absorbance of the C-O stretching region indicates a film thickness at 84 min that is only 64% of its thickness at 70 min. The collapse of the film as the hydrolysis approaches completion is most likely due to increasing attraction of neighboring cellulose chains via hydrogen bond interactions. As acetyl groups were replaced by hydroxyl groups, the free

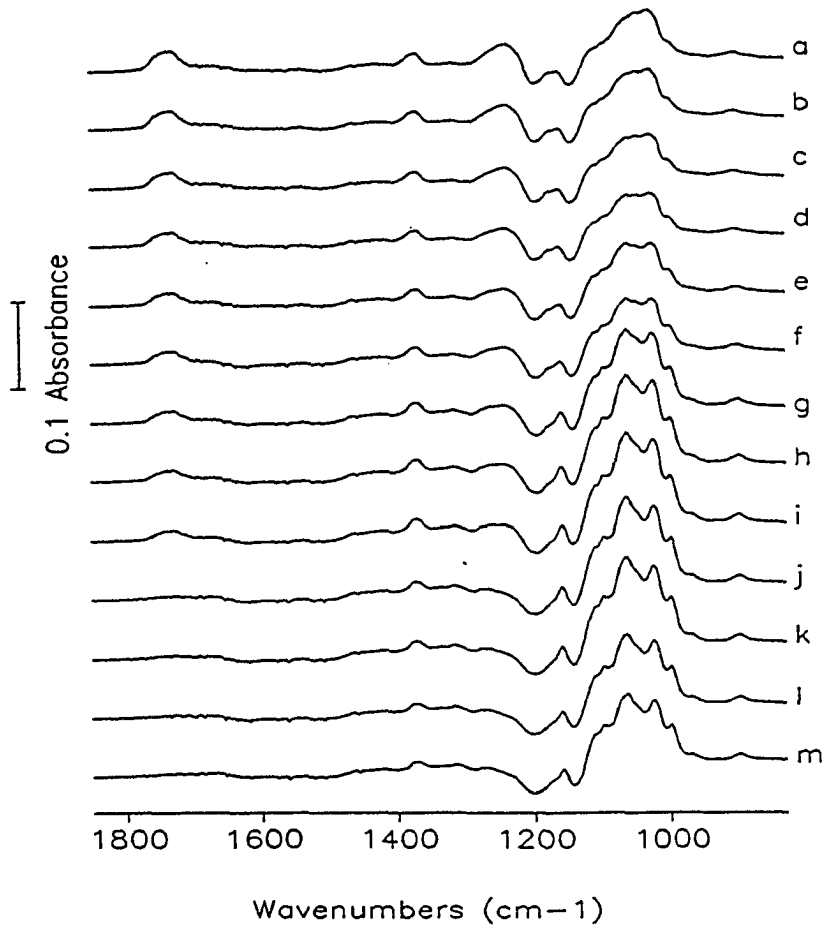

Figure 8. Infrared internal reflection spectra as a function of hydrolysis time: (a) 60 min; (b) 62 min; (c) 64 min; (d) 66 min; (e) 68 min; (f) 70 min; (g) 72 min; (h) 74 min; (i) 76 min; (j) 78 min; (k) 80 min; (l) 82 min; (m) 84 min

volume within the film increased, until at a point corresponding to 93% removal of the acetate, the film collapsed. If the film thickness prior to this collapse was 10.0 μm, the resulting film thickness at 84 min would be 6.4 μm, which is 25% greater than the thickness at the start of immersion.

CONCLUSIONS

The hydrolysis of a thin-film of cellulose acetate has been studied using infrared internal reflection spectroscopy (IR-IRS) at a cylindrical ZnSe internal reflection element. This method offers the possibility for *in-situ* spectroscopic measurements of the film as a function of hydrolysis time. The depth-sensitivity of the method allowed insight into the structural changes (i.e., thickness changes) which occurred in the film. The film expanded to 195% of its initial thickness during the break-in period over the first 40 min of hydrolysis. This expansion was attributed to the uptake of solvent into the film. Late in the hydrolysis reaction (at 93% completion), the film contracted. The net result of these thickness changes was a film thickness that was 25% greater than the thickness prior to immersion. The porosity of the film after complete hydrolysis increases both by the net expansion of the film, and by the replacement by hydroxyl groups of the relatively bulky acetyl groups.

ACKNOWLEDGEMENTS

MDP gratefully acknowledges the support of a Dow Corning Assistant Professorship. Ames Laboratory is operated for the U.S. Department of Energy by Iowa State University under Contract No. W-7405-Eng-82. This work was supported by the Office of Basic Energy Sciences.

REFERENCES

1. Lau, A.; Miller, L. *J. Am. Chem. Soc.* **1983**, *105*, 5271.
2. Sittampalam, G.; Wilson, G. *Anal. Chem.* **1983**, *55*, 1608.
3. Wang, J.; Hutchins, L. *Anal. Chem.* **1985**, *57*, 1536.
4. Ikeda, T.; Schmehl, R.; Denisevich, P.; Willman, K.; Murray, R. *J. Am. Chem. Soc.* **1982**, *104*, 2683.
5. Ohnuki, Y.; Matsuda, H.; Ohsoka, T.; Oyama, N. *J. Electroanal. Chem.* **1984**, *158*, 55.
6. Murray, R. in *Electroanalytical Chemistry*; Bard, A. J., Ed.; Dekker: New York, 1984; vol. 13.
7. Bowden, F.; Tabor, D. *The Friction and Lubrication of Solids*; Oxford Press: London, 1968.
8. Baier, R.; Meyer, A.; Natiella, J.; Natiella, R.; Carter, J. *J. Biomed. Mat. Res.* **1984**, *18*, 337.
9. Gristina, A. *Science* **1987**, *237*, 1588.
10. Jones, T. P.; Porter, M. D. *Anal. Chem.* **1988**, *60*, 404-406.
11. Stole, S. M.; Jones, T. P.; Chau, L.-K.; Porter, M. D. In *Chemical Sensors and Microinstrumentation*; Murray, R.; Dessy, R. E.; Heineman, W. R.; Janata, J.; Seitz, W. R.; Eds.; ACS Symposium Series 403; American Chemical Society: Washington, DC, 1989; chapter 19.
12. Stole, S. M.; Jones, T. P.; Porter, M. D. submitted to *Anal. Chim. Acta*
13. Harrick, N. J. *Internal Reflection Spectroscopy*; John Wiley & Sons, New York, 1967.

14. Mirabella, F. M., Jr. In *Internal Reflection Spectroscopy: Review and Supplement*, Harrick, N. J., Ed.; Harrick Scientific Corp., Ossining, New York, 1985.

15. Xu, J. R.; Balik, C. M. *Appl. Spectrosc.* **1988**, *42*, 1543.

16. Simhony, S.; Katzir, A.; Kosower, E. M. *Anal. Chem.* **1988**, *60*, 1908.

17. Compton, D. A. C.; Hill, S. L.; Wright, N. A.; Druy, M. A.; Piche, J.; Stevenson, W. A.; Vidrine, D. W. *Appl. Spectrosc.* **1988**, *42*, 972.

18. Harrick, N. J. *Internal Reflection Spectroscopy*; Harrick Scientific Corp.: Ossining, New York, 1979.; p. 30.

19. Atalla, R. in *Preservation of Paper and Textile of Historic and Artistic Value,* Williams, J., Ed.; ACS Symposium Series; American Chemical Society: Washington, DC, 1981.

20. Ward, K.; Seib, P. in *The Carbohydrates*, Pigman, W.; Horton, D.; Eds.; Academic Press: New York, 1970; vol. IIA.

21. Hawley, M. C.; Downey, K. W.; Selke, S. M.; Lamport, D. T. A. In *Cellulose: Structure, Modification, and Hydrolysis*; Young, R. A.; Rowell, R. M.; Eds.; John Wiley & Sons: New York, 1986; p 313.

SECTION III. OPTICAL pH SENSOR BASED ON THE CHEMICAL MODIFICATION OF A POROUS POLYMER FILM

OPTICAL pH SENSOR BASED ON THE CHEMICAL MODIFICATION OF A POROUS POLYMER FILM

Thomas P. Jones and Marc D. Porter

Department of Chemistry and Ames Laboratory–USDOE

Iowa State University

Ames, IA 50011

Published in *Anal. Chem.* **1988**, *60*, 404-406.

INTRODUCTION

Several studies have recently described the immobilization of colorimetric reagents at optical fibers as an effective approach to the construction of sensors for pH and metal ion determination.[1-7] To date, fabrication schemes have principally focused on binding chemically selective reagents at a variety of polymeric materials[1,2,8,9] and sintered glasses,[2,10] and on attaching polymeric dyes directly to the distal end of the fiber.[11,12] Although such sensors have proven useful for biomedical purposes[1,3] and have shown considerable promise for application to process control and environmental analyses,[13] their performance often suffers from (1) a slow response time as a result of barriers to mass transport at the polymeric support, (2) a limited dynamic range and low sensitivity due to a weak analytical signal, and (3) long-term instability as a result of the degradation of the immobilized reagent or its desorptive loss from the support.

As part of our interest in this area, we have been examining alternative design and fabrication schemes to enhance sensor performance. This has consisted, in part, of identifying and testing a variety of polymeric materials that could serve as *porous* support structures to minimize barriers to mass transport and, in part, of searching for colorimetric reagents that possess the requisite optical and chemical properties to improve both the sensitivity and the long-term stability of the response. As these studies progressed, it also became apparent that the reactivity of the immobilized reagent can differ dramatically from that of its analogous

solution form. Thus to aid the development of sensors with specific performance characteristics, it will become increasingly important to develop a detailed understanding of the fundamental chemical and physical interactions (intermolecular interactions between the reagent, support, solvent, and analyte), which can alter the reactivity of the immobilized reagent.

In this paper, the fabrication and preliminary evaluation of a pH sensor, which was constructed by immobilizing Congo Red (3,3′-[[1,1′-biphenyl]-4,4′-diylbis(azo)]bis[4-amino-1-naphthalenesulfonic acid]) at a base-hydrolyzed cellulose acetate film, are described. Advantageous features of this design include a rapid equilibration time (<1.3 s) and a large dynamic range (>4 pH units). The rapid response results from the *porous* structure of the hydrolyzed polymeric support, which minimizes barriers to mass transport between the analyte and immobilized indicator. The large dynamic range results both from the polyprotic acid-base reactivity of Congo Red and the high optical absorptivity of its various ionic forms. Additionally, the sensor is easily fabricated by immersing a hydrolyzed cellulose acetate film into a dye bath that contains Congo Red. The optical and chemical properties of the sensor as a function of pH were evaluated by conventional transmission spectroscopy; absorbance vs. time transients for rapid changes in solution pH were monitored in an optical-fiber transmission mode. Differences between the chemical reactivity of Congo Red in solution and after immobilization are also described.

EXPERIMENTAL

Sensor Construction

Cellulose acetate films (Polysciences, Inc., Warrington, PA) were cast onto microscope slides by spin-coating techniques. The films were prepared by flooding the surface with polymer solution and spinning at 1000 rpm. The cellulose acetate concentration was 10% (w/v) in cyclohexanone. Before coating, the edges of the slides were lightly etched with 600-grit abrasive paper to enhance adherence of the film. After drying, the films were hydrolyzed in 0.1 M KOH for 24 h. This step, as shown by recent electrochemical and scanning electron microscopy studies[14,15] and a structural characterization by infrared reflection spectroscopy,[16] converts the cellulose acetate film into a highly porous "cellulosic" material. Film thicknesses were measured prior to hydrolysis with an Alphastep surface profile (Tencor Instruments, Mountainview, CA). A knife edge was used to remove several portions of the film from the substrate with the resulting step used for the thickness measurement. The thicknesses are reported as the average of measurements for at least three different locations on the film; the uncertainty is reported as the range of these measurements.

Congo Red, obtained as its disodium salt (Aldrich, Milwaukee, WI), was immobilized at the porous polymeric film with a classical dye bath recipe.[17] This consisted of immersing a hydrolyzed film in an electrolytic dye bath for 10 min. The aqueous dye bath was composed of Congo Red (3.6×10^{-4} M), Na_2SO_4 (0.025% (w/v)), and K_2CO_3 (0.025% (w/v)). The temperature of the dye bath was held just below its boiling point. After removal from the

dye bath, excess reagent was washed from the substrate with deionized water. Prior to its use, Congo Red was recrystallized twice from an ethanol/water solution.[18]

Dyes such as Congo Red are known as direct dyes.[17,19,20] This terminology derives from the ability of these dyes to adsorb strongly to cellulose-based polymers simply by immersing the polymer into a hot dye solution with a high ionic strength. The factors that govern the formation and absorption strength of such dyes are a complex mixture of chemical, physical, and structural effects. For Congo Red, it is apparent the chemical interactions of both its amine and azo groups with the hydroxyl groups of the cellulosic support play an important role in the formation of the immobilized structure.[21] The relative importance of the molecular planarity (flatness) and solubility, both of which have been found to contribute at differing degrees to the binding strength of such dyes, remains the subject of extensive controversy.[20,22]

Flow Cell

An operational diagram of the flow cell for the sensor in a fiber-optic transmission configuration is shown in Figure 1. The incoming light entered the solution cavity, which was defined by the front window, the sensor, and the thickness of a silicone rubber gasket, through an array of quartz optical fibers (200 μm diameter, Ensign-Bickford Optics Co., Avon, CT). The beam then passed thorough the thin-film sensor and was collected and transmitted to a monochromator by a second array of fibers. The arrays, which consisted of five fibers arranged in a vertical orientation, were

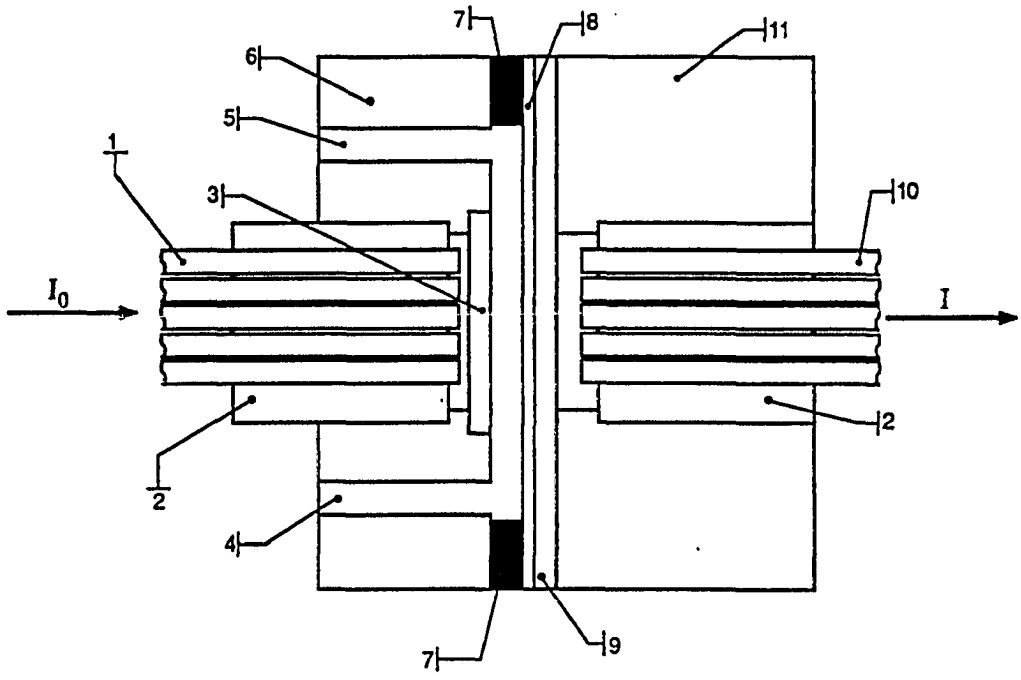

Figure 1. Schematic diagram of the flow cell for the thin film sensor: (1) input optical-fiber bundle, (2) fiber mounting cylinders, (3) front window, (4) solution inlet channel, (5) solution outlet channel, (6) front plate, (7) slotted gasket, (8) thin-film pH sensor, (9) glass plate for film support, (10) light collection optical-fiber bundle, (11) back plate

sealed into slotted Plexiglas® cylinders and mounted to the cell with setscrews. A xenon arc lamp (Oriel Corp., Stamford, CT) was used as a light source; the transmitted radiation was dispersed with a 0.22-m grating monochromator and monitored with a digital photometer (Spex DPC-2, Spex Ind., Edison, NJ), which was operated in analog mode. The front and back plates of the cell were machined from Plexiglas® to respective thicknesses of 1.2 and 2.0 cm. The window was sealed into place with silicone rubber cement. The solution inlet and exit channels were drilled to a diameter of 0.2 cm and connected to Teflon tubing with flanged fittings. The cell was sealed with a 0.15-cm-thick silicone rubber gasket of which an inner portion was removed to define the solution channel. The solution flow rate, maintained with a gravity feed system, was 0.98 m:/s. Solutions were changed with a low-dead-volume multiport injection valve. The time required to affect a complete change (99.9%) of the solution in the cell, measured by injecting a dilute Congo Red solution, was 1.22 ± 0.18 s (standard deviation, n = 17); it required 0.31 ± 0.06 s to change 63% of the solution. The absorbance vs. time response of the sensor to changes in solution pH was measured in a fiber-optic transmission mode by alternate injections of solutions with different pH values. The optical properties of the sensor were characterized as a function of pH in a conventional transmission mode with a DMS-200 UV-vis spectrometer (Varian Instrument Co., Palo Alto, CA). To accommodate these latter measurements, the cell, after removal of the arrays of optical fibers, was mounted on a base-plate accessory in the spectrometer sample chamber.

The pH of the solutions was measured with a 140A Accumet pH meter (Fisher Scientific, Pittsburgh, PA).

Reagents

The pH of the solutions was controlled by varying the amounts of HCl or NaOH or by citrate and phosphate buffers (McIlvaine buffers). All solutions were prepared with deionized water.

RESULTS AND DISCUSSION

Optical Properties of the Sensor vs. pH

The optical properties of Congo Red in solution and immobilized at a hydrolyzed cellulose acetate film are shown as a function of pH in parts a and b of Figure 2, respectively. The thickness of the cellulose acetate film prior to hydrolysis was 2.9 ± 0.1 μm. It is evident that the immobilized and solution forms of the dye exhibit marked differences both in their optical properties and their acid-base reactivities. The spectra in Figure 2a indicate that the solution form of Congo Red behaves as a polyprotic acid, undergoing a succession of protonation steps below a pH of 6.0. This results in the observed differences in the solution absorption spectra where, for example, the dye has an absorption maximum of 485 nm at a pH of 6.0 and of 572 nm at a pH of 1.5. These spectra, together with preliminary potentiometric and spectrophotometric data, indicate that there are at least two and possibly as many as four[23] acid-base equilibria in this pH range. A more detailed characterization of the acid-base reactivities and optical properties of the solution form of Congo Red was hindered by its aggregation below a pH of 3. Thus, those spectra in Figure 2a below a pH of 3 should be considered only as a qualitative representation of optical properties of Congo Red.

The optical response of a Congo Red pH sensor is shown in Figure 2b. Theses spectra indicate that this sensor exhibits a dynamic range of more than 4 pH units. Furthermore, the absorbance of the solution form of the dye at 485 nm decreases by 44% when the pH decreases from 5.5 to 4.0, whereas that of immobilized dye at 511 nm decreases by less than 2%. Thus the acid

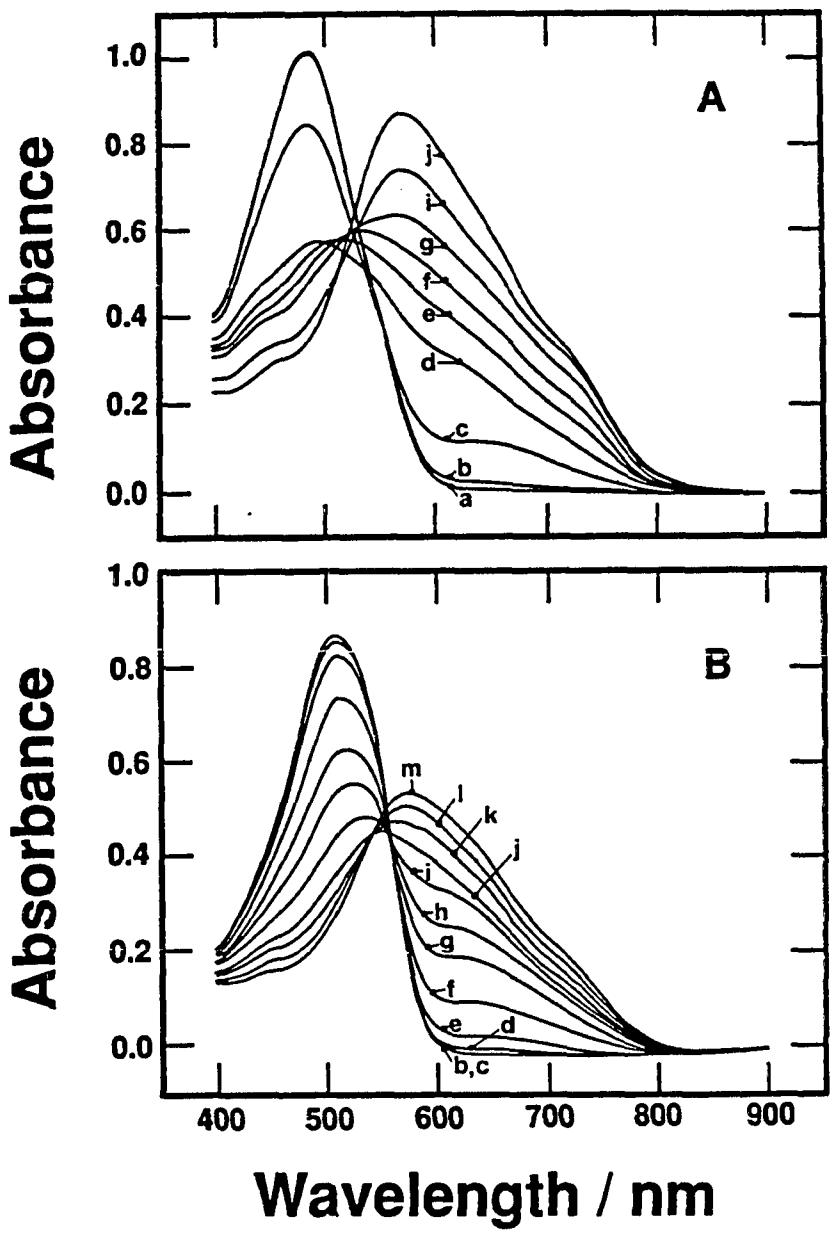

Figure 2. Absorption spectra for Congo Red in solution (A) and immobilized at hydrolyzed cellulose acetate (B) at several pH values: (a) 6.0, (b) 5.5, (c) 5.0, (d) 4.5, (e) 4.0, (f) 3.5, (g) 3.0, (h) 2.5, (i) 2.0, (j) 1.5, (k) 1.0, (l) 0.5, (m) 0.0. Thickness of cellulose acetate film prior to hydrolysis was 2.9 ± 0.1 μm. A spectrum for Congo Red in solution could not be obtained at a pH of 2.5 as a result of excessive dye aggregation

strength of the immobilized dye is almost an order of magnitude greater than that of its solution analog. Such changes in reactivity, although not yet understood at a molecular level, have been observed for a variety of absorbed phthalein indicators,[24] for a monomolecular layer of an aniline azo dye,[25] and for other direct azo dyes.[16] More importantly, however, these results clearly demonstrate the feasibility of constructing optical pH sensors that are based on immobilizing direct dyes such as Congo Red at a porous cellulose acetate film.

It is also important to note that the absorption spectra of the immobilized dye are red-shifted in comparison to those of its solution form, having maxima at 511 and 577 nm at respective pH values of 5.5 and 0.0. This suggests that the structural conformation of the immobilized dye is more planar than that of its solution analogue.[26]

Response Time

The optical response of the sensor to a rapid change in pH is shown in Figure 3. The wavelength for these measurements was 620 nm with the flow cell and sensor operating in a fiber-optic transmission configuration. The pH of the solution was changed from 10.9 to 2.0. Upon injection of pH 2.0 solution, the optical intensity decreases rapidly, corresponding to an increase in the concentration of the acidic form(s) of the immobilized indicator. Equilibration (99.9% completion) is achieved in less than 1.5 s. The average equilibration time for five successive injections was 1.26 ± 0.31 s; the response reaches 63% (1 - 1/e) of its maximum absorbance value in 0.32 ± 0.03 s. This corresponds to a response that is 10 times more rapid

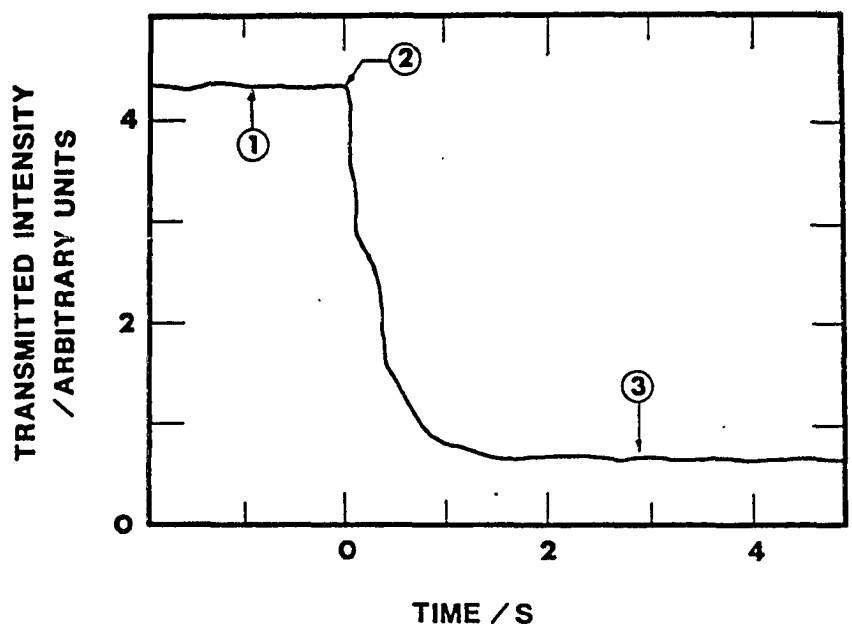

Figure 3. Response time of the pH sensor constructed by the immobilization of Congo Red at hydrolyzed cellulose acetate: (1) equilibrated response at pH 10.9 solution; (2) injection of a pH 2.0 solution; (3) equilibrated response at a pH of 2.0

than those of other thin-film pH sensor.[1,8,12] Furthermore, a comparison to the time required to change the solution in the cell (see Experimental) indicates that the measured response represents an upper limit of the switching time for this sensor.

Response Stability

The stability of the sensor response was examined by repetitively injecting acidic (pH 2) and basic (pH 10.9) solutions into the cell and monitoring the optical response. After an initial "break-in" period (for a dry film), which usually required two to three injections, the absorbance at 577 and 511 nm varied by less than 2%. The break-in period appeared to result from the slow incorporation of solvent into a dry, hydrophobic film. As solvent enters the polymeric matrix, the film expands, providing a more consistent exposure of the immobilized dye to the analyte. An additional test of the response stability, based on monitoring the absorbance at 577 nm (pH 6.0), showed a change of less than 3% over a 6-h period. The hydrolyzed support was stable from pH values of 13-0. Below a pH of zero, the film degraded as a result of extensive cleavage of the glucosidic ether linkages.[16]

Metal-Ion Interference

The interference of metal ion complexation with the optical response of the sensor was examined by using Hg^{2+} as the test ion. In its solution form, Congo Red selectively chelates with Hg^{2+} at a pH greater than 5.5[27] to form a complex which has an absorption maximum at 543 nm. However, when Congo Red is immobilized at a hydrolyzed cellulose acetate film, the

absorption spectra with and without Hg^{2+} ($[Hg^{2+}] = 1.0 \times 10^{-3}$ M) present in solution are indistinguishable. This demonstrates that the sensor is free from interference due to complexation with Hg^{2+}. Furthermore, this indicates that the interactions responsible for the immobilization prohibit the amine and/or azo groups of Congo Red from participating in the formation of a Hg^{2+} complex.[28] Thus, it seems likely that the sensor will be free from other metal ion interferences. This result, combined the the response of the sensor at low pH, suggests its application to the analysis of solutions with high mineral ion content, such as acid rain and coal acid mine drainage. Studies are in progress that will extend the selectivity characterization.

CONCLUSIONS

The rapid response time, large dynamic range, and ease of fabrication make this pH sensor an attractive addition to existing sensors. More importantly this study demonstrates the general utility of immobilizing direct dyes at porous cellulose acetate films for engineering sensors with new and/or improved performance characteristics. Efforts to extend this approach to constructing optical sensors with a broader pH range and faster response are in progress. Studies to explore the fundamental interactions that govern the formation, structure, reactivity, and stability of such sensors are also underway.

ACKNOWLEDGMENT

Discussions with S. M. Stole and L. K. Chau are acknowledged.

Registry No. Congo Red, 573-58-0; cellulose acetate 9004-35-7.

REFERENCES

1. Peterson, J. I.; Goldstein, S. R.; Fitzgerald, R. V.; Buckhold, D. K. *Anal. Chem.* **1980**, *52*, 864-869.
2. Saari, L. A.; Seitz, W. R. *Anal. Chem.* **1982**, *54*, 823-824.
3. Peterson, J. I.; Vurek, G. G. *Science* **1984**, *224*, 123-127.
4. Seitz, W. R. *Anal. Chem.* **1984**, *56*, 16A-34A.
5. Hirschfeld, T. *Fresenius' Z. Anal. Chem.* **1986**, *324*, 618-624.
6. Zemal, J. N.; Van der Spiegel, J; Fare, T. ; Young, J. In *Fundamentals and Applications of Chemical Sensors*; Schuetzle, D., Jammerle, R., Butler, J. W., Eds.; ACS Symposium Series 309; American Chemical Society: Washington, DC, 1986; Chapter 1.
7. Angel, S. M. *Spectroscopy (Springfield, Oreg.)* **1987**, *2*, 38-48.
8. Zhujun, Z.; Seitz, W. R. *Anal. Chim. Acta* **1985**, *171*, 47-55.
9. Kirkbright, G. F.; Narayanaswamy, R.; Welti, N. A. *Analyst (London)* **1984**, *109*, 1025-1028.
10. Offenbacher, H.; Wolfbeis, O. S.; Fürlinger, E. *Sens. Actuators* **1986**, *9*, 73-84.
11. Munkholm, C; Walt, D. R.; Milanovich, F. P.; Klainer, S. M. *Anal. Chem.* **1986**, *58*, 1427-1430.
12. Jordan, D. M.; Walt, D. R.; Milanovich, F. P. *Anal. Chem.* **1987**, *59*, 437-439.
13. Callis, J. B.; Illman, D. L.; Kowalski, B. R. *Anal. Chem.* **1987**, *59*, 624A-637A.
14. Wang, J.; Hutchins, L. D. *Anal. Chem.* **1985**, *57*, 1536-1541.

15. Wang, J; Hutchins-Kumar, L. D. *Anal. Chem.* **1986**, *58*, 402-407.

16. Stole, S. M.; Jones, T. P.; Chau, L. K.; Porter, M. D. In *Chemical Sensors and Microinstrumentation*; Murray, R. W.; Dessy, R. E.; Heineman, W. R.; Janata, J.; Seitz, W. R.; Eds.; ACS Symposium Series 403; American Chemical Society: Washington, DC, 1989; chapter 19.

17. Fieser, L. F.; Williamson, K. L. *Organic Experiments*, 5th ed.; D. C. Heath: Lexington, MA, 1983.

18. Gore, T. S.; Unni, M. K.; Venkataraman, K. *J. Sci. Ind. Res.* **1956**, *15B*, 618-626.

19. Noller, C. R. *Textbook of Organic Chemistry*, 3rd ed.; W. B. Saunders: Philadelphia, PA, 1966.

20. Rattee, I. D.; Breuer, M. M. *The Physical Chemistry of Dye Adsorption*; Academic: New York, 1974.

21. Boss, R. A. *TAPPI* **1959**, *42*, 185A-190A.

22. *Cellulose Chemistry and Technology*; Arthur, J. C., Ed.; ACS Symposium Series 48; American Chemical Society; Washington, DC, 1977.

23. Muramatsu, M. *Bull. Chem. Soc. Jpn.* **1958**, *31*, 864-871.

24. Kirkbright, G. F.; Narayanaswamy, R.; Welti, N. *Analyst (London)* **1984**, *109*, 15-17.

25. Mimms, L. T.; McKnight, M. A.; Murray, R. W. *Anal. Chim. Acta* **1977**, *89*, 355-361.

26. Brode, W. R. In *The Rodger Adams Symposium*; Volwiler, E. H., Ed.; Wiley: New York, 1955, Chapter 1.

27. Tandon, K. N. *Talanta* **1966**, *13*, 161-163.

28. Pribil, R. *Applied Complexometry*; Pergamon: New York, 1982.

SECTION IV. AN OPTICAL SENSOR BASED ON INFRARED SPECTROSCOPY

AN OPTICAL SENSOR BASED ON INFRARED SPECTROSCOPY

Thomas P. Jones and Marc D. Porter

Department of Chemistry and Ames Laboratory–USDOE

Iowa State University

Ames, IA 50011

Published in *Appl. Spectrosc.* **1989**, *43*, 908-911.

INTRODUCTION

The development and application of chemical sensors based on the immobilization of thin films of colorimetric indicators at optical fibers and other waveguide materials have become increasingly active areas of research.[1-15] These types of sampling devices have proven useful for biomedical purposes[1,3] and have shown considerable promise for application to process control and for environmental analyses.[13] To date, the response of these sensors has been monitored primarily with fluorescence and UV-visible absorbance and reflectance techniques. This circumstance is a result of the widespread availability of optical fiber materials with a high transmissivity in these spectral regions. However, these techniques provide little structural information and are not inherently selective, relegating to a large degree the specificity of an analysis to the selective reactivity of the immobilized colorimetric indicator.

Recently, sensors based on Raman and infrared spectroscopies have been described.[16-21] These efforts have focused on combining the advantages of fiber-optic sampling with the structural information that is inherent with vibrational spectroscopies. Raman spectroscopy has been used in its resonance enhanced mode for solution sampling[16,17] and in its surface-enhanced mode for the detection of organic components adsorbed from aqueous solutions at pretreated silver,[18] copper, and gold[19] surfaces. In the resonance-enhanced mode, a portion of an optical fiber bundle transports the excitation beam from a laser source to the sample; the remaining fibers collect the scattered radiation and transmitted it to the input optics of a

monochromator. The potential utility of such a sampling arrangement in a surface enhanced mode has been discussed.[19] With IR sensors, the evanescent wave from IR-transmitting fibers has been used to detect adsorbed films containing organic moieties after solvent evaporation[20] and to monitor the progress of a composite curing reaction.[21] The development of IR sensors stems in part from breakthroughs in the fabrication of waveguide materials with a useful IR transmissivity. To date, however, the potential utility of vibrational spectroscopies for the selective detection of the response of a thin film sensor remains to be addressed.

As part of our interest in this area,[14,15] we have been examining the effects of immobilization chemistry and other intermolecular interactions on the response characteristics of thin film sensors. As a result of these interactions, a sensor may display response characteristics that are markedly different from that of the solution analog of the bound indicator. For instance, Congo Red (3,3'-[[1,1'-biphenyl]-4,4'-diylbis(azo)bis[4-amino-1-naphthalenesulfonic acid]], disodium salt) immobilized at a porous cellulosic film exhibits an acid strength that is nearly an order of magnitude greater than its solution form. Other sensors display even more dramatic changes in reactivity, as we have recently summarized.[15] One approach to probe these interactions is to utilize the molecular specificity and sampling capabilities of infrared internal reflection spectroscopy (IRS). This technique provides a facile means to detect subtle changes in the composition and structure of thin films in the presence of strongly absorbing solvents,[22,23] as well as monitoring the diffusion of small organic

molecules into such materials.[24] During such a characterization of a Congo Red pH sensor, we realized the potential utility of IRS as a probe for detecting the response of a thin film sensor. In this communication, we describe the construction and performance characteristics of a thin film pH sensor based on infrared spectroscopy and briefly discuss the potential utility of such detection schemes.

EXPERIMENTAL

Sensor Construction

The sensor was fabricated by the immobilization of Congo Red at a base hydrolyzed film of cellulose acetate which had been previously coated on a ZnSe internal reflection element (IRE) of a CIRCLE® cell (Spectra Tech, Inc., Stamford CT). A film of cellulose acetate (Aldrich, Inc., Milwaukee, WI) was coated onto the IRE by the slow evaporation of a polymer solution (2.5% w/v cellulose acetate in cyclohexanone). The optical element was positioned horizontally in a chuck attached to an electric motor, and was rotated at 300 rpm to ensure a uniform film thickness. After drying for 24 h, the thickness of the resulting film was 5.1 μm, as estimated by the mass difference of the IRE before and after film deposition. The polymer-modified IRE was then mounted in the cell, and hydrolyzed in 0.07 M NaOH. The progression of hydrolysis as a function of time was monitored by the decrease in the absorbance of the ν(C=O) for the acetate functional group of the polymer. These data indicated that the hydrolytic removal of the acetyl group was complete after 4 h. As has been previously shown, the base-hydrolysis of cellulose acetate imparts a porous microstructure to the film that selectively excludes the permeation of high-molecular-weight organic compounds and other macromolecular materials.[15,25,26] The construction of the pH sensor was completed by the immobilization of Congo Red at the porous cellulosic film by a conventional dye recipe.[27] Although the subject of extensive controversy, immobilization is achieved primarily by

chemical interactions between the amine groups of Congo Red and the hydroxyl groups of the cellulose support.[28]

A schematic diagram of the sensor and flow cell is shown in Figure 1. A pair of mirrors in a "Cassegrain-like" arrangement directs the IR beam onto the IRE at an average angle of incidence of 45°. A similar pair of mirrors collects and redirects the beam to an IR detector after propagation through the IRE. Teflon® O-rings were used to mount the IRE in the flow cell. The O-rings restrict solution contact to a 6.0-cm segment of the thin film sensor. With this arrangement, the light undergoes ~10-11 reflections as it passes through the IRE.

IR Spectroscopy

Spectra were collected with a Nicolet 740 Fourier transform infrared spectrometer (Madison, WI). Each spectrum represents the ratio of 1024 sample and 1024 reference scans, and required 9.5 min for collection of one sample/reference data set. Interferograms were coadded at 4 cm^{-1} resolution with Happ-Genzel apodization. The optical signal was monitored with a liquid-N_2 cooled narrow-band MCT detector. The spectrometer was purged with liquid N_2 boil-off to minimize absorption by water vapor and CO_2.

Reagents

The pH of the solutions was controlled by varying the concentration of HCl. The ionic strength of these solutions was maintained at 0.1 M with

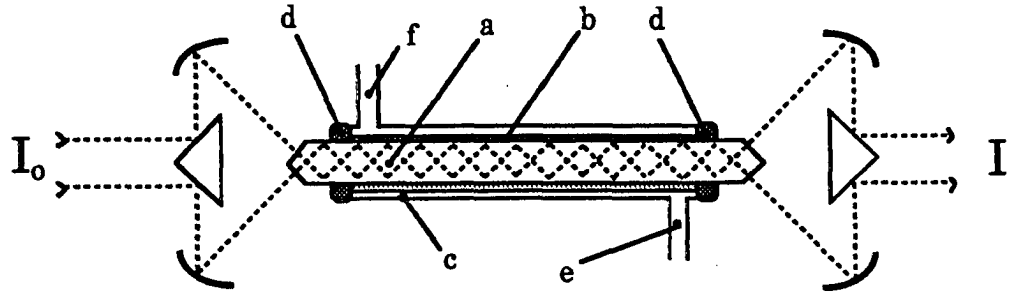

Figure 1. Thin film sensor and CIRCLE® cell: (a) ZnSe internal reflection element; (b) thin film sensor; (c) flow cell; (d) Teflon® O-rings; (e) solution inlet; and (f) solution outlet. The dashed lines represent the light path through the cell

KCl. All solutions were prepared with deionized water (Millipore Corp., Bedford, MA).

RESULTS AND DISCUSSION

Band Assignments

Infrared internal reflection spectra for Congo Red immobilized at a base-hydrolyzed cellulose acetate film are shown at pH values of 5.5 and 0.0 in Figures 2a and 2b, respectively. These spectra are given as $-\log(R_2/R_1)$, where R_2 is the single-beam spectrum for the thin film sensor and R_1 is that for the hydrolyzed film prior to the immobilization of Congo Red. This method of data presentation aided the assignments of vibrational modes by compensating for small changes in the band shapes of the aqueous solvent as a function of pH. Such changes are observed as a consequence of the porous microstructure of the polymer film, even though the penetration depth for the evanescent wave is only ~1.4 μm as estimated with Harrick's Equation. As previously determined with visible spectroscopy,[15] the immobilized form of Congo Red has pK_a values of 0.8 and 2.8. Thus, the spectrum in Figure 2a represents the fully deprotonated form of the indicator. In contrast, the spectrum in Figure 2b is attributed to an extensively (although not completely) protonated form of the indicator. The cellulosic support degrades below a pH of zero as a result of the extensive cleavage of the glucosidic ether linkages.

Several of the features in Figure 2 are relatively unaffected by the protonation/deprotonation process. Those features between ~1600-1470 cm^{-1} are assigned to C=C stretches of the naphthyl and biphenyl rings of Congo Red. The features at 1045 and 1186 cm^{-1} are attributed respectively to the

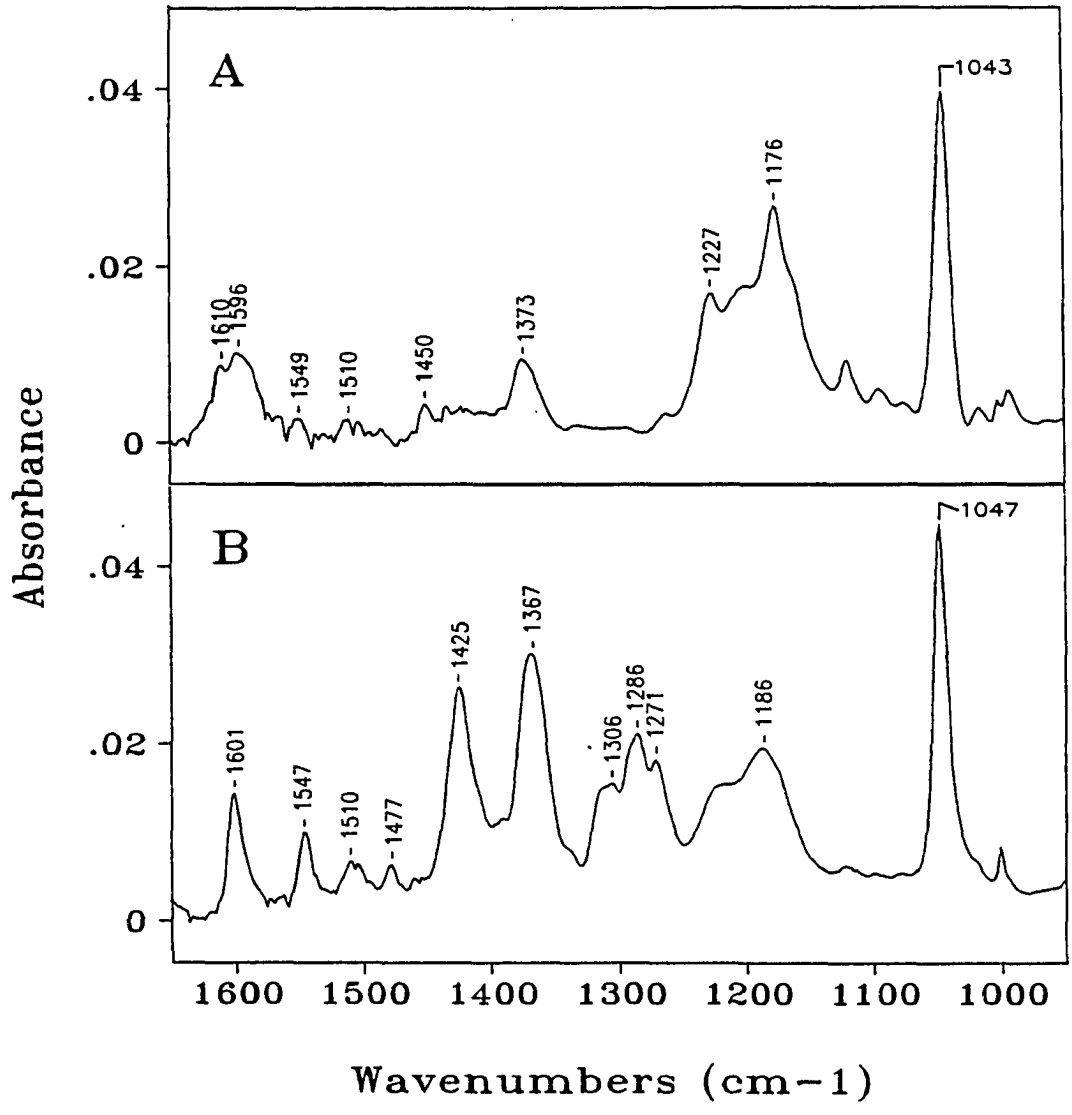

Figure 2. Infrared internal reflection spectra for Congo Red immobilized at a base-hydrolyzed cellulose acetate film: (A) pH value of 5.5; (B) pH value of 0.0

symmetric and asymmetric stretches of the naphthyl sulfonate groups. The latter mode overlaps with an unassigned band at 1176 cm^{-1} that exhibits a pH dependence.

A number of bands in the spectra in Figure 2 display a marked pH dependence. The feature at 1547 cm^{-1} is assigned to N-H bending of a protonated azo group.[29] The absorbance of this feature increases with decreasing pH, consistent with this assignment. Other features that exhibit a strong pH dependence are found at 1425 and 1367 cm^{-1}, and are tentatively assigned to C=N stretches.

The N=N stretch of asymmetrically substituted azo moieties is usually found near 1450 cm^{-1}.[30] These modes typically have a low dipole transition moment, and are therefore difficult to observe with infrared spectroscopy. In Figure 2a, the feature at 1450 cm^{-1} undergoes a decrease in absorbance with a decrease in pH. This mode is assigned to the N=N stretch of an unprotonated azo group. The remaining vibrational modes in these spectra are as yet unidentified.

Performance of an IR Thin Film Sensor

The utility of IRS for detecting the compositional changes in a thin film sensor is demonstrated in Figure 3. This Figure shows the change in the IR spectra for Congo Red immobilized at a porous cellulosic film at intervals of 0.5 pH units between a pH of 4.0 and 0.5. These spectra are given as $-\log(R_i/R_{5.5})$, where R_i is the single-beam spectrum of the thin film sensor at a given pH, and $R_{5.5}$ is the single-beam spectrum of the thin film sensor at pH 5.5. Each spectrum was then subjected to a second-order

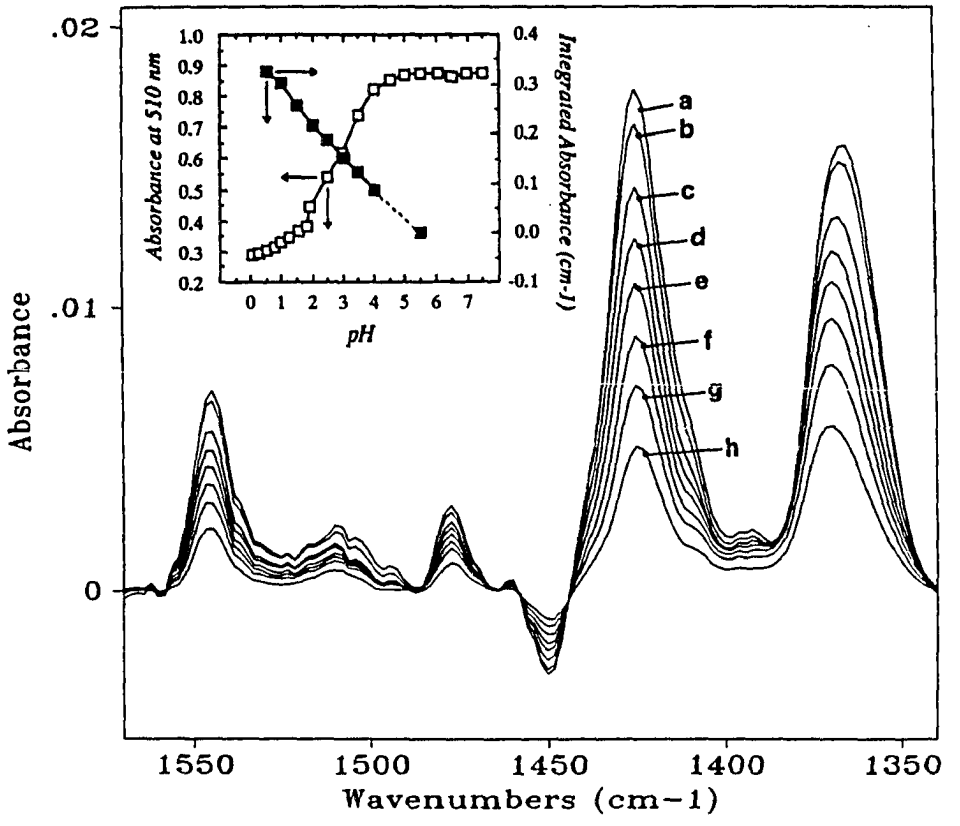

Figure 3. Infrared sensor response between a pH of 0.5 and 4.0: (a) 0.5; (b) 1.0; (c) 1.5; (d) 2.0; (e) 2.5; (f) 3.0; (g) 3.5; (h) 4.0. Each spectrum is relative to that at pH 5.5 (see text for details). Inset: (■) Integrated absorbance of ν(C=N) at 1425 cm^{-1} as a function of pH; (□) absorbance at 510 nm as a function of pH from previously published data. Connecting lines are only a guide to the eye

polynomial base-line linearization (based on the selection of only three data points) to compensate for changes in the solution spectrum as a function of pH. Consistent with the observations in Figure 2, the absorbance of each of the bands in Figure 3 undergoes a continuous change between a pH of 4.0 and a pH of 0.5. Those bands attributed to the N-H bending mode and C=N stretches exhibit an increase in absorbance as pH decreases. In contrast, the absorbance of the N=N stretch decreases as pH decreases.

The inset in Figure 3 shows plots of the integrated absorbance of the ν(C=N) at 1425 cm^{-1} and the absorbance at 510 nm as a function of pH. The latter represents the absorbance of the fully protonated form of immobilized Congo Red, as previously reported.[14] In both cases, the optical response changes rapidly below a pH of 4.0, approaching a constant value near a pH of zero. The changes in the feature at 1425 cm^{-1}, although not yet fully understood in terms of the structure of the immobilized indicator, indicate the continuous protonation/deprotonation of the azo group over this pH range. Such a process is consistent with the small difference between the two pK_a values of immobilized Congo Red. More importantly, the agreement of the trends observed with the two different spectroscopies confirms the feasibility of detecting the response of thin film sensors with IR spectroscopy.

CONCLUSIONS

The feasibility of using infrared spectroscopy for detecting the response of a thin film sensor has been demonstrated. These measurements were made by coating a pH-sensitive polymer film onto a ZnSe internal reflection element. Such an approach offers a variety of new opportunities to construct sensors with specific performance characteristics by extending the selection of immobilized reagents from those that contain a chromophore to those with an infrared-active vibration. However, as is usually the case for spectrochemical analyses, the selection of the optical mode for the detection of the response of a thin film sensor will be strongly dependent on the application. Currently, the detection of a sensor response with UV-visible spectroscopic methods offers several advantages, including high sensitivity and short data-collection times. In fact, rugged instrumentation based on such approaches, especially for pH, metal ion, and selected bioanalytical applications, is emerging rapidly. On the other hand, vibrational spectroscopies offer possibilities of extending the applicability of thin film sensors. Examples include multielement metal-ion determinations and clinical assays of biocomponents. An example of the former might entail on-line monitoring of the alkaline earth metals Ca(II), Mg(II), and Sr(II). These metals would readily complex at a porous polymer film which was functionalized with a carboxylic acid.[31] In this mode, the carboxylate groups would serve as a cation exchange site for the metal ions. Peak positions, which are separated from each other by ~20 cm^{-1},[32] and integrated

areas for each of these complexes should then provide a means for both identification and quantitation.

Thin film sensors based on infrared spectroscopy may also find applicability in clinical laboratories. For example, a sensor for urea could be constructed by the co-immobilization of urease and an acid-base indicator with a physiological pH response at a base-hydrolyzed cellulose acetate film.[33] The change in pH resulting from the ammonium ion generated by the reaction between urea and the immobilized urease would be monitored with a marker band in the infrared spectrum of the immobilized acid-base indicator. As a result of the molecular specificity of infrared spectroscopy, in conjunction with the exclusion of high-molecular-weight and macromolecular materials by the cellulosic support, such sensors may lead to the development of assays that require little or no sample preparation. Opportunities to develop assays for the direct detection and quantification of biocomponents may also be feasible.

Others issues pertaining to the development of sensors based on infrared spectroscopic detection schemes require further consideration. Efforts to improve data-collection times, to evaluate sensitivity limitations, and to construct rugged IR instrumentation need to be addressed.[34] Opportunities for remote sensing will benefit from the development of materials for the construction of optical fibers with a high transmittance in the infrared spectral region, an area of extensive research activity. The preliminary results reported here will be followed by a more extensive examination of coupling infrared spectroscopy with thin film sensors.

ACKNOWLEDGEMENTS

MDP gratefully acknowledges the support of a Dow Corning Assistant Professorship. Discussions of band assignments with Lai-Kwan Chau, and of possible clinical assays with Jackie Larew and Larry Larew are acknowledged. Ames Laboratory is operated for the U.S. Department of Energy by Iowa State University under Contract No. W-7405-Eng-82. This work was supported by the Office of Basic Energy Sciences.

REFERENCES

1. Peterson, J. I.; Goldstein, S. R.; Fitzgerald, R. V.; Buckhold, D. K. *Anal. Chem.* **1980**, *52*, 864.
2. Saari, L. A.; Seitz, W. R.; *Anal. Chem.* **1982**, *54*, 823.
3. Peterson, J. I.; Vurek, G. G. *Science (Washington, D.C.)* **1984**, *224*, 123.
4. Seitz, W. R. *Anal. Chem.* **1984**, *56*, 16A.
5. Hirschfeld, T. ; *Fresenius' Z. Anal. Chem.* **1986**, *324*, 618.
6. Zemal, J. N.; Van der Spiegel, J.; Fare, T.; Young, J. In *Fundamentals and Applications of Chemical Sensors*, D. Schuetzle, R. Jammerle, J. W. Butler, Eds. (ACS Symposium Series 309, American Chemical Society, Washington, D.C., 1986) Chap. 1.
7. Angel, S. M.; *Spectroscopy* **1987**, *2*, 38.
8. Zhujun, Z.; Seitz, W. R. *Anal. Chim. Acta* **1985**, *171*, 47.
9. Kirkbright, G. F.; Narayanaswamy, R.; Welti, N. A. *Analyst (London)* **1984**, *109*, 1025.
10. Offenbacher, H.; Wolfbeis, O. S.; Fürlinger, E. *Sensors and Actuators* **1986**, *9*, 73.
11. Munkholm, C.; Walt, D. R.; Milanovich, F. P.; Klainer, S. M. *Anal. Chem.* **1986**, *58*, 1427.
12. Jordan, D. M.; Walt, D. R.; Milanovich, F. P. *Anal. Chem.* **1987**, *59*, 437.
13. Callis, J. B.; Illman, D. L.; Kowalski, B. R. *Anal. Chem.* **1987**, *59*, 624A.
14. Jones, T. P.; Porter, M. D. *Anal. Chem.* **1988**, *60*, 404.

15. Stole, S. M.; Jones, T. P.; Chau, L. K.; Porter, M. D. In *Chemical Sensors and Microinstrumentation*; Murray, R. W.; Dessy, R. E.; Heineman, W. R.; Janata, J.; Seitz, W. R.; Eds.; ACS Symposium Series 403; American Chemical Society: Washington, DC, 1989; chapter 19.

16. Schwab, S. D.; McCreery, R. L.; *Anal. Chem.* **1984**, *56*, 2199.

17. Schwab, S. D.; McCreery, R. L.; *Appl. Spectrosc.* **1987**, *41*, 126.

18. Carrabba, M. M.; Edmonds, R. B.; Rauh, R. D. *Anal. Chem.* **1987**, *59*, 2259.

19. Angel, S. M.; Katz, L. F.; Archibald, D. D.; Lin, L. T.; Honigs, D. E. *Appl. Spectrosc.* **1988**, *42*, 1327.

20. Simhony, S.; Katzir, A.; Kosower, E. M. *Anal. Chem.* **1988**, *60*, 1908.

21. Compton, D. A. C.; Hill, S. L.; Wright, N. A.; Druy, M. A.; Piche, J.; Stevenson, W. A.; Vidrine, D. W. *Appl. Spectrosc.* **1988**, *42*, 972.

22. Harrick, N. J. *Internal Reflection Spectroscopy*; John Wiley & Sons, New York, 1967.

23. Mirabella, F. M., Jr. In *Internal Reflection Spectroscopy: Review and Supplement*, Harrick, N. J., Ed.; Harrick Scientific Corp.: Ossining, New York, 1985.

24. Xu, J. R.; Balik, C. M. *Appl. Spectrosc.* **1988**, *42*, 1543.

25. Wang, J.; Hutchins, L. D. *Anal. Chem.* **1985**, *57*, 1536.

26. Wang, J.; Hutchins-Kumar, L. D. *Anal. Chem.* **1986**, *58*, 402.

27. Fieser, L. F.; Williamson, K. L. *Organic Experiments*; D. C. Heath, Lexington, MA, 1983; 5th ed.

28. Boss, R. A. *Tappi* **1959**, *42*, 185A.

29. Hadzi, D. *J. Chem. Soc.* **1956**, 2143.

30. Le Fèvre, R. J. W.; Werner, R. L. *Aust. J. Chem.* **1957**, *10*, 26.

31. Rieman, W.; Walton, H. F. *Ion Exchange in Analytical Chemistry*; Pergamon, Oxford, 1970.

32. Warrier, A. V. R.; Narayanan, P. S. *Spectrochim. Acta, Part A* **1967**, *23*, 1061.

33. Yerian, T.; Christian, G.; Ruzicka, J. *Anal. Chim. Acta* **1988**, *204*, 7.

34. Stinson, S. *Chem. Eng. News* **1989**, *67*, 30.

SECTION V. EVALUATION OF THE STRUCTURAL AND PERFORMANCE CHARACTERISTICS OF A pH SENSOR BASED ON THE CHEMICAL MODIFICATION OF A POROUS POLYMER FILM

EVALUATION OF THE STRUCTURAL AND PERFORMANCE CHARACTERISTICS OF A pH SENSOR BASED ON THE CHEMICAL MODIFICATION OF A POROUS POLYMER FILM

Thomas P. Jones and Marc D. Porter

Department of Chemistry and Ames Laboratory–USDOE

Ames, IA 50011

INTRODUCTION

Development of chemical sensors has in the last few years been a rapidly increasing area of research. A variety of optical sensors based on immobilization of colorimetric indicators at polymeric support materials for determination of pH, metal ions, and anions have been reported.[1-10] These sensors have shown promise for applications in environmental[9] and biomedical[10] analyses, as well as in industrial process control.[9,11] The performance of many of these optical sensors, however, suffers due to one or more of the following: (1) a slow response time due to barriers to mass transport at a polymer support; (2) a weak analytical signal due to low optical absorptivity, fluorescent quantum yield, or concentration of immobilized colorimetric indicator; and (3) poor long-term stability due to degradation or desorptive loss of the immobilized reagent, which often necessitates periodic recalibration of the sensor response. It is essential that the long-term stability and accuracy of sensors be improved, and methods of calibration that do not require periodic recalibration of the sensor be developed. Furthermore, in order to develop *new* sensors with enhanced performance characteristics, the fundamental chemical and physical interactions which govern the response of existing sensors must be understood, including the mode of attachment to the support and its effect on the reactivity of the immobilized species toward an analyte.

In this paper, we report an investigation of the response characteristics and the long-term stability of a pH sensor, which consisted of Congo Red immobilized at a thin cellulosic film, the construction and

preliminary evaluation of which were reported earlier.[12] Several characteristics of the sensor were studied, including the pK_a values of the immobilized reagent, the long-term stability of the sensor, the effect of ionic strength and ion size on the response time, and the concentration of Congo Red in the polymeric support. An evaluation of the calibration and accuracy of the sensor was also performed, including an investigation of the effect of ionic strength on sensor response. Finally, vibrational spectroscopy was utilized in the structural characterization of immobilized Congo Red; resonance Raman spectra of the Congo Red sensor were collected, and these spectra were compared to infrared internal reflection spectra from our earlier study of the Congo Red sensor.[13]

EXPERIMENTAL

Sensor Construction

The fabrication of the sensor has been reported previously.[12] Cellulose acetate films (Aldrich, Inc., Milwaukee, WI) were cast onto microscope slides by spin-coating techniques, which consisted of flooding the surface with a 10% (w/v) solution of cellulose acetate (in cylclohexanone) and spinning at 1000 rpm. After drying, the films were hydrolyzed in 0.1 M KOH for 24 h. Film thicknesses were measured prior to hydrolysis with an Alphastep surface profiler (Tencor Instruments, Mountainview, CA). Congo Red (Aldrich, Milwaukee, WI), was immobilized at the porous polymeric film with a classical dye-bath recipe.[14] This consisted of immersing a hydrolyzed film in an electrolytic dye bath for 10 min. The aqueous dye bath was composed of Congo Red (3.6×10^{-4} M), Na_2SO_4 (0.025% w/v), and K_2CO_3 (0.025% w/v). The temperature of the dye bath was held at 85 to 90°C. After removal from the dye bath, excess reagent was washed from the substrate with deionized water. Prior to its use, Congo Red was recrystallized twice from an ethanol / water solution.[15]

Flow Cell

A flow cell that allowed rapid change of solution pH was used in the collection of UV-visible absorption spectra of the Congo Red pH sensor, as well as time-based measurements of single-wavelength absorbance. An operational diagram of the flow cell is shown in Figure 1. Solution was transported to and from the cell through Teflon tubing with internal

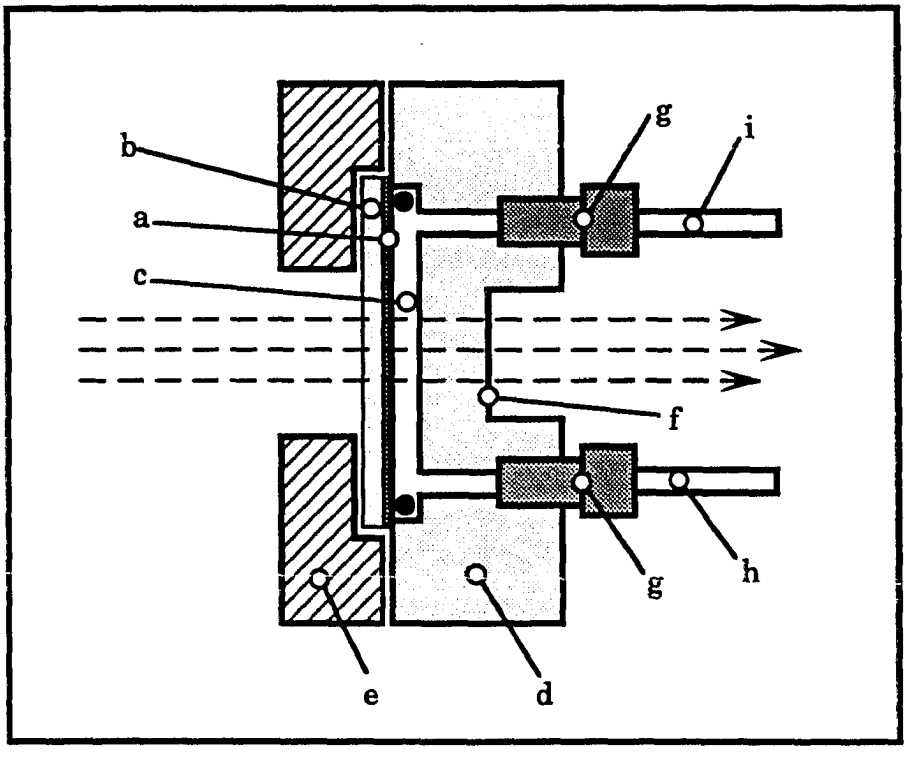

Figure 1. Side view of the flow cell for spectroscopic measurements of immobilized Congo Red: (a) thin-film sensor, (b) glass support, (c) solution channel, (d) cell body, (e) aluminum plate, (f) polished face of cell body, (g) flanged-tubing fitting, (h) solution input tubing, (i) solution outlet tubing. Dotted arrows indicate light path for spectroscopic measurements

diameter of 1.5-mm. The tubing connected via low-pressure flanged fittings at the ends of a solution channel that was defined by the contact area of the sensor with an O-ring of 0.16-cm thickness, the walls of the O-ring, and the Plexiglas® cell body. The cross-sectional area of the solution channel (1.2 mm by 1.2 mm) through the cell matched that of the tubing to minimize dead volume. The flow cell was positioned in the sample compartment of a DMS-200 UV-visible spectrometer (Varian Instrument Co., Palo Alto, CA). The light-path for spectroscopic measurements passed in turn through the glass substrate, the thin-film sensor, solution, and the Plexiglas® cell body. The back face of the cell body, where the light path exited the cell, was polished by 1-μm alumina to facilitate transmission.

Response time

To determine the effect of ionic strength and ion size on the response time of the sensor, the absorbance at 620 nm (at which wavelength only the acidic form of the indicator absorbs light) was monitored as a function of time as the solution composition was alternated. Solution flow was maintained by a gravity-feed system at 1.55 mL/sec. Solutions were changed with a low dead-volume multiport injection valve. The time constant was determined as the time required to affect 63% (1-1/e) of the equilibrated response. The effect of ionic strength on the response time of the sensor was determined by alternating between a solution of 0.1 M HCl and solutions of KCl, which ranged in concentration from 1 mM to 0.1 M. The effect of cation size on the response time of the sensor was determined by alternating a solution of 0.1 M HCl with solutions of 0.1 M KCl, NaCl and LiCl.

Dye-Adsorption Cell

The concentration of Congo Red immobilized at the hydrolyzed cellulose acetate film was determined by monitoring the decrease in absorbance of a solution of Congo Red that was in contact with a hydrolyzed cellulose acetate film. The cell used for these experiments is shown in Figure 2. The area of solution contact of the film was defined by the internal diameter of the O-ring that sealed the glass plate against the cell. The temperature of the cell was controlled by water flow from an IC-2 constant-temperature circulator (Brinkmann Instruments, Inc., Westbury NY). The temperature of the cell was monitored by a Teflon-coated 0.05-mm-diameter thermocouple, the tip of which extended into the solution cavity of the cell. The cell was filled with 2.53 mL of 1.46×10^{-5} M Congo Red, and the concentration of Congo Red in the cell was monitored by the change in absorbance of the solution at 510 nm, through windows that defined an optical path length of 1.20 cm. After the cell was filled with solution, it was sealed to prevent evaporation of solution.

Long-Term Stability

The stability of the sensor at neutral pH was determined over a period of 15 days in a solution of citrate/phosphate buffer[16] at pH 6.0, and the stability of the sensor at acidic pH was determined over a period of 6 days in a solution of 0.1 M HCl at pH 0.96. The solution in the cell was changed before each measurement to remove from the cell any accumulated products of dye bleeding or decomposition. Absorbance spectra were

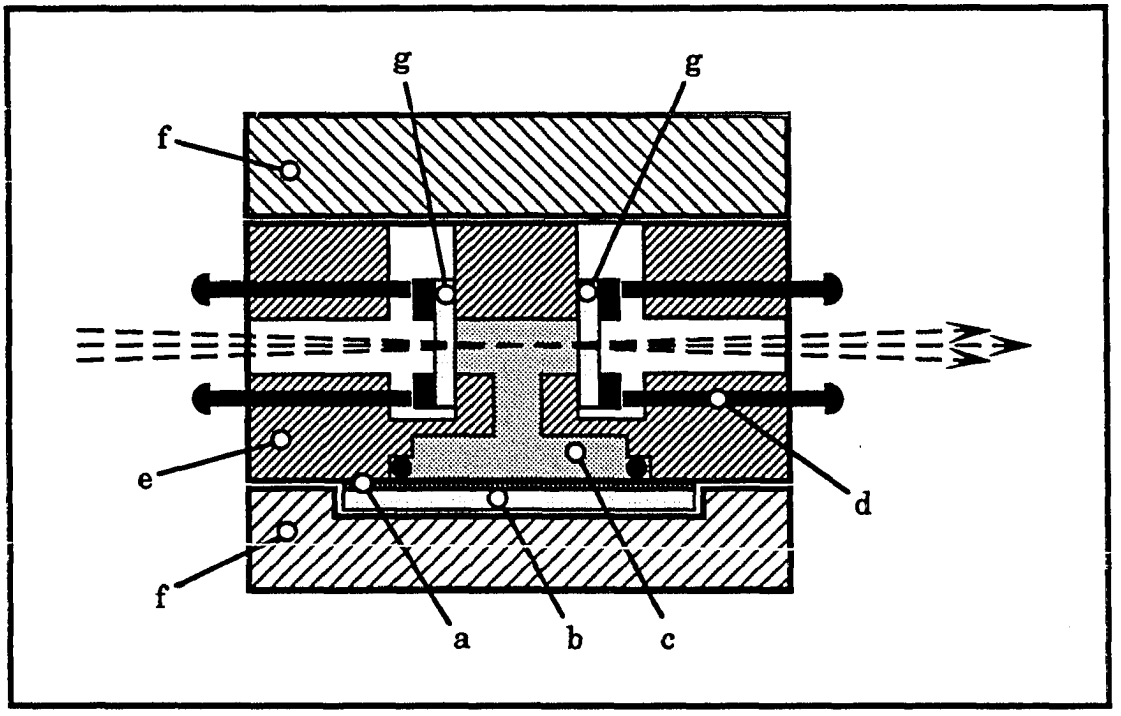

Figure 2. Top view of the dye-adsorption cell for determination of concentration of immobilized Congo Red: (a) thin-film sensor (exaggerated thickness), (b) glass support, (c) solution cavity, (d) window mounting screws, (e) cell body, (f) aluminum heating blocks, (g) quartz windows. Dotted arrows indicate light path for spectroscopic measurements

recorded periodically to determine the amount of Congo Red remaining in the film as a function of time.

Resonance Raman Spectroscopy

Sample preparation

Powdered cellulose acetate (Aldrich, Inc., Milwaukee, WI) was hydrolyzed for 24 h in 1 M KOH, filtered and rinsed with deionized water to remove hydrolysis products and excess KOH. The resulting cellulosic powder was added to a stirred solution of Congo Red (1.8×10^{-3} M), Na_2SO_4 (0.025% w/v), and K_2CO_3 (0.025% w/v), and allowed to react for 24 h at ambient temperature. The dyed cellulosic polymer was filtered and rinsed with deionized water to remove electrolyte, and with a 1:1 (v/v) mixture of deionized water and acetone to remove unreacted Congo Red.

Spectra collection

Powdered samples were placed in a 5.0-mm diameter glass tube, and mixed with solutions of 1 M HCl or 0.1 M KCl. The samples were illuminated with 10 mW of 457-nm light from a dye laser, which was pumped with an argon-ion laser. The resonance-enhanced Raman scattered light was collected by a Triplemate monochromator (Spex Ind., Edison, NJ) and a model 1421 intensified silicon diode-array detector (EG&G Princeton Applied Research Corp., Princeton NJ), which was controlled by an OMA-III data acquisition system (EG&G Princeton Applied Research Corp., Princeton NJ).

Solutions

The pH was varied by preparing a series of solutions of differing concentrations of HCl (pH 0 to 4), or by phosphate and citrate buffers (pH 4-7). Except as indicated otherwise, all solutions were adjusted to an ionic strength of 0.1 M by addition of KCl. The pH of the solutions was measured with an Orion model 701A pH meter (Orion Research Inc., Cambridge, MA) and a general purpose combination pH electrode (Corning Glass, Corning, NY).

RESULTS AND DISCUSSION

Concentration of Immobilized Congo Red

The amount of Congo Red immobilized at a hydrolyzed cellulose acetate film was determined by monitoring the change in absorbance of a solution of Congo Red that was in contact with a film of hydrolyzed cellulose acetate. The thickness of the cellulose acetate film was determined to be 1.5 μm after hydrolysis. During dye adsorption, the absorbance of the solution decreased from 0.790 to 0.590. To verify that the Congo Red lost by solution adsorbs only at the film, the cell was fitted with a clean microscope slide in place of a hydrolyzed cellulose acetate film, and was filled with 1.46×10^{-5} M Congo Red. With this test, the absorbance at 510 nm displayed no change as a function of time, indicating that adsorption at the cellulose acetate film was the only mechanism for the observed decrease in solution absorbance. The initial and final concentrations of Congo Red in solution were determined as 1.45×10^{-5} and 1.09×10^{-5} M, respectively, by the Beer-Lambert Law, using the initial and final absorbance at 510 nm, the cell path length, the volume of solution added to the cell, and the molar absorptivity of Congo Red in solution, 4.53×10^{4} M^{-1} cm^{-1}, which was determined spectroscopically in a 1-cm cuvette. The volume of hydrolyzed cellulose acetate that was subject to Congo Red immobilization, 8.55×10^{-4} cm^3, was defined by the area of contact with solution and the thickness of the film. Using the above values, the concentration of immobilized Congo Red was determined to be 2.1×10^{-2} M. The amount of indicator that is immobilized at a given film is a complex function of fabrication parameters, including temperature, time of

exposure, and dye-bath composition. Using the fabrication procedure, the concentration of Congo Red immobilized at different films varied by 10-20%.

Determination of pK_a Values

Visible absorption spectra of the immobilized Congo Red as a function of pH are shown in Figure 3. As reported earlier,[12] the sensor exhibits change in absorbance from about pH 4 to below pH 0. The spectra indicate the presence of two isosbestic points, at 535 and 559 nm, respectively. The presence of two isosbestic points, which occur where the conjugate acid and base in a protonation step have the same absorptivity,[17] indicates that there are two steps in the protonation of immobilized Congo Red. Figure 4 is a plot of absorbance as a function of pH at the wavelength of each of the isosbestic points. A plot of absorbance at the wavelength of the first isosbestic point as a function of pH shows change in absorbance due only to the second transition, and the absorbance as a function of pH at the second isosbestic point shows change in absorbance due only to the first transition. The equations that describe the absorbance as a function of pH at the two isosbestics are

$$A_{535} = (\alpha_1 \cdot \varepsilon_{1,535} + \alpha_2 \cdot \varepsilon_{2,535} + \alpha_3 \cdot \varepsilon_{3,535})\, b\, C \quad (1)$$

$$A_{559} = (\alpha_1 \cdot \varepsilon_{1,559} + \alpha_2 \cdot \varepsilon_{2,559} + \alpha_3 \cdot \varepsilon_{3,559})\, b\, C \quad (2)$$

where A_{535} and A_{559} are the absorbances at 535 and 559 nm respectively, b is the thickness of the thin-film sensor in cm, C is the molar concentration of Congo Red in all of its various ionic forms; ε_1, ε_2, and ε_3 are the molar absorptivities of the fully protonated, singly protonated, and fully

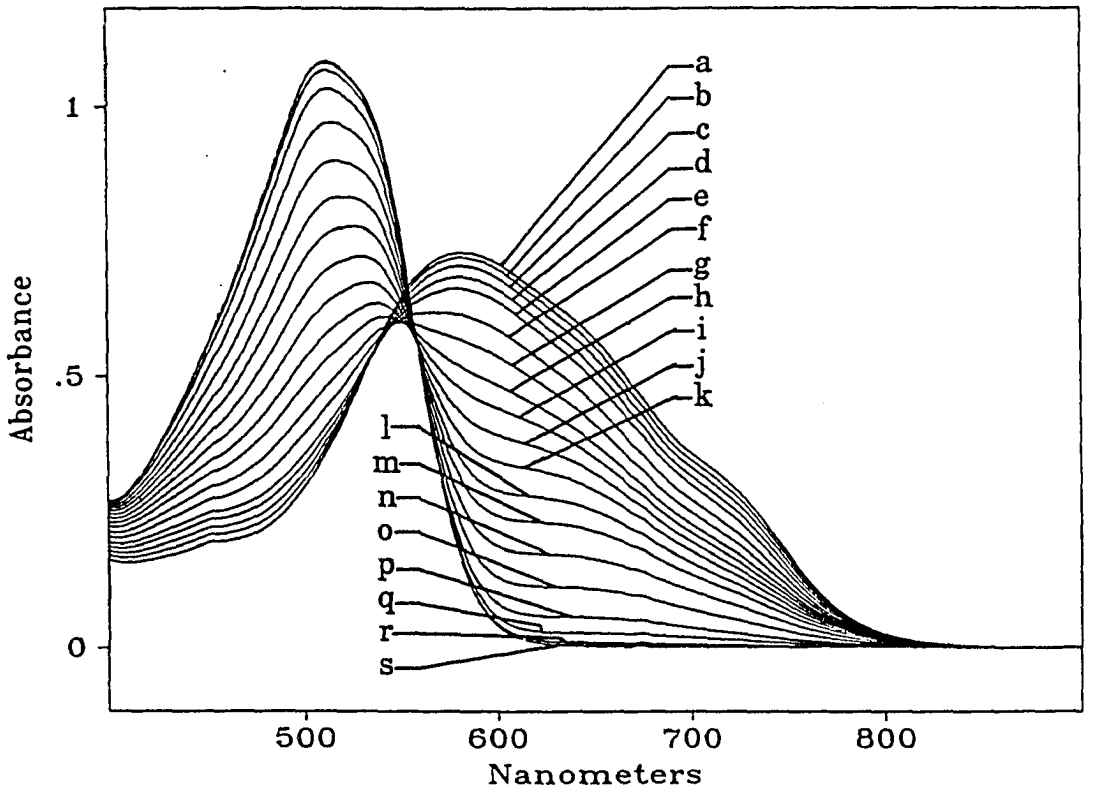

Figure 3. Absorption spectra of immobilized Congo Red at pH values: (a) 0.00, (b) 0.18, (c) 0.45, (d) 0.73, (e) 0.96, (f) 1.22, (g) 1.49, (h) 1.77, (i) 2.00, (j) 2.28, (k) 2.56, (l) 2.85, (m) 3.06, (n) 3.32, (o) 3.56, (p) 3.84, (q) 4.16, (r) 4.98, (s) 5.99. Isosbestic points are at 535 and 559 nm

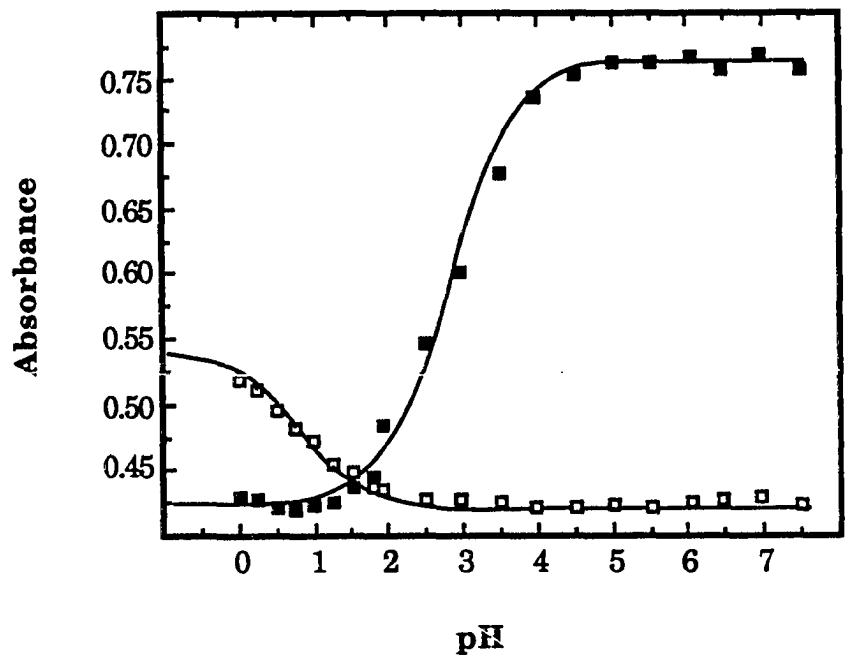

Figure 4. Absorbance vs. pH at isosbestic points: (■) 537 and (□) 559 nm. Curves through points represent calculations by Equations 6 and 7

deprotonated forms of Congo Red, respectively; and α_1, α_2, and α_3 are the distribution coefficients[18] of the fully protonated, singly protonated, and fully deprotonated forms of Congo Red, which are given in terms of the molar hydrogen ion concentration, $[H^+]$,

$$\frac{1}{\alpha_1} = 1 + \frac{K_{a1}}{[H^+]} + \frac{K_{a1}K_{a2}}{[H^+]^2} \tag{3}$$

$$\frac{1}{\alpha_2} = \frac{[H^+]}{K_{a1}} + 1 + \frac{K_{a2}}{[H^+]} \tag{4}$$

$$\frac{1}{\alpha_3} = \frac{[H^+]^2}{K_{a1}K_{a2}} + \frac{[H^+]}{K_{a2}} + 1 \tag{5}$$

where K_{a1} and K_{a2} are the first and second acid-dissociation constants of Congo Red, respectively. As a condition of an isosbestic point, the molar absorptivities $\varepsilon_{1,535}$ and $\varepsilon_{2,535}$ are equal, as are the molar absorptivities $\varepsilon_{2,559}$ and $\varepsilon_{3,559}$. Thus Equations 1 and 2 above simplify to

$$A_{535} = [(\alpha_1 + \alpha_2)\,\varepsilon_{1,535} + \alpha_3\,\varepsilon_{3,535}]\,b\,C \tag{6}$$

$$A_{559} = [\alpha_1\,\varepsilon_{1,559} + (\alpha_2 + \alpha_3)\,\varepsilon_{3,559}]\,b\,C \tag{7}$$

The molar absorptivities of the fully deprotonated form of immobilized Congo Red were calculated as $\varepsilon_{3,535} = 2.31 \times 10^5$ and $\varepsilon_{3,559} = 1.28 \times 10^5$ from spectra at pH 7.0, and the molar absorptivity of the fully protonated form were calculated as $\varepsilon_{1,535} = 1.29 \times 10^5$ and $\varepsilon_{1,559} = 1.64 \times 10^5$ from spectra at pH 0.0. Because the second protonation step is only ~85% complete at pH 0.0, the value of $\varepsilon_{1,559}$ was estimated. From Equations 6 and 7, the pK_a values that resulted in the best fit to the data in Figure 4 were determined to be 0.80 ± 0.15 and 2.80 ± 0.05 for the first and second protonation steps, respectively, using α_i values which were calculated by Equations 3-5, ε_i values given

above, the path length given by the thickness of the film, 2.9×10^{-4} cm, and the concentration of Congo Red in the film, 1.1×10^{-2} M. The higher uncertainty in the pK_a of the first protonation is a result of the estimation of $\varepsilon_{1,559}$.

Resonance Raman Spectra

Resonance enhancement of Raman scattering occurs when the sample undergoes electronic transitions due to absorption by the sample.[19] Raman scattering of vibrational modes associated with the electronic transition are enhanced by factors from 10^2 to 10^6 compared to normal Raman scattering.[21] Resonance Raman spectra of immobilized Congo Red at pH 5.5 and 0.0 are shown in Figures 5A and 5B, respectively. Since the electronic states involved in absorption vary as a function of wavelength, the intensity of resonance-enhanced Raman bands depends on the wavelength of incident light. Therefore, observed changes in peak intensity as a function of pH may be due to the change in resonance enhancement arising from the change in the electronic spectrum, in addition to changes in the cross-section of the vibration. To verify that the observed changes represent changes in the vibrational energy states, a comparison was made between the resonance Raman spectra and spectra obtained by infrared internal reflection spectroscopy.

Table 1 summarizes the peak positions and band assignments for the Raman spectra, as well as infrared peak positions and band assignments from our previous study of Congo Red at hydrolyzed cellulose acetate. Several of the bands observed in the spectra in Figure 5 are relatively

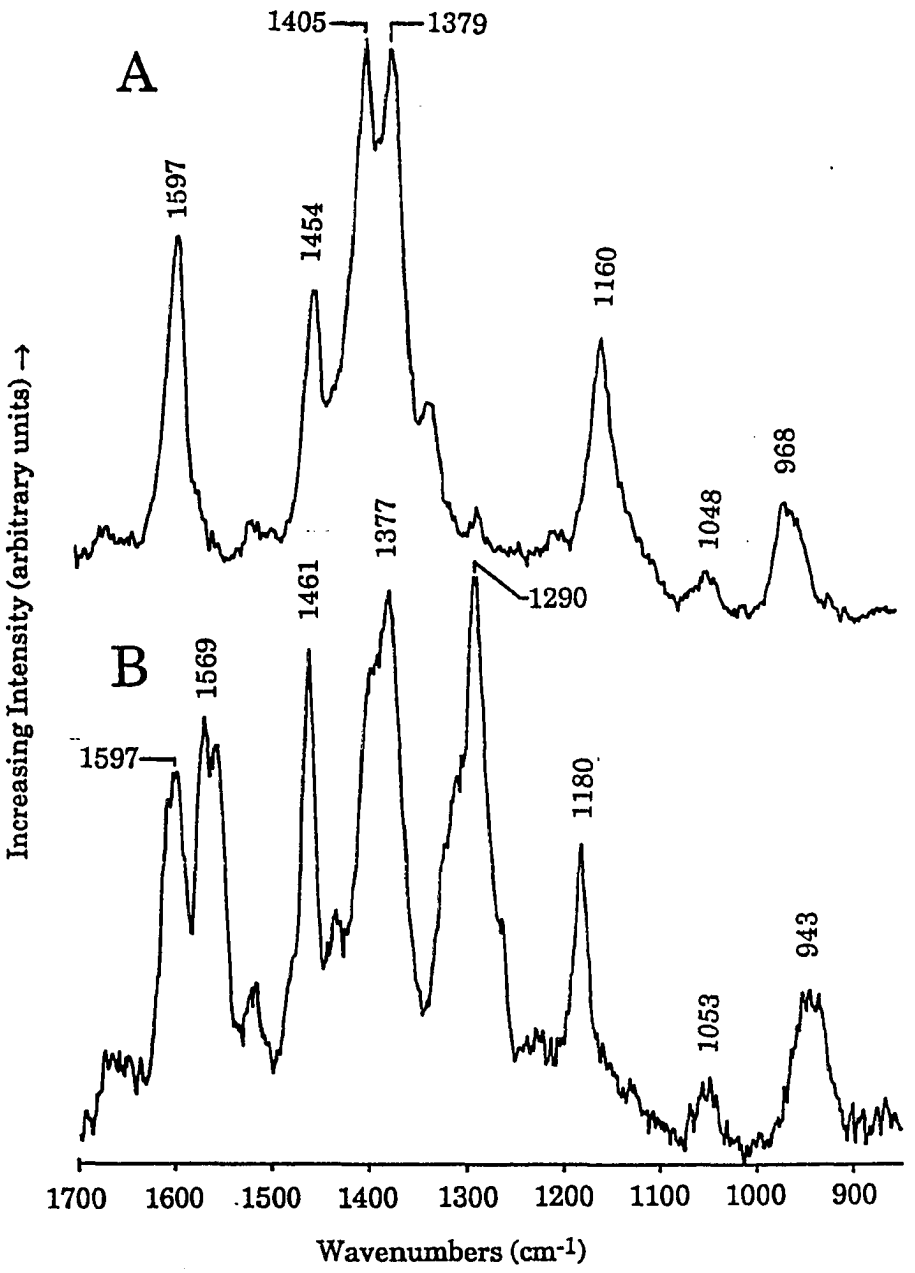

Figure 5. Resonance Raman spectra of Congo Red immobilized at cellulose acetate powder: (A) at pH 5.5 and (B) at pH 0.0

Table 1. Peak assignments from infrared and Raman spectra of immobilized Congo Red at pH 5.5 and 0.0. Peak positions are in wavenumbers (cm^{-1})

	pH 5.5		pH 0.0	
Assignment	Infrared	Raman	Infrared	Raman
ν(ring)	1596[b]	1597[b]	1601[b]	1597[b]
ν(C=C)	-	-	-	1569[b]
ν(C=C)	-	-	-	1559[b]
δ(N-H) azo	-	-	1547[c]	-
ν(ring)	1450[c]	1454[b]	-	1461[a]
ν(N=N) azo	-	1405[a]	-	-
ν(ring)	1373[b]	1379[a]	1367[a]	1377[a]
ν($C=N^+$)	-	-	1286[b]	1290[a]
$\nu(S=O)_a$	1176[b]	1160[b]	1186[b]	1180[b]
$\nu(S=O)_s$	1043[a]	1048[c]	1047[a]	1053[c]

[a]Strong intensity.

[b]Moderate intensity.

[c]Weak intensity.

unaffected by pH. The bands at 1597, 1454, and 1379 cm^{-1} are assigned to ring stretches of the naphthalene rings in Congo Red. The last of these arises from the Kekule stretch of the naphalene ring. These positions are in agreement with bands observed for substituted naphthalene compounds.[20] The bands at 1160 and 1050 cm^{-1} are assigned to the asymmetric and symmetric (S=O) stretches of the sulfonate group, respectively.

A number of bands in Figure 5 display marked changes as a function of pH. The strong band at 1405 cm^{-1} in Figure 5A disappears completely when Congo Red is protonated, and is attributed to the azo (N=N) stretch. This assignment replaces the one from our previous study of the infrared spectra of immobilized Congo Red.[13] A strong band at 1290 cm^{-1} appears in the spectrum in Figure 9B, and is assigned as the stretch of the amine $C=N^+$ as indicated by the structure in Figure 10c. The position of this band agrees with the $C=N^+$ stretch observed in the amine group of *o*-nitroanaline. The bands at 1569 and 1559 cm^{-1} in Figure 5B are attributed to C=C stretches. Changes in these C=C stretches arise from the structural distortions of the naphthalene rings which are caused by protonation. Although changes in the C=C stretching region are observed in both the infrared and resonance Raman spectra, the differences observed between these two methods are likely due to the resonance enhancement of various modes in the Raman spectra.

Sensor Calibration

Because slight variations in the fabrication conditions limits the reproducibility in the amount of indicator immobilized in a sensor, a calibration method which is independent of the concentration of immobilized indicator was utilized. An acid-base indicator in which both the protonated and deprotonated forms absorb light can be used to determine the pH of a solution (even if the concentration of the immobilized indicator is not known) by measuring the absorbance at two appropriate wavelengths. The absorbance of a diprotic acid indicator, represented by H_2A, HA^-, and

A^{2-} for the fully protonated, monoprotonated, and fully deprotonated forms, respectively, at two different wavelengths, λ_x and λ_y, are given by

$$A_x = \varepsilon_{x1} \cdot b \cdot C \cdot \alpha_1 + \varepsilon_{x2} \cdot b \cdot C \cdot \alpha_2 + \varepsilon_{x3} \cdot b \cdot C \cdot \alpha_3 \quad (8)$$

$$A_y = \varepsilon_{y1} \cdot b \cdot C \cdot \alpha_1 + \varepsilon_{y2} \cdot b \cdot C \cdot \alpha_2 + \varepsilon_{y3} \cdot b \cdot C \cdot \alpha_3 \quad (9)$$

where ε is the molar absorptivity, C is the total concentration of the indicator in all its forms, and α represents the distribution coefficient, as given by Equations 3-5; the subscripts 1, 2, and 3 indicate the indicator forms H_2A, HA^-, and A^{2-}, respectively. Dividing Equation 8 by Equation 9 results in the cancellation of b and C:

$$\frac{A_x}{A_y} = \frac{\varepsilon_{x1} \cdot \alpha_1 + \varepsilon_{x2} \cdot \alpha_2 + \varepsilon_{x3} \cdot \alpha_3}{\varepsilon_{y1} \cdot \alpha_1 + \varepsilon_{y2} \cdot \alpha_2 + \varepsilon_{y3} \cdot \alpha_3} \quad (10)$$

In the above equation, the molar absorptivities (ε_{x1}, ε_{x2}, ε_{x3}, ε_{y1}, ε_{y2}, and ε_{y3}) are constants, and the distribution coefficients (α_1, α_2, and α_3) depend only on pH (assuming activity coefficients are constant). Therefore, the absorbance ratio (A_x/A_y) is a function only of pH, and (with the selection of appropriate wavelengths) it can be used to construct a calibration curve that is independent of indicator concentration. In the Congo Red sensor, wavelengths of 621 nm and 510 nm were chosen because the absorbance at 621 nm increases continuously with decreasing pH, and the absorbance at 510 nm does the opposite; therefore not only is the "absorbance ratio" (A_{621}/A_{510}) uniquely defined for every value of pH in the transition range, but it also undergoes a large change as a function of pH. Figure 6 shows a plot of pH as a function of this absorbance ratio for a cellulose acetate film. The curve through the points represents a fifth-order polynomial least-squares fit of the data. The equation describing the fit is

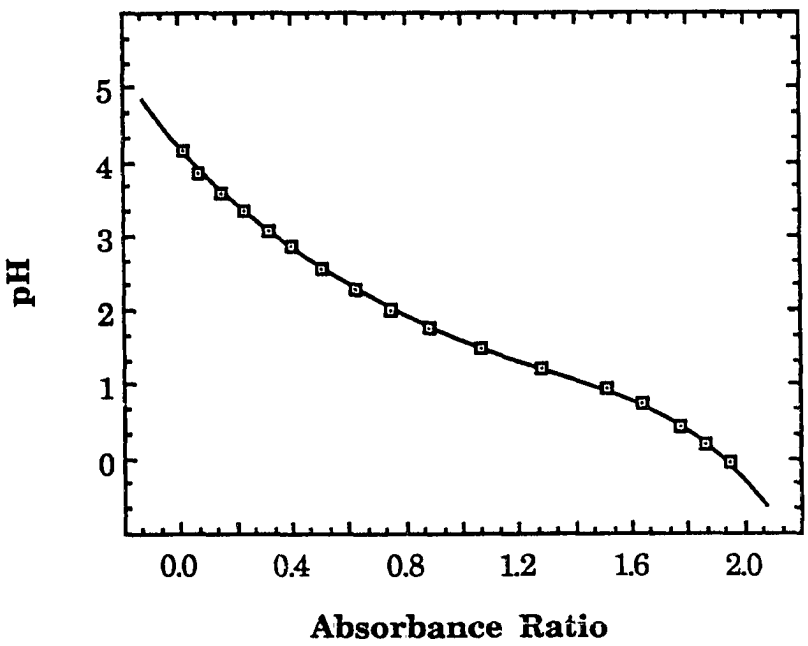

Figure 6. Calibration curve for the pH sensor. Curve represents fifth-order polynomial curve-fit of the data, and is given by Equation 11. The error in the absorbance ratio is smaller than the size of the data points

$$pH = 4.17 - 4.245r + 2.686r^2 - 1.684r^3 + 0.9081r^4 - 0.2419r^5 \quad (11)$$

where r represents the absorbance ratio. The validity of Equation 11 was tested against two other Congo Red sensor films of differing Congo Red concentrations; in each case the pH calculated by Equation 11 was compared with the pH determined potentiometrically. The results from Equation 11 agreed within ±0.05 pH units of the measured values at the central portion of the calibration curve (pH 1 to 3), and to within ±0.10 pH units at the extremes (pH 0 to 1 and pH 3 to 4).

Effects of ionic strength on calibration

Because optical sensors are based on the equilibrium of complex formation involving ionic reactants and/or products, the optical response of a sensor depends on the ionic strength of the solution in which it is immersed. The activity coefficients of indicators such as Congo Red, however, are difficult to predict due to their large size and the presence of multiple ionic charges. It is, therefore, important that the effect of ionic strength on the calibration of optical sensors be investigated. The accuracy of the sensor calibration was investigated as a function of ionic strength. The absorbance ratio (A_{621}/A_{510}) was measured for a Congo Red sensor film immersed in solutions with pH 3.2 and ionic strengths ranging from 0.001 to 0.50. The pH was calculated by Equation 11 and compared to the pH measured potentiometrically. The resulting error ranged from -1.5 to +0.01 pH units at ionic strengths of 0.001 M and 0.501 M, respectively (the calibration curve was prepared at ionic strength of 0.10 M). This deviation is comparable to errors caused by ionic-strength changes observed for other

optical sensors.[21] These errors indicate the importance of correction for ionic strength effects in the calibration of optical sensors, either by using solutions of constant ionic strength or by including activity coefficients in the calibration equation. The acceptable limit of error arising from ionic strength variations to a large degree depends on the application of the sensor. For applications involving environmental analysis of acidic solutions of high ionic strength, for which the Congo Red sensor is best suited, an error of ±0.3 pH units caused by ionic strength variations is most likely acceptable.

Response Time

The effect of ionic strength and the size of counterions on the response times for protonation and deprotonation of the sensor were studied. The response time data for deprotonation of the sensor indicated that the sensor response is limited by the diffusion of hydrogen ions and positive counterions. Because the response to protonation of the sensor, however, was at least as fast as the time required for the cell to completely change solution (0.2 s), it was not possible to determine the effects of ionic strength and ionic size on the response time for protonation.

Effect of ionic strength

The response time for 63% of maximum response (1-1/e) for deprotonation of the sensor as a function of ionic strength are shown in Figure 7A. The data represent the time for the response to a change from a

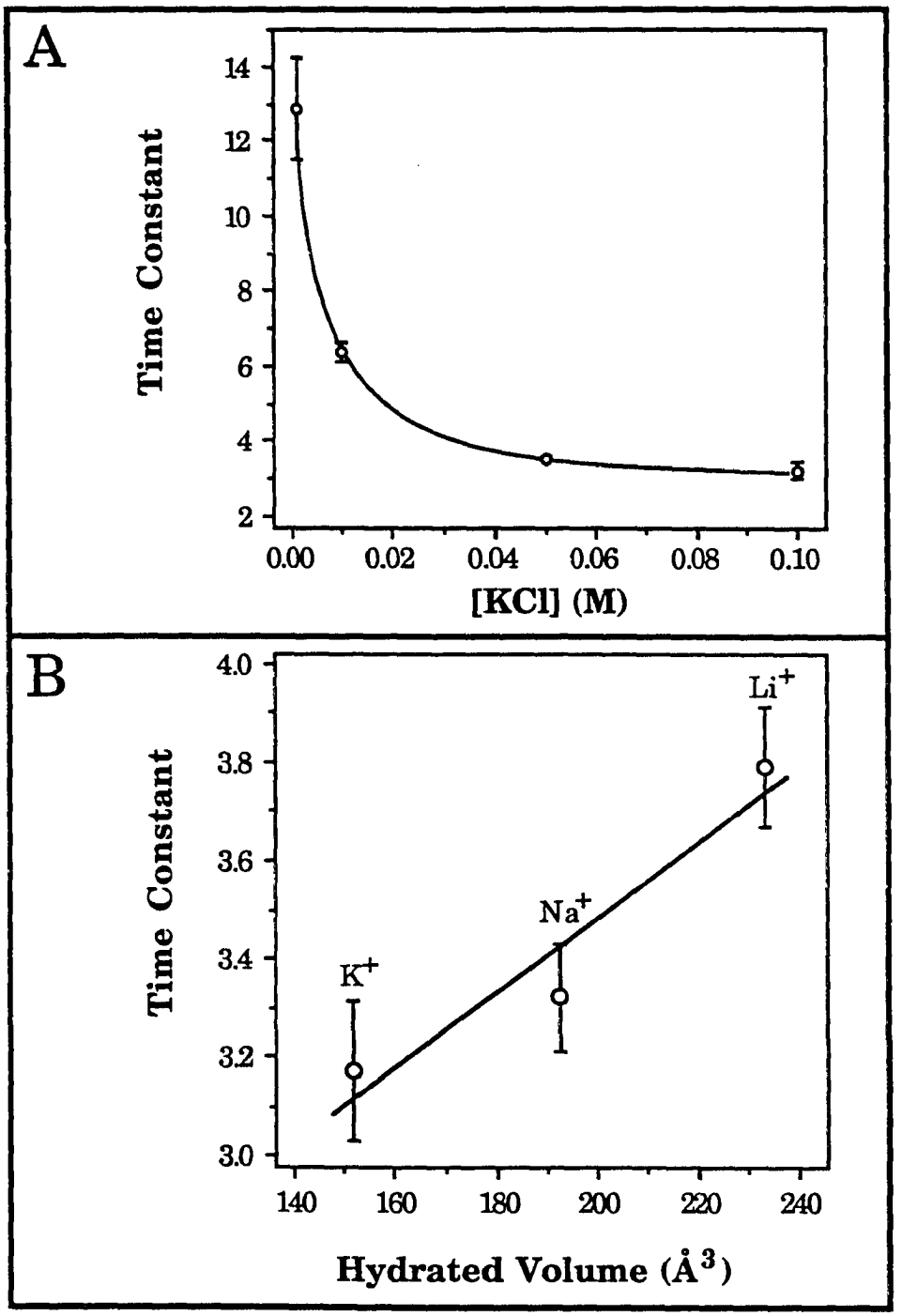

Figure 7. Response time of Congo Red pH sensor as a function of: (A) ionic strength, (B) hydrated ion volume

solution of 0.1 M HCl to a solution of KCl with a concentration varying from 1 mM to 0.1 M. The error bars represent the standard deviation of 3 measurements. The data in Figure 7A indicate that the response time of the sensor is near the maximum for solutions with ionic strengths above 0.05 M.This fact, combined with the range of protonation (from pH 0 to 4), suggest applications to analyses of acidic solutions of high mineral-ion content, such as acid mine drainage.

Effect of hydrated volume on response time

The response times for 63% of maximum response as a function of hydrated cation volume[22] are shown in Figure 7B. The data represent the time for the response to deprotonation by a change from a solution of 0.1 M HCl to solutions of 0.1 M KCl, 0.1 M NaCl or 0.1 M LiCl. The error bars represent the 95% confidence interval based on 20 to 24 measurements. Figure 7B indicates that the response time increases with the hydrated volume of the cation.

Discussion of ionic-strength effects

The rate of diffusion of ions in solution is a function of their hydrated volume. The cations K^+, Na^+, and Li^+ have hydrated radii of 1.25, 1.84, and 2.38 Å, respectively[22] (note that for the *hydrated* ions, $K^+ < Na^+ < Li^+$). Because response times for deprotonation of the Congo Red sensor increased for solutions of decreasing cation concentrations, as well as for solutions of increasing hydrated cation volume, the data in Figures 7A and 7B indicate that the response time for deprotonation was dependent on the mass

transport of positive counter-ions (i.e., K^+, Na^+, or Li^+) into the film. Due to the ~0.02 M concentration of immobilized sulfonate groups (from immobilized Congo Red), the sensor was analogous to a low-capacity cation exchange resin, and in its fully deprotonated form, the negative charge of the sulfonate groups was offset by positive counter ions, e.g., K^+, Na^+, or Li^+. Figure 8 shows our proposed structures for the fully deprotonated, monoprotonated, and fully protonated forms of Congo Red. The net charge of the fully deprotonated, monoprotonated, and fully protonated forms of Congo Red are -2, -1, and 0, respectively. For the complete deprotonation of the sensor, two hydrogen ions per Congo Red molecule diffused out of the sensor to solution, necessitating the diffusion of two positive counterions into the sensor for the preservation of electroneutrality. For the protonation, the diffusion was reversed: two hydrogen ions diffused into the sensor, and electroneutrality was preserved by the diffusion of positive counterions out of the sensor. The longer response time for solutions of lower ionic strength and larger hydrated cation volume observed in Figures 7A and 7B, respectively, support this interpretation.

Long-Term Stability

Stability at pH 6.0

A plot of absorbance at 512 nm as a function of time in a solution at pH 6.0 is shown in Figure 9. The absorbance decreased from an initial value of 1.03 to 0.87 after 15 days of constant immersion in solution at pH 6.0, which represents a loss of 15% of the initial amount of Congo Red. Extrapolation of

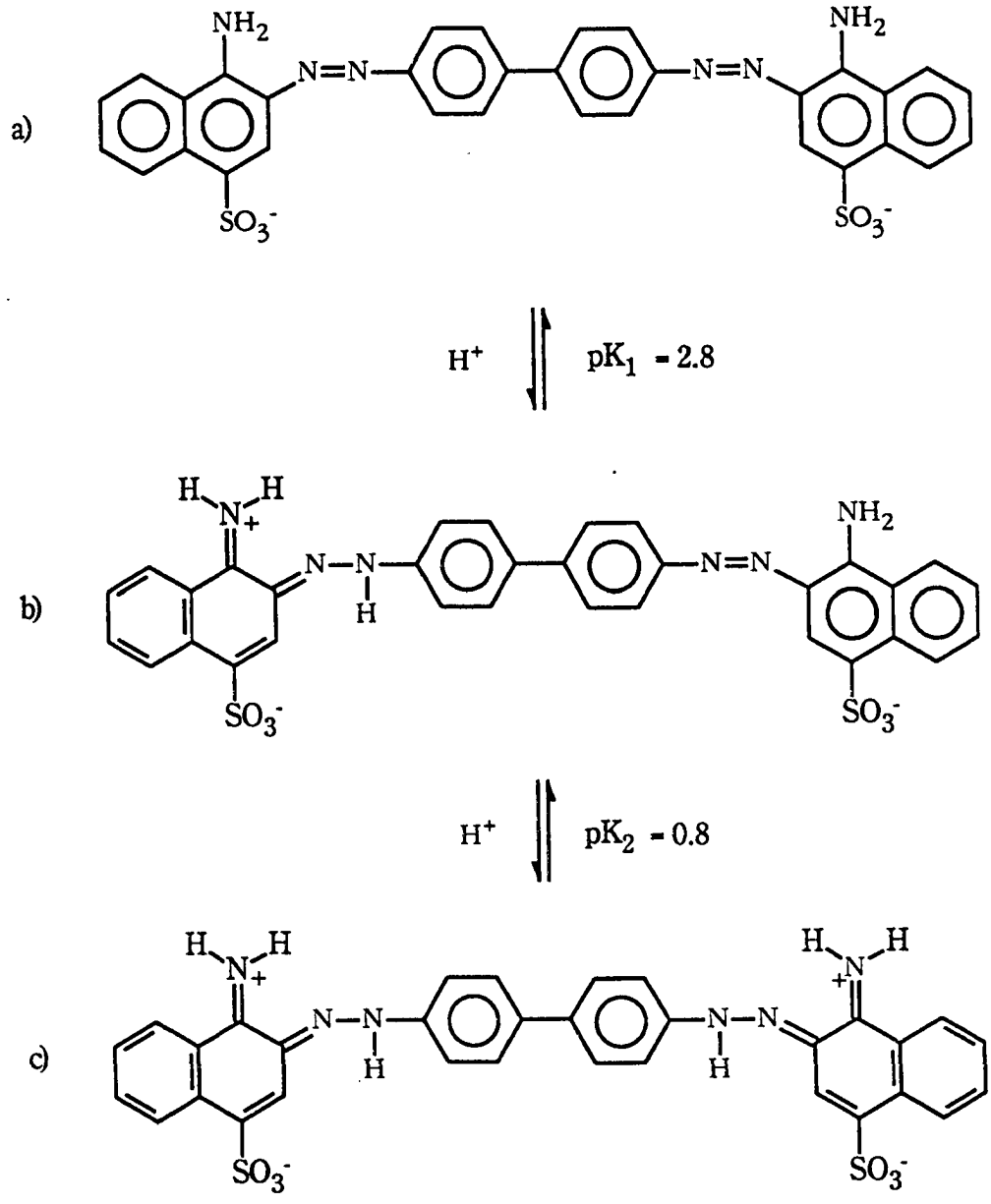

Figure 8. Acid-base reactivity of immobilized Congo Red: (a) fully deprotonated form, (b) monoprotonated form, (c) fully protonated form

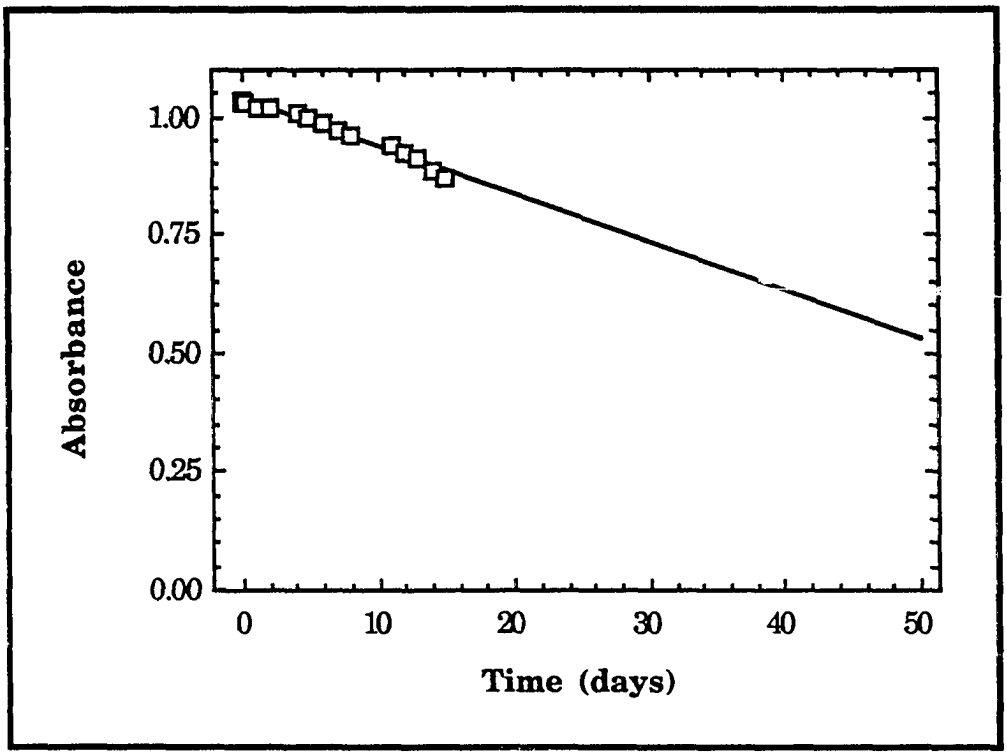

Figure 9. Long-term stability of Congo Red pH sensor at pH 6.0. Line through points represents an extrapolation of rate of degradation

this rate of loss indicates that after 50 days in solution, approximately half of the initial amount of dye would be present. Because the sensor can be calibrated independent of indicator concentration (*vide infra*) the sensor remains calibrated, as long as the remaining amount of indicator results allows calculation of the "absorbance ratio" with sufficient precision. In order to calculate the "theoretical" limit of degradation at which the precision of the sensor remains acceptable, the uncertainty in pH as determined by the calibration (Equation 11) was calculated as a function of indicator concentration. First, the uncertainty in the absorbance ratio was calculated based on a noise level of ±0.001 absorbance units for measurements of absorbance at the two wavelengths. The uncertainty of the pH was then determined from the uncertainty in the absorbance ratio using the derivative of Equation 11 with respect to the absorbance ratio (r). These calculations indicate that the pH of a solution can be determined to within ±0.10 pH units by a Congo Red sensor in which only 5% of the original concentration of immobilized Congo Red remains. Assuming a constant level of "bleeding" of the Congo Red from the sensor, this "theoretical" limit would be reached after 95 days of constant immersion.

Stability at pH 1.0

Absorption spectra of the Congo Red sensor immersed in a solution of 0.1 M HCl (pH 0.96) were recorded. Over the course of several days, the shape and peak maxima of the spectrum undergo considerable change, as the peak maximum shifts to 620 nm and increases in absorbance, and a second peak becomes evident at 715 nm. In acidic solutions, Congo Red

aggregates,[12] and the resulting peak shapes and peak maxima are similar to aggregated solutions of Congo Red. The aggregation indicates that the immobilized Congo Red retains some mobility within the sensor, but because the aggregation in the polymer film proceeded at a much slower rate than in solution (by a factor of $\sim 10^{-3}$), these data suggest that the mobility of Congo Red in the hydrolyzed cellulose acetate film was greatly reduced in comparison to its mobility in solution, where the aggregation was complete in 2-5 minutes at pH 1. The aggregation of Congo Red sensor films which had been immersed in 0.1 M HCl for several days was reversed, however, by briefly immersing the sensor film in an 0.1 M KOH solution. Although an aggregated sensor can be renewed quickly by immersion in base, this limitation must be considered in the application of the sensor. This limitation could be overcome by the covalent immobilization of Congo Red to the polymeric support, which would also reduce indicator "bleeding" and improve long-term stability.

CONCLUSIONS

A thorough investigation of the structure and performance characteristics of an optical sensor based on Congo Red immobilized at a hydrolyzed cellulose acetate film has been performed. A calibration method which is independent of the concentration of indicator in the sensor was utilized; using this method, the sensor was able to measure pH with an accuracy of ±0.05 to ±0.10 pH units over its transition range. The sensor had good long-term stability, with a projected maximum lifetime of 90 days of continuous immersion in solution. The effect of ionic strength on the accuracy of the sensor was also investigated.

The requirements of a sensor in terms of response time, long-term stability, accuracy and calibration are primarily dictated by the application. For instance, applications in environmental, biomedical, and process control analyses have different requirements. The performance characteristics of the Congo Red pH sensor suggest its application to acidic solutions of high mineral-ion content, such as acid mine drainage, due to its optical response in an acidic pH range, coupled with its fast response time in solutions of high ionic strength and low reactivity to metal ions.[12]

Evidence from our characterizations of immobilized Congo Red allowed conclusions to be made regarding the acid-base reactivity of Congo Red immobilized at hydrolyzed cellulose acetate. Absorbance as a function of pH at the two isosbestic points demonstrate the existence of two protonation steps, with pK_a values of 2.80 ± 0.05 and 0.8 ± 0.15 for the first and second protonations, respectively. Bands in both the infrared and

Raman spectra of immobilized Congo Red support the conclusion that these reactions involve protonation at the two azo groups. The effects of ionic strength and the size of cationic counterions on the response time indicated the the response time of the sensor is a function of the diffusion of cationic counterions.

ACKNOWLEDGEMENTS

TPJ gratefully acknowledges Prof. Therese Cotton of the ISU Department of Chemistry for the use of the Raman spectrometer, and Dr. Bernard Rospendowski for assistance in collection of data. MDP gratefully acknowledges the support of a Dow Corning Assistant Professorship. Discussions of band assignments with Lai-Kwan Chau are acknowledged. Ames Laboratory is operated for the U.S. Department of Energy by Iowa State University under Contract No. W-7405-Eng-82. This work was supported by the Office of Basic Energy Sciences.

REFERENCES

1. Wohltjen, H. *Anal. Chem.* **1984**, *56*, 87A-103A.
2. Janata, J.; Bezegh, A. *Anal. Chem.* **1988**, *60*, 62R-74R.
3. Seitz, W. R. *Anal. Chem.* **1984**, *56*, 16A-34A.
4. Narayanaswamy, R. *Anal. Proc. (London)* **1985**, *22*, 204-206.
5. Alder, J. F. *Fresenius' Z. Anal. Chem.* **1986**, *324*, 372-375.
6. Wolfbeis, O. S. *Fresenius' Z. Anal. Chem.* **1986**, *325*, 387-392.
7. Angel, S. M. *Spectroscopy (Springfield, Oreg.)* **1987**, *2*, 38-4.
8. Wolfbeis, O. S. *Anal. Proc. (London)* **1987**, *24*, 14-15.
9. Hirschfeld, T.; Callis, J. B.; Kowalski, B. R. *Science* **1984**, *226*, 312-318.
10. Peterson, J. I.; Vurek G. G. *Science* **1984**, *224*, 123-12.
11. Callis, J. B.; Illman, D. L.; Kowalski, B. R. *Anal. Chem.* **1987**, *59*, 624A-637A.
12. Jones, T. P.; Porter, M. D. *Anal. Chem.* **1988**, *60*, 404-406.
13. Jones, T. P.; Porter, M. D.; *Appl. Spectrosc.* **1989**, *43*, 908-911.
14. Fieser, L. F.; Williamson, K. L. *Organic Experiments*, 5th ed.; D. C. Heath: Lexington, MA, 1983.
15. Gore, T. S.; Unni, M. K.; Venkataraman, K. *J. Sci. Ind. Res.* **1956**, *15B*, 618-626.
16. Perrin, D. D.; Dempsey, B. *Buffers for pH and Metal Ion Control.*; London, Chapman, and Hall: New York, 1974; chapter 10.
17. Ingle, J. D.; Crouch, S. R. *Spectrochemical Analysis*; Prentice Hall, Englewood Cliffs, NJ, 1988; p. 373.
18. Ringbom, A. *J. Chem. Ed.* **1958**, *35*, 282.

19. Morris, M. D.; Wallan, D. J. *Anal. Chem.* **1979**, *51*, 182A-190A.

20. Dollish, F. R.; Fateley, W. G.; Bentley, F. F. *Characteristic Raman Frequencies of Organic Compounds,* John Wiley & Sons: New York, 1974; p. 185.

21. Janata, J. *Anal. Chem.* **1987**, *59*, 1351-1356.

22. Conway, B. E. *Ionic Hydration in Chemistry and Biophysics*; Elsevier Scientific Publishing Co.: New York, 1981; p. 73.

SECTION VI. A DUAL-WAVELENGTH FIBER-OPTIC SENSOR BASED ON SOLID-STATE INSTRUMENTATION

A DUAL-WAVELENGTH FIBER-OPTIC SENSOR BASED ON SOLID-STATE INSTRUMENTATION

Thomas P. Jones and Marc D. Porter
Department of Chemistry and
Center for Advanced Technology Development
Iowa State University
Ames, IA 50011

INTRODUCTION

The development of thin-film optical sensors for pH and metal-ion determinations has emerged as an area of extensive research activity.[1-11] Impetus for this emergence is driven in large part by the need for reliable, durable, and low-cost sensors for environmental and clinical applications. Surprisingly, few reports describing such instrumentation have appeared,[12-14] a circumstance that points to the complexities of realizing analytical instrumentation to meet the demands of the above applications. Central to cited efforts has been the use of low-cost solid-state components (e.g., light-emitting diodes (LEDs) as light sources and photodiodes as detectors) for the construction of optical sensor instrumentation that operated in a single-wavelength mode.[12,13] A two-wavelength scheme has expanded on these capabilities by inclusion of a near-infrared "reference wavelength" to compensate for fiber-bending intensity losses.[14] In each of these cases, however, variations in LED intensity led to instability in the sensor response.

As is apparent, several issues toward the development of reliable, low-cost optical sensor instrumentation have yet to be fully addressed. In addition to light-source fluctuations, questions concerning the selectivity, calibration, and stability of thin-film sensing elements have only been partially resolved. Furthermore, many targeted applications demand extensive miniaturization of both optical and electrical components, and in instances where implantation into a biological host is necessitated, biocompatibility is of considerable importance. It is clear that further

progress in this area will require interdisciplinary research efforts which draw upon expertise in a variety of areas, including synthesis, materials, electronics, and spectroscopy.

In this article, we describe the development and performance characteristics of a solid-state optical photometer that operates in a two-wavelength mode for absorbance measurements of thin-film sensors. Optical fibers are used to transmit light between LEDs, a thin-film sensor probe, and the photodiode detectors. Novel features of this design include the incorporation of a reference detector to compensate for fluctuations in output intensities of LEDs and a thin-film sensor probe that employs a graded-index lens (GRIN) to couple light efficiently from an input fiber to a collection fiber. A GRIN beamsplitter is also used to transmit light simultaneously to sample and reference detectors. An electronic modulation scheme is employed to compensate for stray light that couples into the end of the sensor probe. Results are presented for the application of this instrumentation to the determination of pH with our previously described thin-film sensors. Potential environmental applications of this instrument, based on its small size and mechanical durability (i.e., no moving parts), are also discussed.

EXPERIMENTAL

Optics

A diagram of the optical configuration of the optical sensor instrument is shown in Figure 1. A beam splitter divided the radiation from red and green LEDs between two fibers, one of which transmitted light to the sensor probe and the other to a reference detector. The LEDs, beam splitter, detectors, and amplifying electronics were mounted on a circuit board, and enclosed in a light-tight aluminum box (18 × 13 × 8 cm) to minimize stray light.

The ends of red and green light-emitting diodes (red, HLMP-3750; green, HLMP-3950; Hewlett-Packard Company, Palo Alto, CA), were polished flat successively with 32, 15, and 3-μm polishing sheets. Polishing provides both a smooth and flat end surface near the emitting element enhancing collection by the fiber optic. The red and green LEDs had emission maxima of 635 and 565 nm, respectively, and bandwidths (at half-height) of 40 and 35 nm, respectively. Fiber optics with a 400-μm core diameter and 15-μm-thick polymer cladding (HCR-MO400T-06, Ensign-Bickford Optics Company, Avon, CT) were also polished successively with 32, 15, 3, and 0.3-μm polishing sheets. A 1-cm portion of the protective Tefzel® buffer was removed from the fiber at the ends which connected to the beam splitter and sensor probe, and the fibers were cemented in place with epoxy. The ends of the fiber which connected to the sources and detectors were cemented in place with epoxy without removal of the protective buffer.

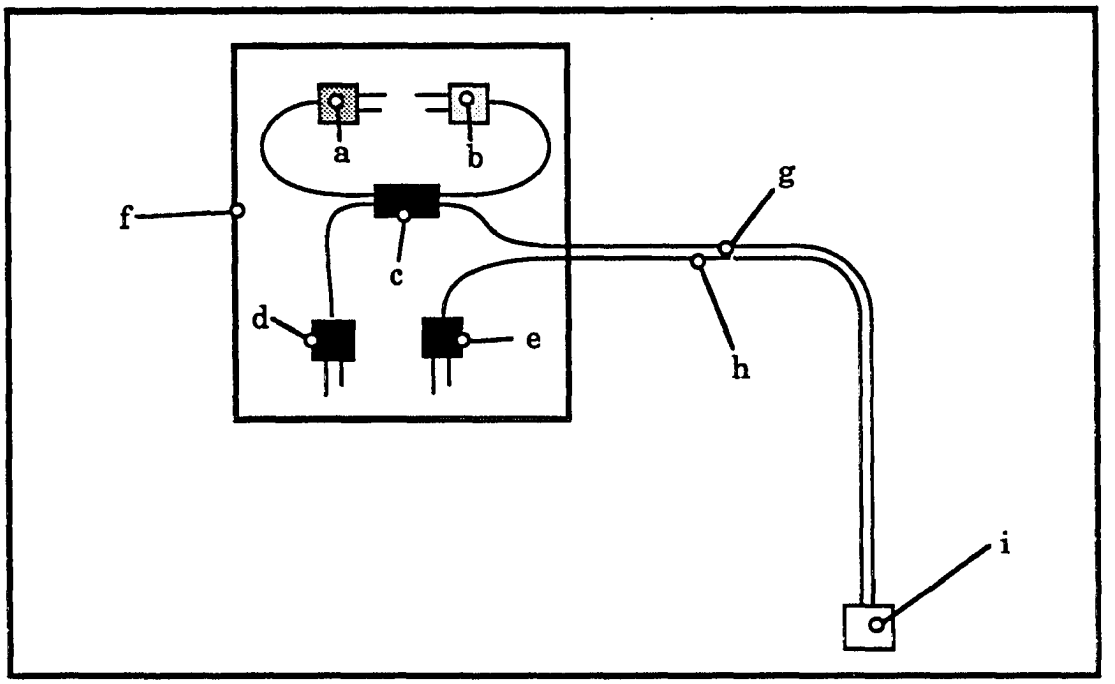

Figure 1. Schematic of optics: (a) green LED, (b) red LED, (c) beam splitter, (d) reference detector, (e) sample detector, (f) light isolation box, (g) sample input fiber to probe, (h) sample collection fiber from probe, (i) sensor probe

Beam splitter

The beam splitter, which is shown in Figure 2, consisted of two 2.0-mm diameter Selfoc® graded-index (GRIN) lenses (SLW-2.0, NSG America, Somerset, NJ) that are 5.11 mm long. The GRIN lenses were held end-to-end in a cylindrical brass housing by Delrin® end caps, which properly positioned the fiber optics for coupling light between the fibers. A 17-nm chromium film, which had been vapor-deposited on the end of one of the GRIN lenses, acted as a beam splitter, dividing the light intensity from each of the LED sources equally between the sample and reference fibers.

Sensor Probe

A diagram of the sensor probe is shown in Figure 3. A GRIN lens coupled light from an input fiber to a collection fiber. The back surface of the GRIN lens was coated with a reflective silver film (800 nm thickness) and protected from degradation by solution contact with a coating of epoxy resin. Light that propagated through the probe passed twice through the sensor film, which was held between the front surface of the GRIN lens and the fibers by a stainless-steel plate. The light losses of the sensor probe optics for both 565 and 635-nm light were measured by the observed decrease in detector response when the probe was connected from the beam splitter to the detector relative to the response of an equal length of fiber.

Thin-film sensor material

The sensor was fabricated according to a scheme we reported previously[15,16] by spin-coating a 15% (w/v) solution of cellulose acetate in

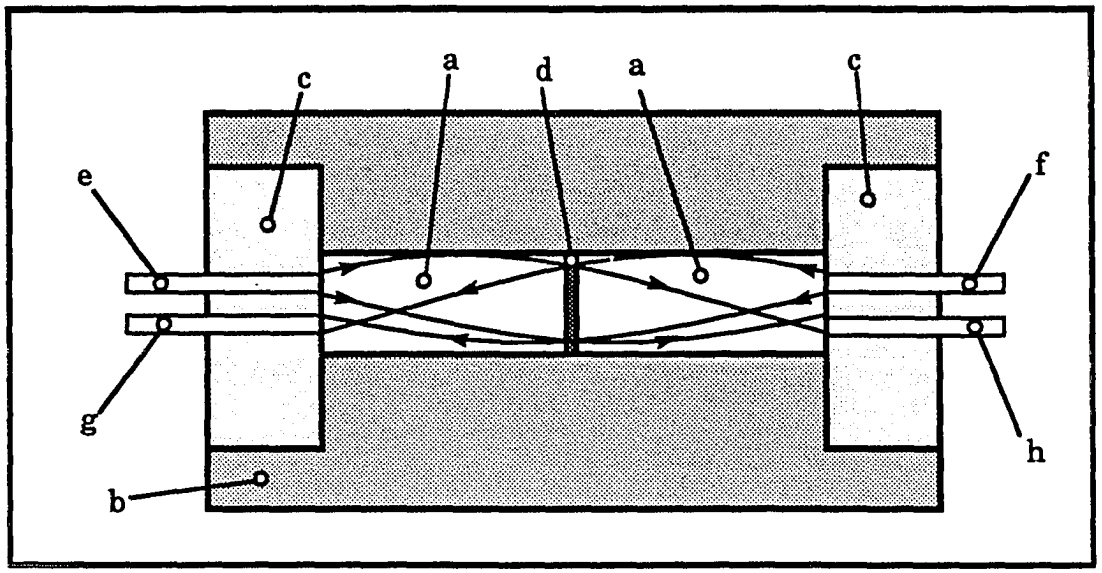

Figure 2. Detail of beam splitter: (a) GRIN lenses, (b) brass housing, (c) Delrin® end-plugs, (d) beam-splitting metal film, (e) input fiber from green LED, (f) input fiber from red LED, (g) fiber to reference detector, (h) fiber to sensor probe. Direction of light propagation is shown by arrows

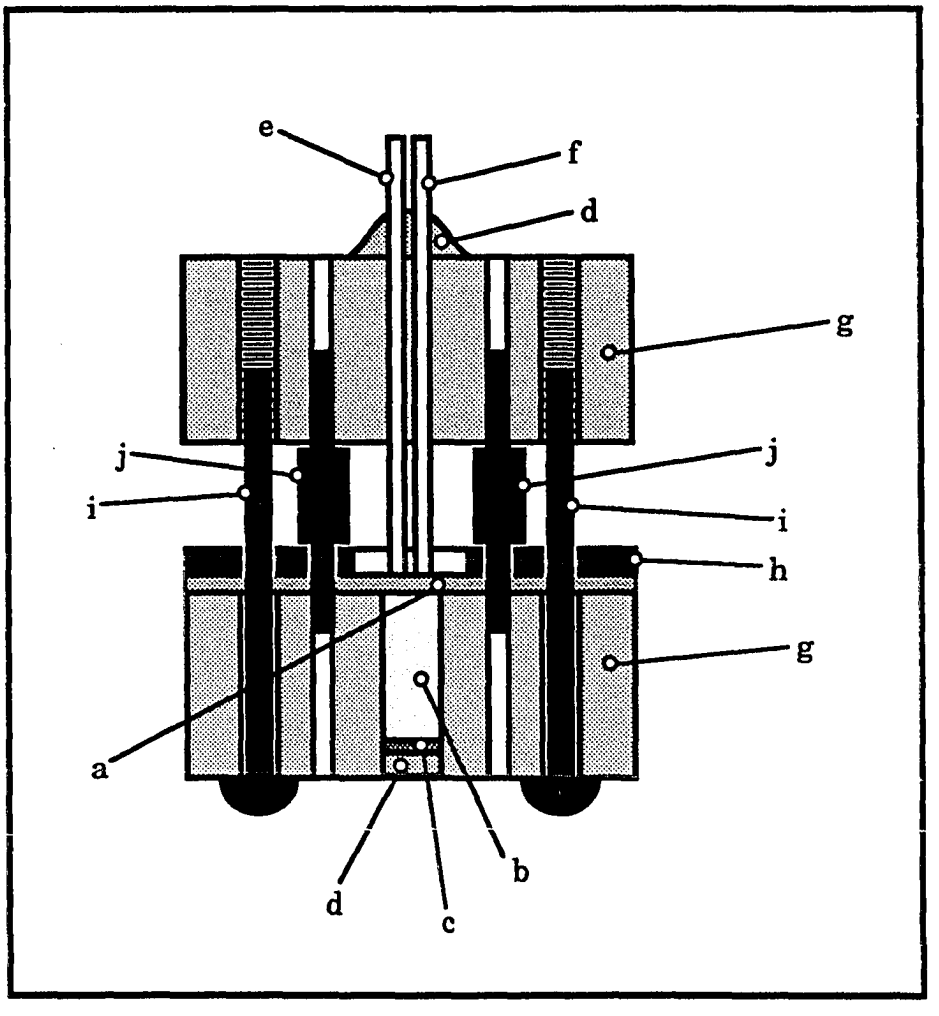

Figure 3. Fiber-optic sensor probe. (a) Thin-film sensor, (b) GRIN lens, (c) mirror, (d) epoxy, (e) input fiber, (f) collection fiber, (g) probe body, (h) stainless-steel plate, (i) screws, (j) stainless-steel pins

cyclohexanone at 2000 rpm onto glass microscope slides. The concentration of cellulose acetate was higher than in our previous reports to provide films with greater mechanical strength. After air drying for 24 h, the films were hydrolyzed in 0.1 M KOH for 24 h. The immobilized reagent (either Congo Red or C.I. Direct Blue 8) was immobilized according to a standard dye-bath recipe.[17] The resulting Congo Red sensor is sensitive in the pH range from 4.5 to 0.0; the C. I. Direct Blue 8 sensor is sensitive between pH 8.5 and 13. The sensor film was mounted in the probe, and held in place by a stainless-steel plate of 1-mm thickness with a 5-mm hole to exposed the pH-sensitive film to solution.

Electronics

A schematic of the detector circuitry is shown in Figure 4. Two such circuits were constructed: one for the sample detector and the one for the reference detector. Two photodetectors (S529-01-5; Devar, Inc., Bridgeport, CT) were used, which contained a 5.0-mm^2 silicon photodiode that was connected to a low-noise pre-amp. The photodetectors were enclosed in electronically shielded cases. One photodetector measured the intensity of light transmitted through the sensor probe, and the second functioned as a reference detector. The output voltage of the photodetectors was amplified by operational amplifiers, with adjustable gain and zero offset. The output voltage of the detector circuits were measured by a microcomputer-based data acquisition system.

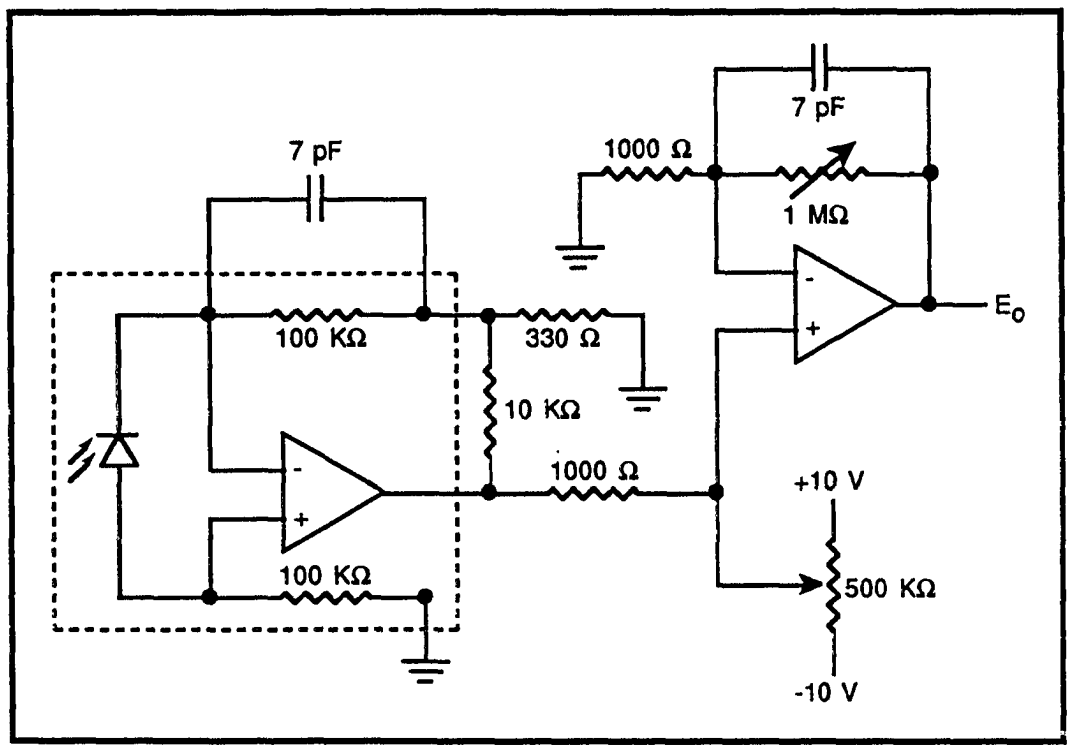

Figure 4. Schematic of detector circuitry. Inside the dotted line indicates internal connections of the S529 photodetector

Data Acquisition and Control System

Data acquisition from the sensor device was performed with a 80386-based microcomputer with data acquisition boards (RTI-815, RTI-850; Analog Devices, Norwood, MA). The data acquisition boards were controlled with Labtech Notebook software (Laboratory Technology Corporation, Wilmington, MA). Both LEDs were electronically modulated at 24 Hz through 8-bit analog-output channels on the RTI-815. The detector outputs were measured with 16-bit analog-input channels on the RTI-850, and represented 24-Hz square-wave functions of detector voltage comprising three stages, each of 1/24-s duration: (1) 635-nm illumination, (2) 565-nm illumination, and (3) background (i.e., ambient light from the probe). Because the voltage of the detector output is a linear function of the intensity of incident light,[18] the absorbance-vs.-time response of the sensor at each of the two wavelengths is given by

$$A = -\log[f_s(V_{s,i} - V_{s,b})]/[f_r(V_{r,i} - V_{r,b})] \quad (1)$$

where V represents detector voltage, f represents a proportionality constant arising from a number of factors (e.g., gain of the detectors, splitting ratio of the beam-splitter, and light attenuation by the sample probe and fiber-optics). The subscripts s and r refer to sample and reference detectors, respectively, and the subscripts i and b represent the detector-illuminated voltage and background voltage, respectively. Equation 2 can be rearranged to give

$$A = -\log[(V_{s,i}-V_{s,b})/(V_{r,i}-V_{r,b})] + C \quad (2)$$

where C represents $-\log(f_s/f_r)$. The value of C that resulted in a zero absorbance in the absence of the sensing film was determined. Subtraction of V_b corrected for detector dark-current, voltage offset of the operational amplifiers, and the effects of stray light. The absorbance-vs.-time trace was signal-averaged over intervals of one second (8 data-points per second), and the resulting data was smoothed with a nine-point Savitsky-Golay smoothing algorithm.

Time Response of Sensors

The absorbances of the sensor at 565 and 650 nm was monitored as a function of time as the sample probe was inserted into solutions of different pH, or as the pH was altered by adding 1M KOH. The solutions were stirred with a magnetic stirring bar, and the probe was rinsed with deionized water between immersions to minimize solution carry-over. The response of the sensor was allowed to reach a steady-state value each time the probe was inserted. The time constant of the sensor response was determined as the time required for 63% of maximum response to be reached.

Reagents

The pH of the solutions was controlled by varying the amounts of HCl or KOH, and sufficient KCl was added to adjust the ionic strength to 0.1. All solutions were prepared with deionized water.

RESULTS AND DISCUSSION

Graded-Index (GRIN) Optics

Graded-index (GRIN) lenses have become useful for fiber-optical applications, primarily in the area of optical communications. GRIN optics offer advantages of small size and low cost, and are often used for such tasks as coupling light from a source to a fiber optic, collimating light from a fiber, and splitting light between multiple fibers. Unlike conventional lenses, which focus light by refraction at a curved surface of a material with a constant refractive index, graded-index lenses focus light via a refractive index gradient. A GRIN lens is a cylinder with flat ends, with a refractive index as a function of radial distance given by

$$N(r) = N_0(1 - Ar^2/2) \quad (3)$$

where A is a constant (units of mm^{-2}), r is the radial distance (units of mm) from the axis of the lens, and N_0 is the refractive index at the axis. The propagation of rays through a GRIN lens is such that a fan of rays starting at a point (such as from a fiber optic) at the GRIN-lens surface are periodically focused as a function of distance along the GRIN-lens axis.[19] Meridional rays propagating through a GRIN lens have a characteristic period of $P = 2\pi/\sqrt{A}$. Because light entering one end of a GRIN lens of length nP/2 mm (where n is an integer) is guided to a mirror-image point on the opposite face of the GRIN lens, light can be coupled with high efficiency between two fiber-optics placed at the ends of a GRIN lens.

GRIN lenses offer a versatile and inexpensive means for the construction of optical components such as beam splitters and fiber-optic

couplers. A fiber-optic beam-splitter (shown in Figure 2) can be constructed with two GRIN lenses (each of length P/4 mm) placed end-to-end; a partially-reflective metal film coated at the interface between them provides a means of splitting the light intensity between two output fibers. Likewise, a GRIN lens (of length P/4 mm) in which the back face is coated with a mirror can be used to couple light between two parallel fibers which are placed at the front face of the cylinder along the diameter at equal distances from the axis.

Time Response of Sensors

The performance of the device was tested with two thin-film sensors: one based on Congo Red, which responds from pH 0 to 4, and C. I. Direct Blue 8, which responds from pH 9.5 to 13. The LEDs were electronically modulated at 24 Hz; the absorbances were calculated from the detector voltages by Equation 2, and the absorbances at 565 and 635 nm were plotted in real-time on the computer screen. Figure 5 shows the time response of the absorbance of the Congo Red sensor at 565 nm and 635 nm as the sensor was inserted into solutions of differing pH. As the probe was inserted into solutions of decreasing pH, the absorbance at both 565 and 635 nm increased until they reached a steady-state response. Figure 6 shows the time response of the absorbance of the C. I. Direct Blue 8 sensor at 565 nm and 635 nm as the sensor probe was inserted into a solution of 0.1 M KCl, and pH was increased by the addition of 1 M KOH. As the the pH increased, the absorbance at both 565 and 635 nm decreased until they reached a steady-state response. The time constant for the Congo Red sensor probe response

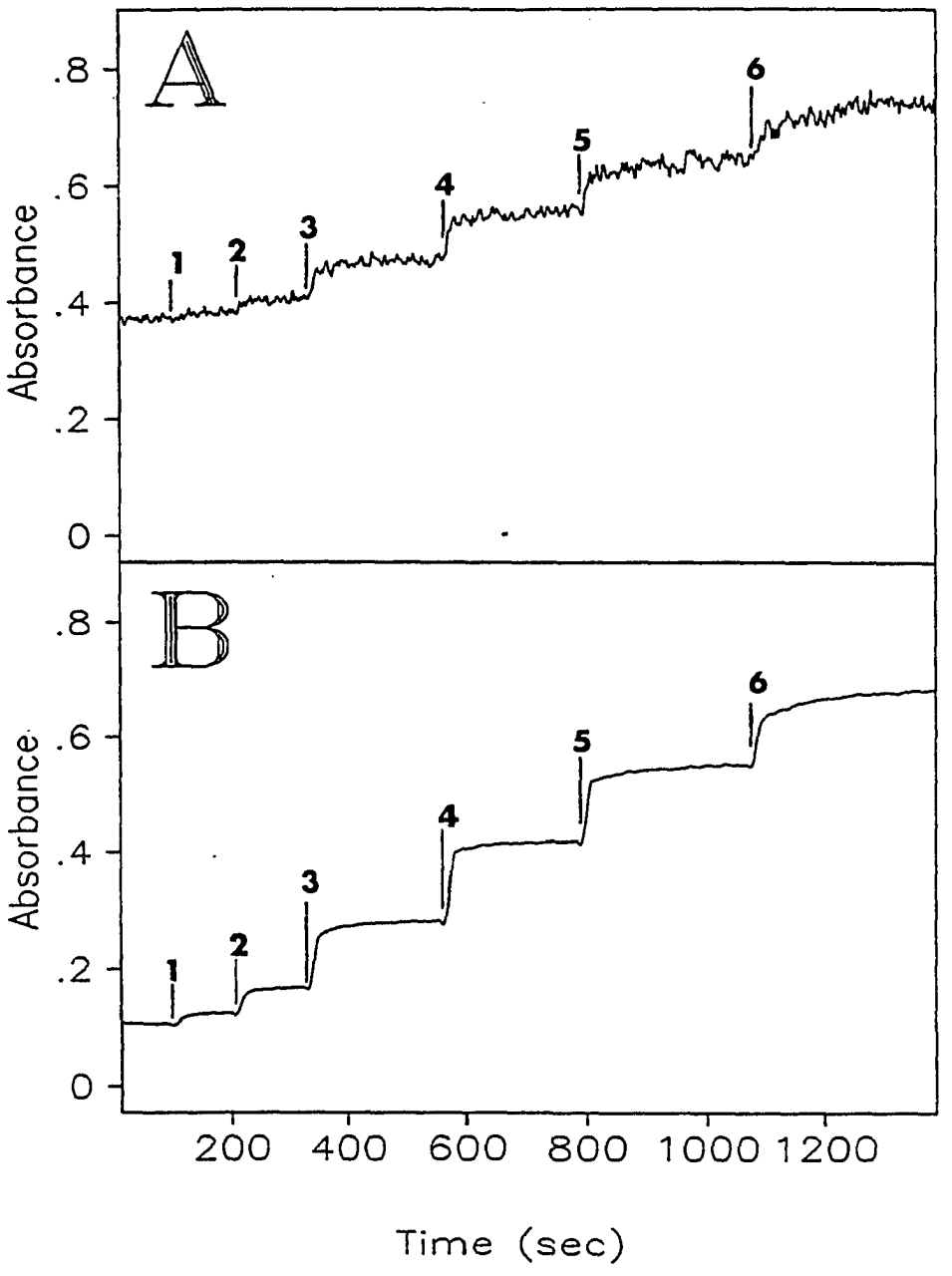

Figure 5. Absorbance time response of the Congo Red sensor at: (A) 565 nm, and (B) 635 nm. Probe was inserted into solutions with pH values of: (0) 3.96, (1) 3.45, (2) 2.98, (3) 2.41, (4) 1.88, (5) 1.37, (6) 0.86

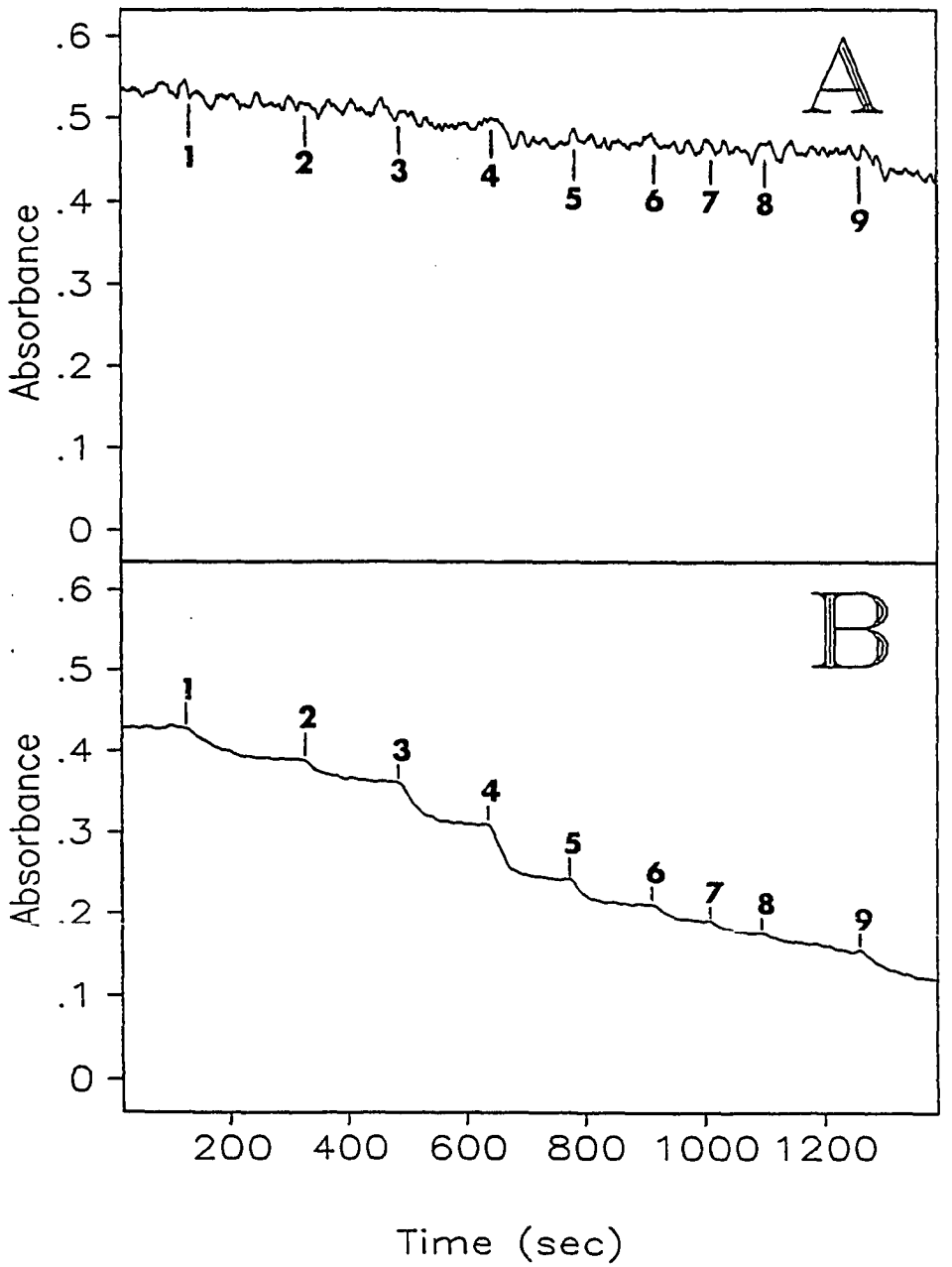

Figure 6. Absorbance time response of the C. I. Direct Blue 8 sensor at: (A) 565 nm, (B) 635 nm. The pH was altered by addition of 1 M KOH to values of: (0) 6.00, (1) 9.82, (2) 10.05, (3) 10.38, (4) 10.81, (5) 11.16, (6) 11.41, (7) 11.64, (8) 11.90, (9) 12.71

was 10 s. The time constant for the C. I. Direct Blue 8 sensor probe response was 25 s. Although these time constants were significantly larger than the value of 0.32 s that was measured for the Congo Red sensor in a flow cell,[20] they represent the time required for solution mixing as well as the sensor response. The stability of the photometer response was determined over a four-hour period, during which no drift was observed in the absorbance.

Figure 7 shows the absorbance at 565 nm and 635 nm as a function of pH for (A) the Congo Red sensor and (B) the C. I. Direct Blue 8 sensor. The error bars in Figure 7 represent the peak-to-peak noise from the data in Figures 5 and 6. The peak-to-peak noise level for the absorbance at 635 nm was ±0.001. This level of noise allows the singe-wavelength detection of changes in pH as small as 0.003 pH units. The peak-to-peak noise level for the absorbance at 565 nm was ±0.010. The higher noise level at 565 nm was a result of two factors: (1) 565-nm light couples through the probe with only ~53% of the efficiency as 630-nm light, and (2) the detector response for 565-nm light is ~30% of the response for 635-nm light.[21] Efforts to improve the noise level of the absorbance measurement at 565 nm are currently underway, including the use of more sensitive detectors, and higher-intensity light sources. Additionally, the data collection rate will be increased to the 2-3 KHz range (presently 24 Hz), resulting in nearly a factor of 10 improvement in noise due to increased signal averaging.

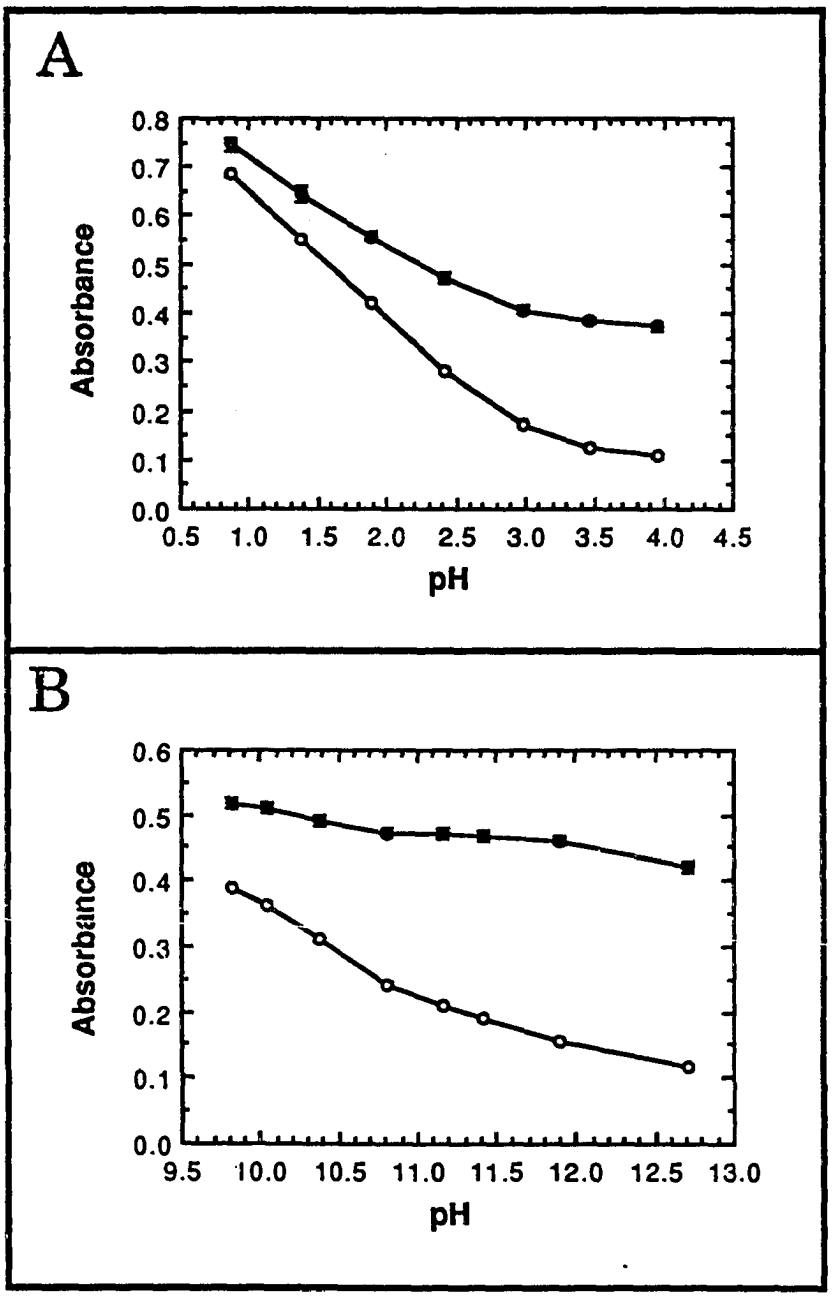

Figure 7. Absorbance as a function of pH of: (A) Congo Red pH sensor, (B) C. I. Direct Blue 8 pH sensor. Plot symbols: (o) absorbance at 635 nm, (●) absorbance at 565 nm

Calibration of the Sensor

One advantage of a "two-color" indicator is that a calibration curve that is independent of indicator concentration can be constructed. Figure 8 shows calibration curves for (A) the Congo Red sensor and (B) the C. I. Direct Blue 8 sensor, which were obtained by plotting the pH as a function of the ratio of the absorbance at 635 nm to the absorbance at 565 nm (A_{635}/A_{565}), which was independent of indicator concentration. The validity of the two-wavelength calibration was demonstrated previously,[20] in which the approach was determined to be reproducible for sensor films containing differing amounts of indicator to within ±0.05 pH units. The data were then fitted with a fifth-order polynomial equation to give

$$pH = 28.75 - 215.6r + 720.3r^2 - 1195r^3 + 972.5r^4 - 311.9r^5 \quad (4)$$

$$pH = 38.94 - 246.6r + 918.6r^2 - 1750r^3 + 1665r^4 - 628.7r^5 \quad (5)$$

for the Congo Red and C. I. Direct Blue 8 sensors, respectively, where r is the absorbance ratio (A_{635}/A_{565}). The horizontal error bars in Figures 8A and 8B represent the uncertainty in the measurement of the absorbance ratio. The vertical error bars in Figures 8A and 8B represent the uncertainty in the calculated pH corresponding to the uncertainty in r, via the derivatives of Equations 4 and 5, respectively. In the Congo Red calibration curve (Figure 8A), the uncertainty in the pH calculated by Equation 4 varies from a low of ±0.03 in the middle of the calibration curve to ±0.08 and ±0.22 at at the high-pH and low-pH ends, respectively. In the C. I. Direct Blue 8 calibration curve (Figure 8B), the uncertainty in the pH calculated by Equation 5 varies

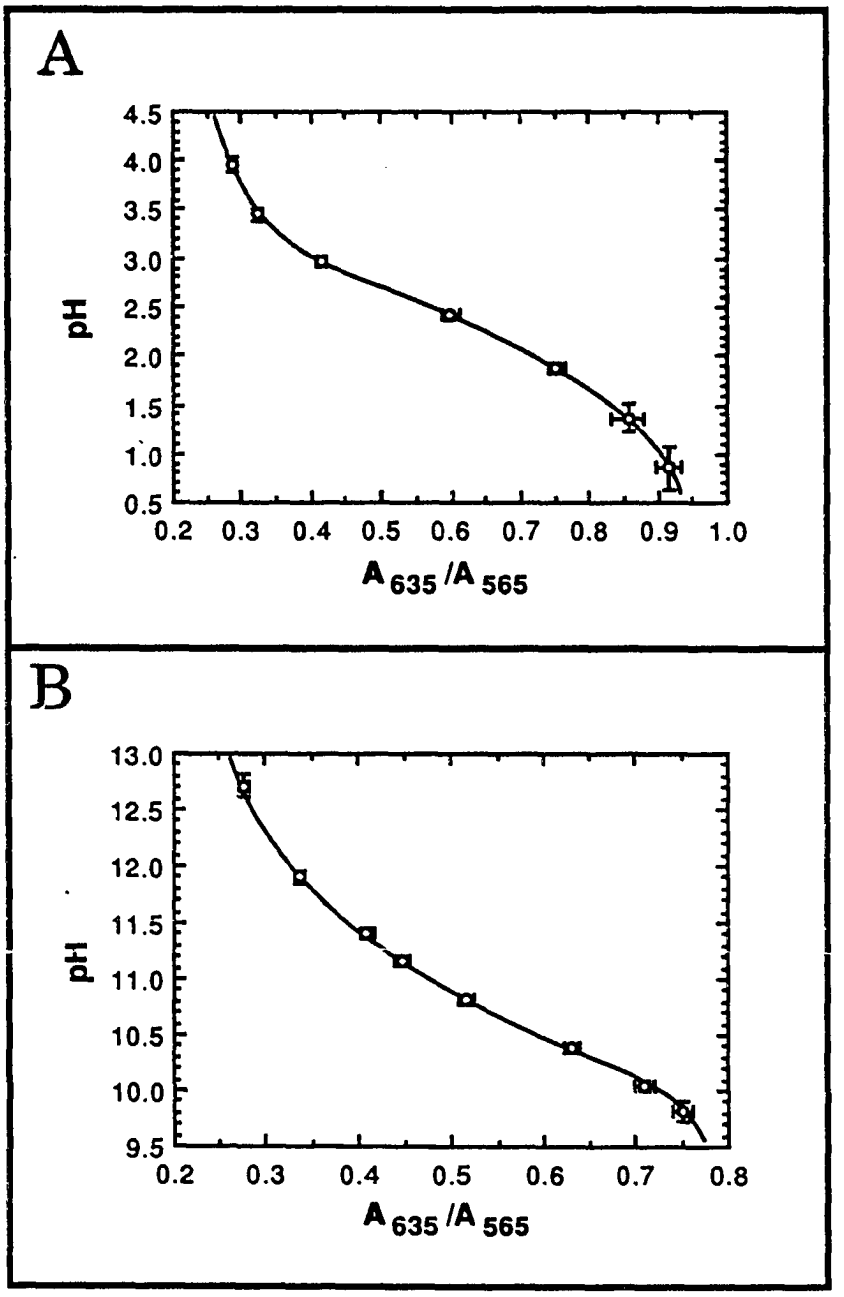

Figure 8. Calibration curves for (A) Congo Red pH sensor, (B) C. I. Direct Blue 8 pH sensor. Horizontal error bars represent uncertainty in the absorbance ratio, and vertical error bars represent corresponding uncertainties in pH values calculated by curve fit

from a low of ±0.03 in the middle of the calibration curve to ±0.10 and ±0.09 at at the high-pH and low-pH ends, respectively. The greater uncertainty in pH at the ends of the calibration curves arises from the large change in pH corresponding to a small change in absorbance ratio.

Although the bandwidth (in excess of 30 nm) of the LEDs causes nonlinearity of Beer-Lambert plots, this non-linearity does not affect the accuracy of for the calibration plots. A narrow-bandpass filter can be used to select light of a narrower wavelength range, but it also reduces throughput, resulting in noise levels which are unacceptable with the current sources. The selection of wavelengths was to a large part limited by the availability of LEDs with high intensity and low power consumption, particularly by the lack of suitable sources of wavelengths below 550 nm.

CONCLUSIONS

A solid-state optical photometer that operates in a two-wavelength mode for absorbance measurements has been developed which allows the determination of pH to within ±0.1 pH units across a dynamic range of 2-3 pH units. Novel features of the design include incorporation of a reference detector to compensate for fluctuations in output intensities of LEDs and a thin-film sensor probe that employs a graded-index (GRIN) lens to couple light efficiently from an input fiber to a collection fiber. A GRIN beamsplitter is also used to transmit simultaneously to the sample and reference detectors.

To improve the precision of the sensor device, a few improvements will be incorporated in the design. Presently, the greatest contribution to the uncertainty of the sensor is the noise level of the absorbance measurement at 565 nm. Calculations indicate that uncertainties of ±0.01 pH units in the center (and ±0.04 at the ends) of the dynamic range will be attainable if the noise level for 565-nm light is reduced to ±0.001 absorbance units. Efforts to attain this goal are currently underway, including faster data collection, which allows for more signal averaging, the use of photodiode detectors with greater sensitivity to 565-nm light, and higher intensity light sources. Additionally, data collection rates in the 2-3 KHz range are planned that will result in a reduction of noise by a factor of 10 due to increased signal averaging.

Future applications of the sensor device include the construction of "remote sensing modules" (RSM), which allow the possibility of continuous

environmental sensing at multiple remote locations, and the development of sensors for biomedical applications, such as the measurement of physiological pH. The RSMs, which contain on-board microprocessors and FM-radio transceivers, could be placed at multiple locations along a watershed, and interrogated by a central data station located in a vehicle or communicating via microwave repeater stations. Development of a prototype of such a device is nearing completion in our laboratory.

ACKNOWLEDGEMENTS

Assistance in electronic circuit design by Shelley J. Coldiron and Bill Deninger is acknowledged. MDP Gratefully acknowledges the support of a Dow Corning Assistant Professorship. This work was supported by the Ames Laboratory–USDOE and the Center for Advanced Technology Development, at Iowa State University, Ames, IA 50011.

REFERENCES

1. Wohltjen, H. *Anal. Chem.* **1984**, *56*, 87A-103A.
2. Janata, J.; Bezegh, A. *Anal. Chem.* **1988**, *60*, 62R-74R.
3. Seitz, W. R. *Anal. Chem.* **1984**, *56*, 16A-34A.
4. Narayanaswamy, R. *Anal. Proc. (London)* **1985**, *22*, 204-206.
5. Alder, J. F. *Fresenius' Z. Anal. Chem.* **1986**, *324*, 372-375.
6. Wolfbeis, O. S. *Fresenius' Z. Anal. Chem.* **1986**, *325*, 387-392.
7. Angel, S. M. *Spectroscopy (Springfield, Oreg.)* **1987**, *2*, 38-4.
8. Wolfbeis, O. S. *Anal. Proc. (London)* **1987**, *24*, 14-15.
9. Hirschfeld, T.; Callis, J. B.; Kowalski, B. R. *Science* **1984**, *226*, 312-318.
10. Peterson, J. I.; Vurek G. G. *Science* **1984**, *224*, 123-12.
11. Callis, J. B.; Illman, D. L.; Kowalski, B. R. *Anal. Chem.* **1987**, *59*, 624A-637A.
12. Giuliani, J. F.; Wohltjen, H.; Jarvis, N. L. *Opt. Lett.* **1983**, *8*, 54.
13. Smardzewski, R. R. *Talanta* **1988**, *35*, 95-101.
14. Guthrie, A. J.; Narayanaswamy, R.; Welti, N. A. *Talanta* **1988**, *35*, 157-159.
15. Jones, T. P.; Porter, M. D. *Anal. Chem.* **1988**, *60*, 404-406.
16. Stole, S. M.; Jones, T. P.; Chau, L. K.; Porter, M. D. In *Chemical Sensors and Microinstrumentation*; Murray, R. W.; Dessy, R. E.; Heineman, W. R.; Janata, J.; Seitz, W. R.; Eds.; ACS Symposium Series 403; American Chemical Society: Washington, DC, 1989; chapter 19.
17. Fieser, L. F.; Williamson, K. L. *Organic Experiments,* 5th ed.; D. C. Heath, Lexington, MA, 1983.

18. Application notes for type 529 integrated optical detectors; Devar, Inc.: Bridgeport, CT., 1990.

19. Marchand, E. W. *Gradient Index Optics*; Academic: New York, 1978.

20. Jones, T. P.; Porter, M. D. submitted to *Anal. Chem.* (see Section V.).

21. Technical specifications, Devar, Inc., Bridgeport, CT., 1990.

SUMMARY AND DISCUSSION

The development, characterization, and application of optical pH sensors have been studied. Studies of the hydrolysis of cellulose acetate indicated that the polymer was an appropriate medium for the immobilization of colorimetric indicators. Sensors for pH were developed, based on the immobilization of direct dyes at hydrolyzed cellulose acetate. A thorough investigation of the response characteristics of the Congo Red pH sensor, including its calibration and accuracy, was performed. Characterizations of the sensor led to the development of a sensor for pH based on infrared spectroscopy. Finally, a solid-state device for remote sensing with thin polymer-film sensors was constructed and its performance was evaluated.

The last five years have seen a tremendous growth in the number of manuscripts and books published in the research area of optical chemical sensors. Despite this growth, to date the promise of low-cost continuous environmental monitoring of pH and metal-ion analysis is still largely unfulfilled. A handful of optical sensors has made it out of the laboratory and into the marketplace, and doubtless more will follow in the future. Devices based on solid-state components will become more powerful with the development of shorter-wavelength light-emitting diodes and diode lasers. New developments in fiber-optics technology will allow lower light-losses. All of these developments will allow more sophisticated detection strategies and enhance the applicability of optical chemical sensors.

ACKNOWLEDGEMENTS

I would like to thank my Major Professor, Prof. Marc D. Porter, for leadership and guidance, and all the members of the Porter research group, especially Scott M. Stole, without whose assistance my work would have been much more difficult. I'd also like to thank Prof. Dennis C. Johnson for his guidance as Co-Major Professor. There are many others in the Chemistry Department at Iowa State for whose assistance I shall always be grateful.

Finally, I'd like to thank my undergraduate professors at Earlham College, particularly Prof. Paul Ogren, who has always been a source of inspiration, for their encouragement to pursue an academic career.